



Utrecht University



Institute of Theoretical Physics

Matching between EFT and UV Complete Models

MASTER'S THESIS

Jaco ter Hoeve

Supervisors:

Dr. Juan ROJO

Nikhef, VU

Prof. Dr. Eric LAENEN

Utrecht University, ITP

July 6, 2020

Abstract

Standard Model Effective Field Theory (SMEFT) provides an elegant mathematical framework that lets us capture imprints of new physics in a model independent way. Considering the Standard Model (SM) as a low energy approximation of a more fundamental theory allows for the addition of higher dimensional operators to the SM Lagrangian. By fitting these operators to high precision data from the Large Hadron Collider (LHC), we can simultaneously constrain a plethora of models beyond the SM (BSM). Here, information about BSM physics gets implicitly encoded in a set of Wilson coefficients. In order to extract these constraints, UV complete models need to be matched onto the SMEFT. In this thesis, we present the matching equations at tree level for a heavy scalar and a heavy vector boson in the Warsaw basis. We derive bounds for the associated couplings and masses by combining the matching equations with a SMEFT fit to LHC top quark data. As an alternative approach, we also derive bounds for the same UV parameters from an explicit BSM phenomenology analysis using differential cross sections for $t\bar{t}$ -production in pp -collisions at $\sqrt{s} = 13$ TeV. Our study shows that an EFT approach is more versatile and provides sensitivity for higher energies than direct BSM searches.

As a second piece of this work, we quantify the degree to which the SMEFT fitting degrees of freedom can be constrained from top-quark processes by performing a sensitivity study. It highlights experiments that are particularly suitable to constrain SMEFT degrees of freedom.

Acknowledgements

This thesis could not have been completed without the help of the following people. First of all, I would like to thank my supervisor Juan Rojo for inspiring me along this journey, and giving me the freedom to explore the world of particle physics. A special thanks also goes to Jake Ethier of course for all the interesting conversations that we have had over the last year and for always making time for me whenever I had questions. I would also like to thank Prof. Eric Laenen for putting me in contact with Juan's research group. In addition I thank my office friends at Nikhef for the many fruitful discussions and the occasional banter.

It goes without saying that I could not have done all this without the people that stand closest to me. Thank you, Maartje, for always being supportive and showing interest in what I do. Thank you, mom and dad, for making me live the life I live and your endless love and support. Finally, to Pauline, thank you for giving my life colour every day, it means so much to me.

Contents

1	Introduction	1
2	The Standard Model	3
3	Effective Field Theories	5
3.1	Fermi’s Theory of Weak Decay	6
3.2	The SM as an EFT	7
3.3	Observables in SMEFT	8
3.4	Example: Top-Quark Decay	9
3.5	Warsaw-basis	19
4	SMEFT Fitting Framework	20
4.1	Nested Sampling	20
4.2	Operator Definitions and Experiments	22
5	Dimensional Reduction: Sensitivity	25
5.1	Preliminaries	25
5.2	The Sensitivity	26
5.3	Results	27
5.4	Discussion	35
6	Top-quark Matching	36
6.1	Model: Heavy Scalar	37
6.1.1	NLO Effects	43
6.2	Model: Heavy Vector Boson	44
7	Phenomenology of UV Extensions	51
7.1	Standard Model Contribution	51
7.1.1	Partonic Cross Sections	52
7.1.2	Differential Hadronic Cross Section	56

7.1.3	Dynamical Renormalization Scale	57
7.1.4	Conversion to Bins and Conventions	58
7.2	Beyond the Standard Model Contribution	59
7.2.1	Heavy Scalar	59
7.2.2	Heavy Vector	60
7.2.3	Interference SM and BSM	61
7.3	FastNLO and MadGraph	62
7.4	χ^2 Analysis	64
7.4.1	Heavy Scalar	64
7.4.2	Heavy Vector	70
8	Conclusion	76
A	Warsaw Basis	78
B	Fierz Identities	80
C	Decay Widths	82
C.1	Heavy Scalar	82
C.2	Heavy Vector Boson	83

Chapter 1

Introduction

The discovery of the Higgs boson at the Large Hadron Collider (LHC) in 2012 [1], has caused a vast increase in the search for new physics beyond the standard model (BSM). Given that there is no direct evidence of new physics directly around the corner, the LHC's program is largely focused on high precision measurements. Here, the hope is to find statistically significant deviations from the standard model (SM) that provide evidence for new interactions or particles beyond the LHC's reach. These imprints can most conveniently be captured by the standard model effective field theory (SMEFT). When faced with separation of scales, or significant energy gaps, SMEFT provides a convenient mathematical framework for parameterising new physics in a model-independent way [2]. This makes it an incredibly valuable tool in our search for new physics.

In the SMEFT, the SM gets extended by higher dimensional operators that can capture high energy effects as imprints below a certain cutoff scale Λ . Above Λ , new particles or interactions are believed to exist. The operators are weighted by a priori unknown coefficients, the *Wilson coefficients*. Without assuming any particular ultraviolet (UV) extension, these coefficients can only be determined by performing fits to high precision data from the LHC. New physics will then be detected as non-vanishing Wilson coefficients, thereby constraining a large class of possible extensions of the SM. A big part of current research in particle physics is devoted to inferring these Wilson coefficients from the data and putting confidence level bounds on their values.

Many attempts in this direction have already been made, predominantly by the SMEFiT collaboration [3], but a fully global fit that incorporates all relevant experimental data has yet to be performed. The work presented in [3] focuses on the top-quark sector of the SM and introduces a novel framework called SMEFiT to constrain and find bounds on the 34 degrees of freedom that are relevant in the study of top-quark interactions at the LHC. Future attempts will include the extensions of this work to the Higgs-sector and possibly the electroweak sector of the SM as well. This will increase the number of degrees of freedom entering the fit, which makes it an even more statistically and computationally challenging problem.

Naturally, a second step that should be carried out alongside the SMEFT analysis involves

connecting the parameters appearing in explicit UV extensions to the SMEFT degrees of freedom (Wilson coefficients). This is done through what is called *matching*. It restores the model dependence and, as a result, bounds can be found on the UV parameters, which are primarily masses and couplings. So both the SMEFT fitting problem as well as matching computations play central roles. Together, they provide a powerful and diverse framework that enables one to search for new physics at energies beyond those that are currently accessible.

In this thesis, we study and carry out this two-step process. Using bounds on the SMEFT degrees of freedom, we constrain two specific UV extensions of the SM – a heavy scalar and heavy vector model. The goal is to add to the class of UV-extensions a set of bounds that helps to constrain potentially new physics.

The remainder of this work is structured as follows. First, we present the necessary background material aimed at the level of a student with experience in quantum field theory. This covers a quick introduction to the SM in chapter 2, followed by an introduction to effective field theories in chapter 3. In section 3.4, we carry out a detailed calculation that shows how the decay of the top-quark gets modified in the SMEFT with respect to the SM. This is both insightful and instructive. After introducing the basics behind the SMEFT fitting framework in chapter 4, we then move on to presenting new material developed as part of this thesis.

Chapter 5 presents a new statistical measure applied to the SMEFT, called the sensitivity. It turns out that not every SMEFT degree of freedom is as sensitive to experimental data as others. Therefore, the sensitivity helps to distinguish between these cases and highlights experiments that are particularly important for constraining the SMEFT degrees of freedom. The main part of this thesis is covered by chapters 6 and 7. There, we present new results that show how to match explicit UV extensions onto the SMEFT for two different models: a heavy scalar and a heavy vector extension. We specifically take care here to present our results in the so-called *Warsaw*-basis. This gives bounds on the parameters that characterise the UV-extension, such as masses and couplings, from an effective field theory perspective. The analysis done in chapter 7, on the other hand, offers an alternative approach for obtaining bounds on the same UV-parameters by working within the UV-extension itself. This relies on minimising a figure of merit, the famous chi-squared. A comparison between the different approaches in chapters 6 and 7 then forms our main result. Finally, in chapter 8 we summarise our main conclusions and outline future research ideas that build on this work.

Chapter 2

The Standard Model

We start this thesis by giving a lightning introduction to the Standard Model of particle physics. Considering the vastness of this subject, we focus only on those areas that are important for the upcoming chapters. For further details, many good references exist, such as [4, 5]. The content in this chapter primarily serves to fix our notation, and is based around the introductory discussion in [6].

The SM is a quantum field theory that transforms under the gauge group

$$SU(3)_c \times SU(2)_L \times U(1)_Y, \quad (2.0.1)$$

where the subscripts c , L , and Y stand for colour, left (chirality) and hypercharge respectively. The associated Lagrangian is given by

$$\mathcal{L}_{\text{SM}} = \mathcal{L}_{\text{Gauge}} + \mathcal{L}_{\text{Dirac}} + \mathcal{L}_{\text{Yukawa}} + \mathcal{L}_{\text{Higgs}}. \quad (2.0.2)$$

Here, $\mathcal{L}_{\text{Gauge}}$ describes the kinetic terms for the Gauge fields, written as

$$\mathcal{L}_{\text{Gauge}} = -\frac{1}{4}B_{\mu\nu}B^{\mu\nu} - \frac{1}{4}W_{\mu\nu}^I W^{I\ \mu\nu} - \frac{1}{4}G_{\mu\nu}^A G^{A\ \mu\nu}, \quad (2.0.3)$$

where

$$\begin{aligned} B_{\mu\nu} &= \partial_\mu B_\nu - \partial_\nu B_\mu \\ W_{\mu\nu}^I &= \partial_\mu W_\nu^I - \partial_\nu W_\mu^I + gf^{IJK}W_\mu^J W_\nu^K \\ G_{\mu\nu}^A &= \partial_\mu G_\nu^A - \partial_\nu G_\mu^A + g_s f^{ABC}G_\mu^B G_\nu^C \end{aligned}$$

define the field strength tensors and B_μ , W_μ^I and G_μ^A denote the gauge fields of the groups $U(1)_Y$, $SU(2)_L$ and $SU(3)_c$ respectively. The kinetic terms for the fermionic fields are described by $\mathcal{L}_{\text{Dirac}}$:

$$\begin{aligned} \mathcal{L}_{\text{Dirac}} &= \sum_i \bar{q}_L^i \not{D} q_L^i + \sum_i \bar{l}_L^i \not{D} l_L^i + \sum_i \bar{u}_R^i \not{D} u_R^i \\ &+ \sum_i \bar{d}_R^i \not{D} d_R^i + \sum_i \bar{e}_R^i \not{D} e_R^i, \end{aligned} \quad (2.0.4)$$

where q_L and l_L transform in the fundamental representation of $SU(2)$, with components

$$q_L = \begin{pmatrix} u_L \\ d_L \end{pmatrix} \quad \text{and} \quad l_L = \begin{pmatrix} \nu_L \\ e_L \end{pmatrix}. \quad (2.0.5)$$

The symbols u , d and e generally denote up-type quarks, down-type quarks and charged leptons respectively. The subscripts L/R refer to left/right-handed fermionic fields that transform as doublets/singlets under $SU(2)$. Starting from a four component Dirac spinor ψ , its left and right-handed fields are obtained by acting with the projection operators

$$P_L = \frac{1}{2}(1 - \gamma^5) \quad \text{and} \quad P_R = \frac{1}{2}(1 + \gamma^5). \quad (2.0.6)$$

The superscript $i = 1, 2, 3$ labels the generations. Furthermore, in order to make sure the terms in $\mathcal{L}_{\text{Dirac}}$ transform covariantly under the SM gauge group, we define the covariant derivative as

$$D_\mu = \partial_\mu - ig'YB_\mu - ig\frac{\tau^I}{2}W_\mu^I - ig_s\frac{\lambda^A}{2}G_\mu^A. \quad (2.0.7)$$

Here, Y , $\tau^I/2$ and $\lambda^A/2$ denote the generators of the abelian group $U(1)$, and the non-abelian groups $SU(2)$ and $SU(3)$ respectively.

In order to get mass terms for the fermionic fields they are coupled to the Higgs field φ according to

$$\mathcal{L}_{\text{Yukawa}} = -Y_d^{ij}\bar{d}_R^i\varphi^\dagger q_L^j - Y_u^{ij}\bar{u}_R^i\tilde{\varphi}^\dagger q_L^j - Y_e^{ij}\bar{e}_R^i\varphi^\dagger l_L^j + \text{h.c.} \quad (2.0.8)$$

Here, φ defines the Higgs field that transforms as a doublet under $SU(2)_L$ and is written as

$$\varphi = \begin{pmatrix} \varphi^+ \\ \varphi^0 \end{pmatrix}, \quad (2.0.9)$$

where φ^+ and φ^0 are complex scalars. Furthermore, Y_l^{ij} , with $l \in \{d, u, e\}$, define the Yukawa matrices in generation space. The Lagrangian describing the Higgs field itself is given by

$$\mathcal{L}_{\text{Higgs}} = D_\mu\varphi(D^\mu\varphi)^\dagger - V(\varphi), \quad (2.0.10)$$

where $V(\varphi)$ defines the potential of the Higgs fields, responsible for spontaneous symmetry breaking.

All terms in the SM Lagrangian are Lorentz and gauge invariant. Furthermore, it only includes marginal operators and can therefore make predictions to arbitrarily large energies down to the Planck scale. With this quick overview of the SM, we will now turn to effective field theories. Combining this with the SM itself will then lead to the Standard Model Effective Field Theory (SMEFT).

Chapter 3

Effective Field Theories

A striking result in (high energy) physics is that one can get away with knowing very little. For instance, the hydrogen spectrum can be calculated in quantum mechanics quite precisely without referring to the existence of quarks and gluons inside the proton. As a second example, the orbits of planets can be accurately described without having to worry about their sizes or constituents. Also, the multipole expansion in electrodynamics describes a collection of electric charges from a far away region regardless of their precise distribution. These three observations are collectively captured by the notion of *separation of scales*. In short, this says that any physics that takes place at one particular energy scale, is describable without having detailed knowledge of physics outside this energy regime. In field theoretic language this means that short-distance (ultra-violet) physics decouples from large-distance (infrared) physics, as also formally stated by Appelquist's theorem [7].

The mathematical translation of this set of ideas is captured by an *effective field theory* (EFT). Given a physical system, the first step towards building an effective field theory is to identify the relevant degrees of freedom at the scale that one considers. Let us start with a full theory that contains two fields, one light field ϕ and one heavy field ψ with masses m_ϕ and m_ψ respectively. We can now construct an effective theory that gives an adequate description at energy scales smaller than m_ψ and that only features the light field ϕ . The heavy field is said to be “integrated out”, see figure 3.1.

Despite the fact that the EFT will no longer carry any explicit dependence on ψ , the heavy field still leaves indirect effects on scales $E < m_\psi$ that can be approximated to arbitrary accuracy. Therefore, an EFT provides a framework that allows us to capture the right amount of physics to have both a simple description and an accurate one, in the sense that high energy corrections can be added to the effective theory through an expansion in a small ratio of scales.

To make the abstract introduction above concrete, we begin this chapter with an extremely modest example: Fermi's theory of weak decay. It is the prime example when discussing effective field theories. It also provides us with an early example of matching.

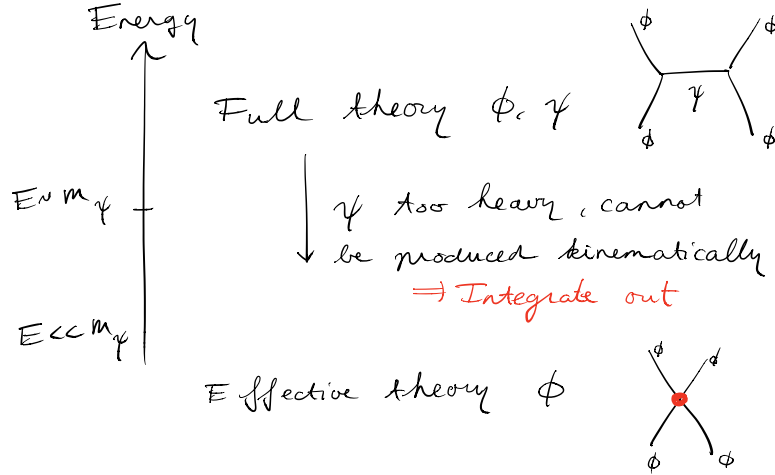


Figure 3.1: The conceptual picture behind effective field theories. The full theory depends on the light and heavy fields ϕ and Ψ respectively. At energies $E < m_\psi$ the effective theory gives an accurate description which features ϕ only. The heavy field is said to be “integrated out”.

3.1 Fermi’s Theory of Weak Decay

Before the theory of weak-interactions was fully understood, Enrico Fermi proposed the idea of a four-fermion interaction in order to explain the phenomenon of neutron beta decay [8]. With hindsight, we know that this model is incomplete, as it does not include the W -bosons. However, it provides an accurate phenomenological description at low energies. In other words, Fermi’s theory of Weak Decay can be derived as an effective theory starting from the SM Lagrangian.

Within the SM, the decay $n \rightarrow p + e^- + \bar{\nu}_e$ happens through coupling of the W -bosons to the quarks and leptons according to

$$\mathcal{L}_W = \frac{g}{\sqrt{2}} V_{ij} \bar{q}_i \gamma^\mu P_L q_j W_\mu^\pm + \frac{g}{\sqrt{2}} \bar{e} \gamma^\mu P_L \nu_e W_\mu^\pm + \dots, \quad (3.1.1)$$

where V_{ij} are the CKM matrix elements, and $P_L = \frac{1}{2}(1 - \gamma^5)$ is the left-handed projector operator. Let us now consider the process $d \rightarrow u + e^- + \bar{\nu}_e$. Its amplitude at tree level is given by

$$\mathcal{M} = \left(\frac{ig}{\sqrt{2}} \right)^2 V_{du} (\bar{d} \gamma^\mu P_L u) (\bar{e} \gamma^\nu P_L \nu_e) \times \frac{-ig_{\mu\nu}}{p^2 - M_W^2}, \quad (3.1.2)$$

In the regime $p^2 \ll M_W^2$, with p the momentum of the W -boson, W cannot be kinematically produced, and the matrix element can be simplified by Taylor expanding the propagator:

$$\frac{1}{p^2 - M_W^2} = -\frac{1}{M_W^2} \left(1 + \frac{p^2}{M_W^2} + \dots \right)$$

Therefore, at leading order the matrix element becomes

$$\mathcal{M} = \frac{i}{M_W^2} \left(\frac{ig}{\sqrt{2}} \right)^2 V_{du} (\bar{d} \gamma^\mu P_L u) (\bar{e} \gamma_\mu P_L \nu_e) + \mathcal{O} \left(\frac{1}{M_W^4} \right). \quad (3.1.3)$$

This same matrix element can also be obtained by the following *effective Lagrangian*:

$$\mathcal{L}_{\text{eff}} = -\frac{4G_F}{\sqrt{2}} V_{du} (\bar{d}\gamma^\mu P_L u) (\bar{e}\gamma_\mu P_L \nu_e), \quad (3.1.4)$$

where G_F is called Fermi's constant, which can be related to the UV-parameters g and M_W via *matching*. In general, matching connects the EFT parameters to the parameters of the full theory by demanding the EFT to produce the same matrix element as the full theory. In the case of Fermi's theory described by the Lagrangian in (3.1.4), this requirement leads to:

$$\frac{G_F}{\sqrt{2}} = \frac{g^2}{8M_W^2}. \quad (3.1.5)$$

We will see a more detailed examples of matching in chapter 6. In principle the effective theory can now be made more accurate by going to higher orders in the ratio of scales p^2/M_W^2 , but for now this simple example suffices.

3.2 The SM as an EFT

The SM was introduced in chapter 2 and is a renormalisable theory from which we can construct effective theories through perturbative matching, as we just saw in section 3.1. However, let us now take a different viewpoint and consider the SM itself as an effective theory of some other, more fundamental theory. This is an interesting statement by itself. So far, all the effective theories we have considered, are only valid up to some finite energy scale. Beyond this, the EFT breaks down and we have to resort to the full theory again. The SM, in contrast, is valid all the way down to the Planck scale, where quantum gravity is thought to take over. However, there are clear indications that the SM is incomplete. For example, it does not feature any candidates for dark matter particles, and the neutrinos are assumed massless even though they exhibit oscillations [9]. Inspired by the idea of effective field theories, we now require the SM to be valid only up to $E \simeq \Lambda$, with $\Lambda \ll m_H$ (125 GeV). Consequently, there is no need anymore to restrict ourselves to only marginal operators (having mass-dimension equal to four), and we can write down the following effective Lagrangian:

$$\mathcal{L}_{\text{SMEFT}} \equiv \mathcal{L}_{\text{SM}} + \frac{1}{\Lambda} \sum_{i=1}^{N_{d5}} C_i^{(5)} \mathcal{O}_i^{(5)} + \frac{1}{\Lambda^2} \sum_{i=1}^{N_{d6}} C_i^{(6)} \mathcal{O}_i^{(6)} + \dots \quad (3.2.1)$$

This defines the SMEFT-Lagrangian, where the dots represent higher order terms in $1/\Lambda$. It is a series expansion in the energy scale Λ where the SM stops being valid. Beyond Λ , new particles, or forces, are believed to appear. The idea is to capture these new interactions as imprints at energies below Λ by effective, or higher dimensional, operators. The superscript k in the operators $\mathcal{O}_i^{(k)}$ indicates the operator's mass dimension and the $C_i^{(k)}$ are the *Wilson coefficients*. As far as the latter are concerned, there are two options. One, the Wilson coefficients can be fixed by the full

theory if it is known to us (this is called the *top-down approach*). Two, in case the full theory is unknown (*bottom-up approach*), like in the SMEFT, they can only be constrained from experimental data.

The only dimension-five operator one can write down violates lepton number conservation [10, 11], and the same goes for all dimension-seven operators. Therefore, the first new physics corrections are parameterised by dimension-six operators. As for dimension-eight operators, a complete and non-redundant set has recently been claimed to be found in ref. [12]. However, this still needs to be processed and implemented in fitting codes. So in practice, the SMEFT-Lagrangian is truncated after dimension six:

$$\mathcal{L}_{\text{SMEFT}} \equiv \mathcal{L}_{\text{SM}} + \frac{1}{\Lambda^2} \sum_{i=1}^{N_{d6}} C_i^{(6)} \mathcal{O}_i^{(6)}. \quad (3.2.2)$$

Why should we bother writing down an effective field theory in the first place? There are a couple of important reasons as to why this could be of interest to us. First of all, every theory can be thought of as an EFT, as long as we consider it as a low energy approximation of some underlying more complete UV theory. Secondly, EFTs oftentimes simplify calculations by dealing with only one scale at a time and including only the relevant degrees of freedom. Most importantly though, they can parameterise additions to new physics, as in the case of SMEFT. This allows for a model independent description of new physics that is systematically improvable by going to higher orders.

Requirements

Not just any higher dimensional operator can be written down in the SMEFT-Lagrangian. They need to fulfill a number of conditions. First of all, they should be composed of SM-fields only. Secondly, the operators should be invariant under the SM gauge group $SU(3) \times SU(2) \times U(1)$ and under Lorentz transformations. For example, the following is a valid SMEFT-operator at dimension-six:

$$\mathcal{O}_{qq}^{1(ijkl)} = (\bar{q}_i \gamma^\mu q_j)(\bar{q}_k \gamma_\mu q_l). \quad (3.2.3)$$

It has dimension six indeed, as the quark field q carries mass dimension 3/2. Furthermore, it is a Lorentz scalar, so Lorentz invariance is trivially met. Lastly, the quark fields transform in the fundamental representation of $SU(3)$ and (3.2.3) is thus invariant under the SM gauge group.

3.3 Observables in SMEFT

Having defined the SMEFT-Lagrangian in equation (3.2.2), we can ask ourselves the question how observables, such as cross sections and decay rates, get modified due to the higher dimensional operators. In general, observables are modified with respect to their SM prediction according to

$$\sigma = \sigma_{\text{SM}} + \sum_i^{N_{d6}} \kappa_i \frac{C_i^{(6)}}{\Lambda^2} + \sum_i^{N_{d6}} \tilde{\kappa}_{ij} \frac{C_i^{(6)} C_j^{(6)}}{\Lambda^4}, \quad (3.3.1)$$

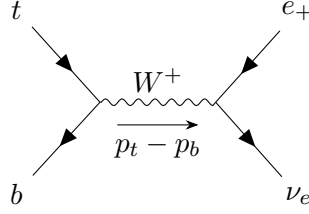


Figure 3.2: Top quark decay in the SM at tree level

where we have only kept terms up to quadratic order in the SMEFT corrections, i.e. up to Λ^{-4} . In principle, dimension-eight operators do also contribute at order Λ^{-4} , but, as we mentioned before, a complete set of non-redundant operators has not yet been implemented. The last term in equation (3.3.1) therefore originates in its entirety from SMEFT-corrections, as opposed to the middle term, which accounts for interference effects with the SM. The κ_i 's present kinematical factors that can be calculated exactly in the SMEFT. It is both interesting and illuminating to see how explicit expressions for the κ_i 's arise, and for that reason, we consider top-quark decay in the SMEFT as an example in the next section.

3.4 Example: Top-Quark Decay

The goal of this section is to provide an explicit calculation in full detail that shows how to obtain expressions for the κ_i 's appearing in equation (3.3.1). We consider the decay of the top-quark [13] and we will be working at order Λ^{-2} .

Top-quark decay occurs in the SM at tree level according to figure 3.2, where the decay products are formed by a bottom-quark, a positron and an electron-neutrino. If we take all fermions but the top-quark to be massless, the only two independent dimension-six operators that contribute at tree level and modify the Wtb -vertex turn out to be given by [13, 14]:

$$O_{\varphi q}^{(3)} = (\varphi^\dagger i \overleftrightarrow{D}_\mu^I \varphi) (\bar{q} \tau^I \gamma^\mu q) \quad (3.4.1)$$

$$Q_{tW} = (\bar{q} \sigma^{\mu\nu} t) \tau^I \tilde{\varphi} W_{\mu\nu}^I, \quad (3.4.2)$$

where the Hermitian derivative is defined as

$$\varphi^\dagger i \overleftrightarrow{D}_\mu^I \varphi \equiv i \varphi^\dagger \left(\tau^I D_\mu - \overleftarrow{D}_\mu \tau^I \right) \varphi \quad \text{with} \quad \varphi^\dagger \overleftarrow{D}_\mu \varphi \equiv (D_\mu \varphi)^\dagger \varphi. \quad (3.4.3)$$

Hence, $O_{\varphi q}^{(3)}$ can also be written as

$$\begin{aligned} O_{\varphi q}^{(3)} &= -i (D_\mu \varphi)^\dagger \tau^I \varphi (\bar{q} \gamma^\mu \tau^I q) + i (\varphi^\dagger \tau^I D_\mu \varphi) (\bar{q} \gamma^\mu \tau^I q) \\ &= -i (D_\mu \varphi)^\dagger \tau^I \varphi (\bar{q} \gamma^\mu \tau^I q) + \text{h.c.} \end{aligned} \quad (3.4.4)$$

Furthermore, in equations (3.4.1) and (3.4.2), φ denotes the $SU(2)$ Higgs-doublet and $\tilde{\varphi}_i = \epsilon_{ij} \varphi^{j*}$, with ϵ the completely anti-symmetric Levi-Civita tensor. The $SU(2)$ generators $\tau^I/2$ are the usual

Pauli-matrices, $D_\mu = \partial_\mu - ig'YB_\mu - ig\frac{\tau^I}{2}W_\mu^I - ig_s\frac{\lambda^A}{2}G_\mu^A$ is the SM covariant derivative, q denotes a left-handed quark doublet transforming in the fundamental representation of $SU(2)$ and $W_{\mu\nu}^I$ is the field-strength tensor, defined as

$$W_{\mu\nu}^I = \partial_\mu W_\nu^I - \partial_\nu W_\mu^I - g\epsilon^{IJK}W_\mu^J W_\nu^K. \quad (3.4.5)$$

Finally, the field t is a right-handed quark singlet that transforms trivially under $SU(2)$.

With the notation set, we can now go on and note that the SMEFT-Lagrangian from equation (3.2.2) takes the following simple form:

$$\mathcal{L}_{\text{SMEFT}} = \mathcal{L}_{\text{SM}} + \frac{C_{\varphi q}^{(3)}}{\Lambda^2} \mathcal{O}_{\varphi q}^{(3)} + \frac{C_{tW}}{\Lambda^2} \mathcal{O}_{tW}. \quad (3.4.6)$$

Here, the coefficients $C_{\varphi q}^{(3)}$ and C_{tW} are the Wilson-coefficients, which we ultimately want to constrain using experimental data. After spontaneous symmetry breaking, i.e. when the Higgs field φ attains a non-zero vacuum expectation value (VEV), $\mathcal{O}_{\varphi q}^{(3)}$ and \mathcal{O}_{tW} turn out to give rise to the following terms in the SMEFT-Lagrangian:

$$\mathcal{L}_{\text{SMEFT}} = \mathcal{L}_{\text{SM}} + \left(-2\frac{C_{tW}}{\Lambda^2} \bar{v}b\sigma^{\mu\nu}t_R\partial_\nu W_\mu^- + \text{h.c.} \right) + \left(\frac{C_{\varphi q}^{(3)}}{\Lambda^2} \frac{gv^2}{\sqrt{2}} \bar{b}\gamma^\mu t_L W_\mu^- + \text{h.c.} \right). \quad (3.4.7)$$

As an intermediate step towards our ultimate goal of computing the κ_i 's in equation (3.3.1), let us pause to show that equation (3.4.7) indeed follows from (3.4.6).

The SMEFT Lagrangian

We first consider the operator $\mathcal{O}_{\varphi q}^{(3)}$. Starting with its expanded form in equation (3.4.4), we write the Higgs field and the covariant derivative as

$$\varphi = \frac{1}{\sqrt{2}} \begin{pmatrix} 0 \\ v \end{pmatrix} \quad \text{and} \quad D_\mu = \partial_\mu - ig\frac{1}{2}\tau^I W_\mu^I. \quad (3.4.8)$$

With this, the following factor in $\mathcal{O}_{\varphi q}^{(3)}$ is seen to take the form

$$\begin{aligned} -i(D_\mu\varphi)^\dagger\tau^I\varphi &= -i\left(-ig\frac{1}{2}\tau^J W_\mu^J \frac{1}{\sqrt{2}} \begin{pmatrix} 0 \\ v \end{pmatrix}\right)^\dagger \tau^I \frac{1}{\sqrt{2}} \begin{pmatrix} 0 \\ v \end{pmatrix} \\ &= g\frac{v^2}{4} \left(\begin{pmatrix} W_\mu^3 & W_\mu^1 - iW_\mu^2 \\ W_\mu^1 + iW_\mu^2 & -W_\mu^3 \end{pmatrix} \begin{pmatrix} 0 \\ 1 \end{pmatrix} \right)^\dagger \tau^I \begin{pmatrix} 0 \\ 1 \end{pmatrix} \\ &= g\frac{v^2}{4} \begin{pmatrix} W_\mu^1 + iW_\mu^2 & -W_\mu^3 \end{pmatrix} \tau^I \begin{pmatrix} 0 \\ 1 \end{pmatrix}. \end{aligned}$$

If we insert this into (3.4.4), we get

$$\begin{aligned}
O_{\phi q}^{(3)} &= g \frac{v^2}{4} \begin{pmatrix} W_\mu^1 + iW_\mu^2 & -W_\mu^3 \end{pmatrix} \tau^I \begin{pmatrix} 0 \\ 1 \end{pmatrix} \bar{q} \gamma^\mu \tau^I q + \text{h.c.} \\
&= g \frac{v^2}{4} \begin{pmatrix} W_\mu^1 + iW_\mu^2 & -W_\mu^3 \end{pmatrix} \tau^I \begin{pmatrix} 0 \\ 1 \end{pmatrix} \begin{pmatrix} \bar{t}_L & \bar{b}_L \end{pmatrix} \gamma^\mu \tau^I \begin{pmatrix} t_L \\ b_L \end{pmatrix} + \text{h.c.}, \tag{3.4.9}
\end{aligned}$$

where the sum over the repeated index $SU(2)$ -index I is left implicit. Note that the contribution coming from the term $I = 3$ does not involve W_μ^- , and can thus be ignored. We are only interested in Wtb -interactions after all. However, $I = 1$ and $I = 2$ do contribute, and give respectively

$$\begin{aligned}
I = 1 : \quad & \frac{gv^2}{4} \begin{pmatrix} W_\mu^1 + iW_\mu^2 & -W_\mu^3 \end{pmatrix} \begin{pmatrix} 0 & 1 \\ 1 & 0 \end{pmatrix} \begin{pmatrix} 0 \\ 1 \end{pmatrix} \begin{pmatrix} \bar{t}_L & \bar{b}_L \end{pmatrix} \gamma^\mu \begin{pmatrix} 0 & 1 \\ 1 & 0 \end{pmatrix} \begin{pmatrix} t_L \\ b_L \end{pmatrix} + \text{h.c.} = \\
& \frac{gv^2\sqrt{2}}{4} W_\mu^- \begin{pmatrix} \bar{t}_L & \bar{b}_L \end{pmatrix} \gamma^\mu \begin{pmatrix} b_L \\ t_L \end{pmatrix} + \text{h.c.} = \\
& \frac{gv^2\sqrt{2}}{4} W_\mu^- (\bar{t}_L \gamma^\mu b_L + \bar{b}_L \gamma^\mu t_L) + \text{h.c.} \\
I = 2 : \quad & \frac{gv^2}{4} \begin{pmatrix} W_\mu^1 + iW_\mu^2 & -W_\mu^3 \end{pmatrix} \begin{pmatrix} 0 & -i \\ i & 0 \end{pmatrix} \begin{pmatrix} 0 \\ 1 \end{pmatrix} \begin{pmatrix} \bar{t}_L & \bar{b}_L \end{pmatrix} \gamma^\mu \begin{pmatrix} 0 & -i \\ i & 0 \end{pmatrix} \begin{pmatrix} t_L \\ b_L \end{pmatrix} + \text{h.c.} = \\
& - \frac{gv^2\sqrt{2}}{4} W_\mu^- (\bar{t}_L \gamma^\mu b_L - \bar{b}_L \gamma^\mu t_L) + \text{h.c.}
\end{aligned}$$

Adding the terms $I = 1$ and $I = 2$ then gives:

$$\begin{aligned}
O_{\phi q}^{(3)} &= \frac{gv^2}{\sqrt{2}} \bar{b}_L \gamma^\mu t_L W_\mu^- + \text{h.c.} + \dots \\
&= \frac{gv^2}{\sqrt{2}} \bar{b} \gamma^\mu P_L t W_\mu^- + \text{h.c.} + \dots, \tag{3.4.10}
\end{aligned}$$

where in going from the first to the last line, we have used that

$$\bar{b}_L \gamma^\mu t_L = (P_L b)^\dagger \gamma^0 \gamma^\mu P_L t = b^\dagger P_L \gamma^0 \gamma^\mu P_L t = \bar{b} P_L t.$$

So $O_{\phi q}^{(3)}$ contributes to $\mathcal{L}_{\text{SMEFT}}$ by

$$\frac{C_{\phi q}^{(3)}}{\Lambda^2} O_{\phi q}^{(3)} = \frac{C_{\phi q}^{(3)}}{\Lambda^2} \frac{gv^2}{\sqrt{2}} \bar{b} \gamma^\mu P_L t W_\mu^- + \text{h.c.} \tag{3.4.11}$$

We now move on to the other operator, O_{tW} . After the Higgs acquires a VEV, this takes the following form:

$$\begin{aligned}
Q_{tW} &= (\bar{q}\sigma^{\mu\nu}t)\tau^I\tilde{\varphi}W_{\mu\nu}^I \\
&= \begin{pmatrix} \bar{t}_L & \bar{b}_L \end{pmatrix} \sigma^{\mu\nu}(P_R t)\tau^I \frac{1}{\sqrt{2}} \begin{pmatrix} v \\ 0 \end{pmatrix} W_{\mu\nu}^I \\
&= \begin{pmatrix} \bar{t}_L & \bar{b}_L \end{pmatrix} \sigma^{\mu\nu}(P_R t)\tau^I \frac{1}{\sqrt{2}} \begin{pmatrix} v \\ 0 \end{pmatrix} (\partial_\mu W_\nu^I - \partial_\nu W_\mu^I - g\epsilon^{IJK}W_\mu^J W_\nu^K)
\end{aligned} \tag{3.4.12}$$

where we have plugged in the definition of the field strength tensor $W_{\mu\nu}^I$, equation (3.4.5). Let us separately consider the contributions $I = 1$ and $I = 2$. Again, the term $I = 3$ does not result in a Wtb -interaction, and can thus be ignored.

$$\begin{aligned}
I = 1 : \quad & \begin{pmatrix} \bar{t}_L & \bar{b}_L \end{pmatrix} \sigma^{\mu\nu}t_R \begin{pmatrix} 0 & 1 \\ 1 & 0 \end{pmatrix} \frac{1}{\sqrt{2}} \begin{pmatrix} v \\ 0 \end{pmatrix} (\partial_\mu W_\nu^1 - \partial_\nu W_\mu^1 - gW_\mu^2 W_\nu^3 + gW_\mu^3 W_\nu^2) = \\
& \frac{v}{\sqrt{2}} \bar{b}_L \sigma^{\mu\nu}t_R (\partial_\mu W_\nu^1 - \partial_\nu W_\mu^1 - gW_\mu^2 W_\nu^3 + gW_\mu^3 W_\nu^2)
\end{aligned}$$

$$\begin{aligned}
I = 2 : \quad & \begin{pmatrix} \bar{t}_L & \bar{b}_L \end{pmatrix} \sigma^{\mu\nu}t_R \begin{pmatrix} 0 & -i \\ i & 0 \end{pmatrix} \frac{1}{\sqrt{2}} \begin{pmatrix} v \\ 0 \end{pmatrix} (\partial_\mu W_\nu^2 - \partial_\nu W_\mu^2 - gW_\mu^3 W_\nu^1 + gW_\mu^1 W_\nu^3) = \\
& \frac{iv}{\sqrt{2}} \bar{b}_L \sigma^{\mu\nu}t_R (\partial_\mu W_\nu^2 - \partial_\nu W_\mu^2 - gW_\mu^3 W_\nu^1 + gW_\mu^1 W_\nu^3)
\end{aligned}$$

We now add the terms $I = 1$ and $I = 2$ to arrive at

$$\begin{aligned}
O_{tW} &= v\bar{b}_L\sigma^{\mu\nu}t_R(\partial_\mu W_\nu^- - \partial_\nu W_\mu^-) + \dots \\
&= -2v\bar{b}_L\sigma^{\mu\nu}t_R\partial_\nu W_\mu^- + \dots \\
&= -2v\bar{b}\sigma^{\mu\nu}t_R\partial_\nu W_\mu^- + \dots
\end{aligned} \tag{3.4.13}$$

Therefore, the operator O_{tW} contributes to the SMEFT-Lagrangian by the term

$$\frac{C_{tW}}{\Lambda^2} \mathcal{O}_{tW} = -2\frac{C_{tW}}{\Lambda^2} v\bar{b}\sigma^{\mu\nu}t_R\partial_\nu W_\mu^- + \text{h.c.} \tag{3.4.14}$$

Adding the results (3.4.11) and (3.4.14) gives us the Lagrangian from equation (3.4.7) indeed:

$$\mathcal{L}_{\text{SMEFT}} = \mathcal{L}_{\text{SM}} + \left(-2\frac{C_{tW}}{\Lambda^2} v\bar{b}\sigma^{\mu\nu}t_R\partial_\nu W_\mu^- + \text{h.c.} \right) + \left(\frac{C_{\varphi q}^{(3)}}{\Lambda^2} \frac{gv^2}{\sqrt{2}} \bar{b}\gamma^\mu t_L W_\mu^- + \text{h.c.} \right). \tag{3.4.15}$$

The squared amplitude - SM

Having obtained an expression for the SMEFT-Lagrangian after spontaneous symmetry breaking, we are ready to calculate the $t \rightarrow be^+\nu$ squared amplitude at tree level and see how it gets modified

with respect to the SM prediction. Let us first consider the \mathcal{M}_{SM} contribution alone, using the Feynman rules given in (3.4.16). We will see later how this prediction gets modified due to the dimension-six operators in (3.4.1) and (3.4.2).

The image shows three Feynman diagrams and their corresponding mathematical expressions. The first diagram shows a top quark (t) and a bottom quark (b) meeting at a vertex, with a W+ boson (wavy line) outgoing. The second diagram shows a W+ boson (wavy line) meeting at a vertex, with a positron (e+) and an electron neutrino (νe) outgoing. The third diagram shows a W+ boson (wavy line) meeting at a vertex, with a positron (e+) and an electron neutrino (νe) outgoing, and another W+ boson (wavy line) incoming from the left.

$$\begin{aligned}
 & \begin{array}{c} b \\ \nearrow \\ \bullet \\ \nwarrow \\ t \end{array} \begin{array}{c} W^+ \\ \text{wavy line} \end{array} = \frac{igV_{tb}}{2\sqrt{2}}\gamma^\mu(1-\gamma^5) \\
 & \begin{array}{c} e^+ \\ \nearrow \\ \bullet \\ \nwarrow \\ \nu_e \end{array} \begin{array}{c} W^+ \\ \text{wavy line} \end{array} = \frac{ig}{2\sqrt{2}}\gamma^\mu(1-\gamma^5) \\
 & \begin{array}{c} W^+ \\ \text{wavy line} \end{array} \begin{array}{c} W^+ \\ \text{wavy line} \end{array} = \frac{i}{s-m_W^2} \left(-g_{\mu\nu} + \frac{p_\mu p_\nu}{m_W^2} \right) \quad (3.4.16)
 \end{aligned}$$

Applying the Feynman rules in (3.4.16) readily gives

$$i\mathcal{M}_{SM} = \left(\frac{igV_{tb}}{\sqrt{2}} \bar{u}(p_b)\gamma_\mu P_L u(p_t) \right) \cdot \frac{i}{s-m_W^2} \left(-g_{\mu\nu} + \frac{p_\mu p_\nu}{m_W^2} \right) \cdot \left(\frac{ig}{\sqrt{2}} \bar{u}(p_\nu)\gamma_\nu P_L v(p_e) \right).$$

However, the term $p_\mu p_\nu$ does not contribute, as can be understood from the following:

$$\begin{aligned}
 \bar{v}_2 \gamma^\mu u_1 p_\mu &= \bar{v}_2 \gamma^\mu u_1 p_\mu \\
 &= \bar{v}_2 \not{p} u_1 \\
 &= \bar{v}_2 (\not{p}_1 + \not{p}_2) u_1 \\
 &= \bar{v}_2 (m - m) u_1 = 0, \quad (3.4.17)
 \end{aligned}$$

where we have used that $\not{p}u = mu$ and $\bar{v}\not{p} = -m\bar{v}$. Therefore,

$$i\mathcal{M}_{SM} = \frac{ig^2}{2} V_{tb} \frac{1}{(s-m_W^2)} [\bar{u}(p_b)\gamma_\mu P_L u(p_t)\bar{u}(p_\nu)\gamma^\mu P_L v(p_e)]. \quad (3.4.18)$$

From this we can straightforwardly find $|\mathcal{M}_{SM}|^2$ by writing

$$\begin{aligned}
 \mathcal{M}_{SM} &= \frac{g^2 V_{tb}}{2(s-m_W^2)} [\bar{u}(p_b)\gamma_\mu P_L u(p_t)\bar{u}(p_\nu)\gamma^\mu P_L v(p_e)] \\
 \mathcal{M}_{SM}^\dagger &= \frac{g^2 V_{tb}}{2(s-m_W^2)} [\bar{v}(p_e)P_R \gamma^\nu u(p_\nu)\bar{u}(p_t)P_R \gamma_\nu u(p_b)].
 \end{aligned}$$

Hence,

$$|\mathcal{M}_{SM}|^2 = \frac{g^4 V_{tb}^2}{4(s - m_W^2)^2} [\bar{u}(p_b)\gamma_\mu P_L u(p_t)] [\bar{u}(p_t)P_R\gamma_\nu u(p_b)] [\bar{u}(p_\nu)\gamma^\mu P_L v(p_e)] [\bar{v}(p_e)P_R\gamma^\nu u(p_\nu)] \quad (3.4.19)$$

In going from the first to the second line we used that for two general spinors ψ_1 and ψ_2 it holds that

$$\begin{aligned} (\bar{\psi}_1\gamma^\mu P_L\psi_2)^\dagger &= (\psi_1^\dagger\gamma^0\gamma^\mu P_L\psi_2)^\dagger \\ &= \psi_2^\dagger P_L(\gamma^\mu)^\dagger\gamma^0\psi_1 \\ &= \psi_2^\dagger P_L\gamma^0\gamma^\mu\psi_1 \\ &= \psi_2^\dagger\gamma^0 P_R\gamma^\mu\psi_1 \\ &= \bar{\psi}_2 P_R\gamma^\mu\psi_1 \end{aligned}$$

Since the initial state has no average polarization, we will have to sum over the quark spins and take its average. Up to a factor of 1/2 that accounts for the average value, we thus get:

$$\begin{aligned} \sum_{s,s'} [\bar{u}^{s'}(p_b)\gamma_\mu P_L u^s(p_t)] [\bar{u}^s(p_t)P_R\gamma_\nu u^{s'}(p_b)] &= \sum_{s'} \bar{u}^{s'}(p_b)\gamma_\mu P_L \left(\sum_s u^s(p_t)\bar{u}^s(p_t) \right) P_R\gamma_\nu u^{s'}(p_b) \\ &= \sum_{s'} \bar{u}_\beta^{s'}(p_b)(\gamma_\mu P_L)_{\beta\delta}(\not{p}_t + m_t\mathbb{1})_{\delta l}(P_R\gamma_\nu)_{l\alpha} u_\alpha^{s'}(p_b) \\ &= (\not{p}_b + m_b\mathbb{1})_{\alpha\beta}(\gamma_\mu P_L)_{\beta\delta}(\not{p}_t + m_t\mathbb{1})_{\delta l}(P_R\gamma_\nu)_{l\alpha} \\ &= \text{Tr} [\not{p}_b\gamma_\mu P_L(\not{p}_t + m_t)P_R\gamma_\nu] \end{aligned}$$

This can be simplified further by using that $P_L P_R = 0$ and $P_R = \frac{1}{2}(1 + \gamma^5)$:

$$\begin{aligned} \sum_{s,s'} [\bar{u}^{s'}(p_b)\gamma_\mu P_L u^s(p_t)] [\bar{u}^s(p_t)P_R\gamma_\nu u^{s'}(p_b)] &= \text{Tr} [\not{p}_b\gamma_\mu P_L \not{p}_t P_R\gamma_\nu] \\ &= \text{Tr} [\not{p}_b\gamma_\mu \not{p}_t P_R\gamma_\nu] \\ &= \frac{1}{2}\text{Tr} [\not{p}_b\gamma_\mu \not{p}_t \gamma_\nu] + \frac{1}{2}\text{Tr} [\not{p}_b\gamma_\mu \gamma^5 \not{p}_t \gamma_\nu] \quad (3.4.20) \end{aligned}$$

Analogously, we now perform the sum over the outgoing lepton spins:

$$\begin{aligned} \sum_{s,s'} [\bar{u}^{s'}(p_\nu)\gamma^\mu P_L v^s(p_e)] [\bar{v}^s(p_e)P_R\gamma^\nu u^{s'}(p_\nu)] &= \sum_{s'} \bar{u}^{s'}(p_\nu)\gamma^\mu P_L \left(\sum_s v^s(p_e)\bar{v}^s(p_e) \right) P_R\gamma^\nu u^{s'}(p_\nu) \\ &= \sum_{s'} \bar{u}_\beta^{s'}(p_\nu)(\gamma^\mu P_L)_{\beta\delta}(\not{p}_e - m_e\mathbb{1})_{\delta l}(P_R\gamma^\nu)_{l\alpha} u_\alpha^{s'}(p_\nu) \\ &= (\not{p}_\nu + m_\nu\mathbb{1})_{\alpha\beta}(\gamma^\mu P_L)_{\beta\delta}(\not{p}_e - m_e\mathbb{1})_{\delta l}(P_R\gamma^\nu)_{l\alpha} \\ &= \text{Tr} [\not{p}_\nu\gamma^\mu P_L \not{p}_e P_R\gamma^\nu] \\ &= \text{Tr} [\not{p}_\nu\gamma^\mu \not{p}_e P_R\gamma^\nu] \\ &= \frac{1}{2}\text{Tr} [\not{p}_\nu\gamma^\mu \not{p}_e \gamma^\nu] + \frac{1}{2}\text{Tr} [\not{p}_\nu\gamma^\mu \not{p}_e \gamma^5 \gamma^\nu]. \quad (3.4.21) \end{aligned}$$

Combining equations (3.4.20), (3.4.21) and (3.4.19) leads to the following expression for the scattering amplitude:

$$\begin{aligned} \frac{1}{2} \sum_{\text{spins}} |\mathcal{M}_{SM}|^2 &= \frac{g^4 V_{tb}^2}{32(s - m_W^2)^2} \left(\text{Tr} \left[\not{p}_b \gamma_\mu \not{p}_t \gamma_\nu \right] + \text{Tr} \left[\not{p}_b \gamma_\mu \gamma^5 \not{p}_t \gamma_\nu \right] \right) \\ &\quad \times \left(\text{Tr} \left[\not{p}_\nu \gamma^\mu \not{p}_e \gamma^\nu \right] + \text{Tr} \left[\not{p}_\nu \gamma^\mu \not{p}_e \gamma^5 \gamma^\nu \right] \right) \end{aligned} \quad (3.4.22)$$

Note that

$$\begin{aligned} \text{Tr} \left[\not{p}_b \gamma_\mu \not{p}_t \gamma_\nu \right] &= p_b^\rho p_t^\sigma \text{Tr} [\gamma_\rho \gamma_\mu \gamma_\sigma \gamma_\nu] \\ &= 4p_b^\rho p_t^\sigma (g_{\rho\mu} g_{\sigma\nu} + g_{\rho\nu} g_{\mu\sigma} - g_{\rho\sigma} g_{\mu\nu}) \end{aligned}$$

is symmetric in μ and ν , whereas

$$\text{Tr} \left[\not{p}_\nu \gamma^\mu \not{p}_e \gamma^5 \gamma^\nu \right] \propto p_\sigma p_\rho \epsilon^{\nu\sigma\mu\rho}$$

is anti-symmetric in μ and ν . Therefore, the cross-terms in equation (3.4.22) vanish and we are left with:

$$\begin{aligned} \frac{1}{2} \sum_{\text{spins}} |\mathcal{M}_{SM}|^2 &= \frac{g^4 V_{tb}^2}{32(s - m_W^2)^2} \left(\text{Tr} \left[\not{p}_b \gamma_\mu \not{p}_t \gamma_\nu \right] \cdot \text{Tr} \left[\not{p}_\nu \gamma^\mu \not{p}_e \gamma^\nu \right] \right. \\ &\quad \left. + \text{Tr} \left[\not{p}_b \gamma_\mu \gamma^5 \not{p}_t \gamma_\nu \right] \cdot \text{Tr} \left[\not{p}_\nu \gamma^\mu \not{p}_e \gamma^5 \gamma^\nu \right] \right) \end{aligned} \quad (3.4.23)$$

Let us now focus on the first term in equation (3.4.23). This gives

$$\text{Tr} \left[\not{p}_b \gamma_\mu \not{p}_t \gamma_\nu \right] \cdot \text{Tr} \left[\not{p}_\nu \gamma^\mu \not{p}_e \gamma^\nu \right] = 16 [p_b^\mu p_e^\nu + p_\nu^\nu p_e^\mu - p_{\nu e} g^{\mu\nu}] [(p_b)_\mu (p_t)_\nu + (p_b)_\nu (p_t)_\mu - g_{\mu\nu} p_{bt}],$$

where we have introduced the shorthand notation $p_{ij} = (p_i)_\mu (p_j)^\mu$. Expanding this then gives

$$\begin{aligned} \text{Tr} \left[\not{p}_b \gamma_\mu \not{p}_t \gamma_\nu \right] \cdot \text{Tr} \left[\not{p}_\nu \gamma^\mu \not{p}_e \gamma^\nu \right] &= 16(p_{\nu b} p_{et} + p_{\nu t} p_{eb} - p_{\nu e} p_{bt} + p_{\nu t} p_{eb} + \\ &\quad p_{\nu b} p_{et} - p_{\nu e} p_{bt} - p_{bt} p_{\nu e} - p_{bt} p_{\nu e} + 4p_{\nu e} p_{bt}) \end{aligned}$$

Simplifying further leads to

$$\text{Tr} \left[\not{p}_b \gamma_\mu \not{p}_t \gamma_\nu \right] \cdot \text{Tr} \left[\not{p}_\nu \gamma^\mu \not{p}_e \gamma^\nu \right] = 32(p_{b\nu} p_{et} + p_{be} p_{t\nu}) \quad (3.4.24)$$

In order to evaluate the second term in equation (3.4.23), we use the FeynCalc package in *Mathematica* [15–17], which gives the following identity

$$\text{Tr} \left[\not{p}_b \gamma_\mu \gamma^5 \not{p}_t \gamma_\nu \right] \cdot \text{Tr} \left[\not{p}_\nu \gamma^\mu \not{p}_e \gamma^5 \gamma^\nu \right] = -32(p_{b\nu} p_{et} - p_{be} p_{t\nu}). \quad (3.4.25)$$

Substituting identities (3.4.24) and (3.4.25) into equation (3.4.23) yields after a bit of algebra:

$$\frac{1}{2} \sum_{\text{spins}} |\mathcal{M}_{SM}|^2 = \frac{2g^4 V_{tb}^2}{(s - m_W^2)^2} p_{be} p_{t\nu}$$

We can now use the Mandelstam variables to eliminate the momenta:

$$\begin{aligned} s &= (p_t - p_b)^2 = (p_\nu + p_e)^2 = m_t^2 - 2p_{tb} = 2p_{\nu e} \\ t &= (p_t - p_\nu)^2 = (p_b + p_e)^2 = m_t^2 - 2p_{\nu t} = 2p_{be} \\ u &= (p_t - p_e)^2 = (p_b + p_\nu)^2 = m_t^2 - 2p_{et} = 2p_{\nu b} \end{aligned}$$

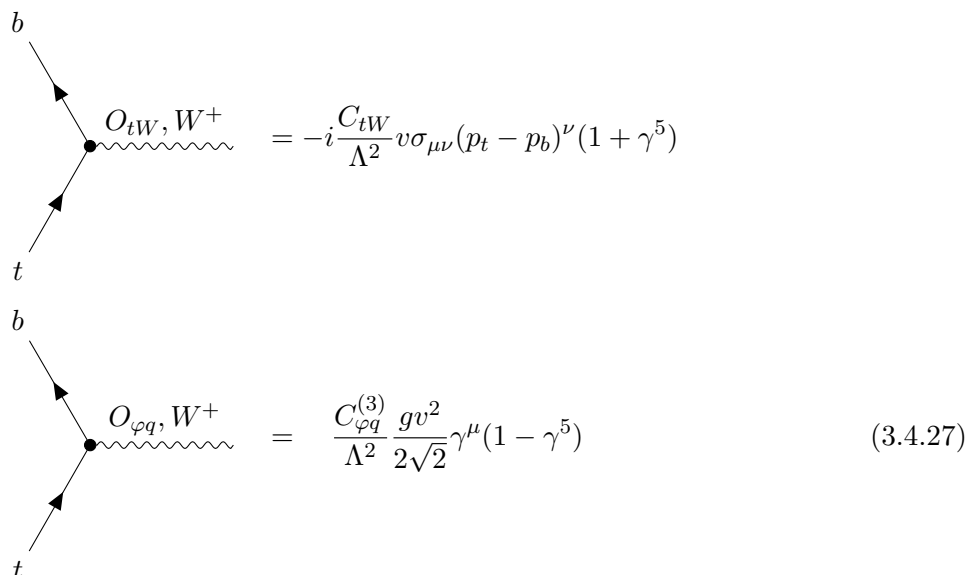
This results in

$$\frac{1}{2} \sum_{\text{spins}} |\mathcal{M}|^2 = \frac{g^4 V_{tb}^2}{2(s - m_W^2)^2} t(m_t^2 - t), \quad (3.4.26)$$

which concludes the derivation of the squared amplitude in the SM. We now move on to the SMEFT correction terms.

The squared amplitude - SMEFT

The effective Lagrangian from equation (3.4.7) comes with a new set of Feynman rules for the Wtb -vertex, see (3.4.27). The operator $O_{\varphi q}^{(3)}$ is seen to only rescale the SM Wtb -vertex by an overall factor, whereas the correction induced by the operator O_{tW} brings down a momentum dependence.



$$\begin{aligned} \begin{array}{c} b \\ \nearrow \\ \bullet \\ \nwarrow \\ t \end{array} \begin{array}{c} O_{tW}, W^+ \\ \text{---} \\ \end{array} &= -i \frac{C_{tW}}{\Lambda^2} v \sigma_{\mu\nu} (p_t - p_b)^\nu (1 + \gamma^5) \\ \begin{array}{c} b \\ \nearrow \\ \bullet \\ \nwarrow \\ t \end{array} \begin{array}{c} O_{\varphi q}, W^+ \\ \text{---} \\ \end{array} &= \frac{C_{\varphi q}^{(3)}}{\Lambda^2} \frac{gv^2}{2\sqrt{2}} \gamma^\mu (1 - \gamma^5) \end{aligned} \quad (3.4.27)$$

Due to these new vertices the squared amplitude changes with respect to its SM prediction:

$$|\mathcal{M}|^2 = |\mathcal{M}_{SM} + \mathcal{M}_{tW} + \mathcal{M}_{\varphi q}|^2 = |\mathcal{M}_{SM}|^2 + (\mathcal{M}_{SM}^\dagger (\mathcal{M}_{tW} + \mathcal{M}_{\varphi q}) + h.c.) + \mathcal{O}\left(\frac{1}{\Lambda^4}\right),$$

where \mathcal{M}_{tW} and $\mathcal{M}_{\varphi q}$ denote the $t \rightarrow be^+\nu_e$ amplitude induced by O_{tW} and $O_{\varphi q}^{(3)}$ respectively. Let us first compute $\mathcal{M}_{\varphi q}$:

$$\begin{aligned} i\mathcal{M}_{\varphi q} &= \left(\frac{C_{\varphi q}^{(3)}}{\Lambda^2} \frac{gv^2}{\sqrt{2}} \bar{u}(p_b) \gamma_\mu P_L u(p_t) \right) \cdot \left(\frac{-ig^{\mu\nu}}{s - m_W^2} \right) \cdot \left(\frac{ig}{\sqrt{2}} \bar{u}(p_\nu) \gamma_\nu P_L v(p_e) \right) \\ &= \frac{C_{\varphi q}^{(3)}}{\Lambda^2} \frac{v^2}{V_{tb}} \mathcal{M}_{SM}. \end{aligned} \quad (3.4.28)$$

Therefore, the contribution of $\mathcal{M}_{\varphi q}$ to the total squared amplitude \mathcal{M}^2 is given by:

$$\begin{aligned} \frac{1}{2} \sum_{\text{spins}} \left[(\mathcal{M}_{SM})^\dagger (\mathcal{M}_{\varphi q}) + (\mathcal{M}_{\varphi q}^\dagger) (\mathcal{M}_{SM}) \right] &= \frac{2C_{\varphi q}^{(3)}}{\Lambda^2} \frac{v^2}{V_{tb}} \frac{1}{2} \sum_{\text{spins}} |\mathcal{M}_{SM}|^2 \\ &= \frac{C_{\varphi q}^{(3)} V_{tb} v^2}{\Lambda^2} \frac{g^4 t (m_t^2 - t)}{(s - m_W^2)^2}, \end{aligned} \quad (3.4.29)$$

where we have used that $C_{\varphi q}^{(3)}$ is real. Next, we want to find \mathcal{M}_{tW} . Using the Feynman rule from figure ??, we find:

$$\begin{aligned} i\mathcal{M}_{tW} &= \left(-2i \frac{C_{tW}}{\Lambda^2} v \bar{u}(p_b) \sigma_{\mu\nu} (p_t - p_b)^\nu P_R u(p_t) \right) \left(\frac{-ig^{\mu\rho}}{s - m_W^2} \right) \left(\frac{ig}{\sqrt{2}} \bar{u}(p_\nu) \gamma_\rho P_L v(p_e) \right) \\ &= \frac{-\sqrt{2}i C_{tW} v g}{\Lambda^2 (s - m_W^2)} (p_t - p_b)^\nu [\bar{u}(p_b) \sigma_{\mu\nu} P_R u(p_t) \bar{u}(p_\nu) \gamma^\mu P_L v(p_e)]. \end{aligned}$$

Defining for convenience

$$A = \frac{-\sqrt{2}i C_{tW} v g}{\Lambda^2 (s - m_W^2)},$$

lets us write the above as

$$i\mathcal{M}_{tW} = A \cdot (p_t - p_b)^\nu [\bar{u}(p_b) \sigma_{\mu\nu} P_R u(p_t) \bar{u}(p_\nu) \gamma^\mu P_L v(p_e)]. \quad (3.4.30)$$

Recalling the SM amplitude from equation (3.4.19) and defining

$$B = \frac{ig^2 V_{tb}}{2(s - m_W^2)},$$

leads to

$$\begin{aligned} i\mathcal{M}_{SM} &= \frac{ig^2 V_{tb}}{2(s - m_W^2)} [\bar{u}(p_b) \gamma_\mu P_L u(p_t) \bar{u}(p_\nu) \gamma^\mu P_L v(p_e)] \\ &= B [\bar{u}(p_b) \gamma_\mu P_L u(p_t) \bar{u}(p_\nu) \gamma^\mu P_L v(p_e)]. \end{aligned} \quad (3.4.31)$$

The interference term between the SM and O_{tW} is thus given by:

$$\begin{aligned} (\mathcal{M}_{SM})^\dagger (\mathcal{M}_{tW}) + h.c. &= AB [\bar{v}(p_e) P_R \gamma^\mu u(p_\nu) \bar{u}(p_t) P_R \gamma_\mu u(p_b)] \\ &\quad \times (p_t - p_b)^\nu [\bar{u}(p_b) \sigma_{\rho\nu} P_R u(p_t) \bar{u}(p_\nu) \gamma^\rho P_L v(p_e)] + h.c. \end{aligned} \quad (3.4.32)$$

Or, after reordering terms:

$$(\mathcal{M}_{SM})^\dagger(\mathcal{M}_{tW}) = AB(p_t - p_b)^\nu [\bar{u}(p_b)\sigma_{\rho\nu}P_R u(p_t)] [\bar{u}(p_t)P_R\gamma_\mu u(p_b)] \\ \times [\bar{u}(p_\nu)\gamma^\rho P_L v(p_e)] [\bar{v}(p_e)P_R\gamma^\mu u(p_\nu)]. \quad (3.4.33)$$

Again, since the incoming state is unpolarized, we perform the sum over spins. For the quarks we get:

$$\sum_{ss'} [\bar{u}^{s'}(p_b)\sigma_{\rho\nu}P_R u^s(p_t)] [\bar{u}^s(p_t)P_R\gamma_\mu u^{s'}(p_b)] = \text{Tr} [\not{p}_b\sigma_{\rho\nu}P_R(\not{p}_t + m_t)P_R\gamma_\mu] \\ = m_t \text{Tr} [\not{p}_b\sigma_{\rho\nu}P_R\gamma_\mu].$$

Likewise for the lepton spins we get

$$\sum_{ss'} [\bar{u}(p_\nu)\gamma^\rho P_L v(p_e)] [\bar{v}(p_e)P_R\gamma^\mu u(p_\nu)] = \text{Tr} [\not{p}_\nu\gamma^\rho\not{p}_e P_R\gamma^\mu].$$

Hence,

$$\frac{1}{2} \sum_{\text{spins}} (\mathcal{M}_{SM})^\dagger(\mathcal{M}_{tW}) = m_t \frac{AB}{2} \text{Tr} [\not{p}_b\sigma_{\rho\nu}P_R\gamma_\mu] \cdot \text{Tr} [\not{p}_\nu\gamma^\rho\not{p}_e P_R\gamma^\mu] (p_t - p_b)^\nu.$$

We evaluate the Dirac traces using the package FeynCalc in *Mathematica* [15–17]. The result reads

$$\frac{1}{2} \sum_{\text{spins}} (\mathcal{M}_{SM})^\dagger(\mathcal{M}_{tW}) = m_t AB (3p_{bv}p_{et} - 2p_{be}p_{bv} + p_{bt}p_{ev} - p_{be}p_{tv}) \\ - iABm_t(p_b)_\mu(p_e)_\nu(p_t)_\rho(p_\nu)_\sigma \epsilon^{\mu\nu\rho\sigma}. \quad (3.4.34)$$

After adding the hermitian conjugate the imaginary part cancels and we are left with:

$$\frac{1}{2} \sum_{\text{spins}} [(\mathcal{M}_{SM})^\dagger(\mathcal{M}_{tW}) + \text{h.c.}] = 2m_t \text{Re}(AB)(3p_{bv}p_{et} - 2p_{be}p_{bv} + p_{bt}p_{ev} - p_{be}p_{tv})$$

Expressed in terms of the Mandelstam variables this equals

$$= \frac{1}{2} \text{Re}(AB)m_t [3u(m_t^2 - u) - 2tu + s(m_t^2 - s) - t(m_t^2 - t)]$$

and after using that $t = m_t^2 - s - u$ and canceling terms, we arrive at

$$= \frac{1}{2} \text{Re}(AB)m_t us. \quad (3.4.35)$$

Reinserting the definitions of A and B , gives

$$\frac{1}{2} \sum_{\text{spins}} [(\mathcal{M}_{SM})^\dagger(\mathcal{M}_{tW}) + \text{h.c.}] = \frac{\text{Re}(C_{tW})V_{tb}m_t m_W}{\sqrt{2}\Lambda^2} \frac{g^2 su}{(s - m_W^2)^2}. \quad (3.4.36)$$

Collecting all contributions to $|\mathcal{M}|^2$, we finally find:

$$\frac{1}{2} \sum_{\text{spins}} |\mathcal{M}|^2 = \frac{V_{tb}^2 g^4 t (m_t^2 - t)}{2(s - m_W^2)^2} + \frac{C_{\varphi q}^{(3)} V_{tb} v^2 g^4 t (m_t^2 - t)}{\Lambda^2 (s - m_W^2)^2} + \frac{\text{Re}(C_{tW}) V_{tb} m_t m_W}{\sqrt{2} \Lambda^2} \frac{g^2 s u}{(s - m_W^2)^2}. \quad (3.4.37)$$

From here we can readily read off the κ'_i s:

$$\kappa_1 \equiv V_{tb} v^2 \frac{g^4 t (m_t^2 - t)}{(s - m_W^2)^2} \quad (3.4.38)$$

$$\kappa_2 \equiv V_{tb} m_t m_W \frac{g^2 s u}{\sqrt{2} (s - m_W^2)^2}. \quad (3.4.39)$$

3.5 Warsaw-basis

Obviously, the operators $O_{\varphi q}^{(3)}$ and O_{tW} are not the only operators we can write down at dimension six. Imposing baryon-number conservation, there are a total of 59 independent dimension-six operators [14]. We list all of them, including the four B -violating operators, in Tables A.2 and A.1 of appendix A, taken from [14]. Finding a complete set of independent dimension-six operators has been an active field of study. The first attempt was made by W. Buchmüller and D. Wyler [18]. However, B. Grzadkowski et al. showed that some of these operators are in fact redundant, since they can be related by Fierz identities, the SM Equations of Motion (EOM) and integration by parts [14]. Tables A.2 and A.1 are classified according to their field content. The symbols X, φ, D, ψ denote field strength tensors, the Higgs fields, the covariant derivative and fermionic fields respectively. Fermions that transform as a left-handed doublet under $SU(2)$ are denoted by L , whereas the right-handed singlets under $SU(2)$ are denoted by R . Fermion generations are labelled by p, r, s, t , and isospin and colour indices are denoted by $j = 1, 2$ and $\alpha = 1, 2, 3$ respectively. For further details we refer to ref. [14]. In our analysis of the top-quark sector we shall only be needing a subset of the operators in Tables A.2 and A.1. These are all operators that involve at least one top-quark. For an exhaustive list here, we refer to appendix A in [3].

Chapter 4

SMEFT Fitting Framework

In this chapter, we present a short overview of the SMEFT fitting framework that is used to obtain bounds on the SMEFT degrees of freedom. The idea is to fit the modified cross sections in the SMEFT to high precision data from the LHC. We can distinguish between two methods as far as obtaining the best-fit parameters in the SMEFT analysis is concerned. We can either use Monte Carlo (MC) fit, which functions by performing gradient-based optimization on a cost function, or Nested Sampling (NS) [19]. The latter provides us with a method that relies on pure sampling techniques only. Consequently, it is more efficient than MC fit in case the parameter space is not too big, i.e. the number of parameters is less than 50.

4.1 Nested Sampling

In this section, we present the NS-algorithm and explain how it is used in our SMEFT-analysis. The starting point is Bayes' theorem, which states that

$$P(\boldsymbol{\theta}|\mathbf{D}) = \frac{\Pr(\mathbf{D}|\boldsymbol{\theta})\Pr(\boldsymbol{\theta})}{\Pr(\mathbf{D})}, \quad (4.1.1)$$

where $\Pr(\boldsymbol{\theta}|\mathbf{D})$ is the posterior probability density and $\Pr(\mathbf{D}|\boldsymbol{\theta}) \equiv \mathcal{L}(\boldsymbol{\theta})$ denotes the likelihood of the data given the hypothesis, which is parameterised by $\boldsymbol{\theta}$. The prior probability density $\Pr(\boldsymbol{\theta}) \equiv \pi(\boldsymbol{\theta})$ encodes our initial belief in the hypothesis, and $\Pr(\mathbf{D})$ is the overall likelihood of the data, and serves to normalize the posterior. This is also called the Bayesian Evidence \mathcal{Z} , and can be found by integrating the likelihood over the whole prior volume $\Omega_{\boldsymbol{\theta}}$:

$$\mathcal{Z} = \int_{\Omega_{\boldsymbol{\theta}}} \mathcal{L}(\boldsymbol{\theta})\pi(\boldsymbol{\theta})d\boldsymbol{\theta}. \quad (4.1.2)$$

Determining \mathcal{Z} thus faces us with a high-dimensional integral over the entire parameter space, which makes it a computationally high-demanding problem. MC methods do exist however that find a way around this problem. One of these methods is Nested Sampling. Not only does it allow us to

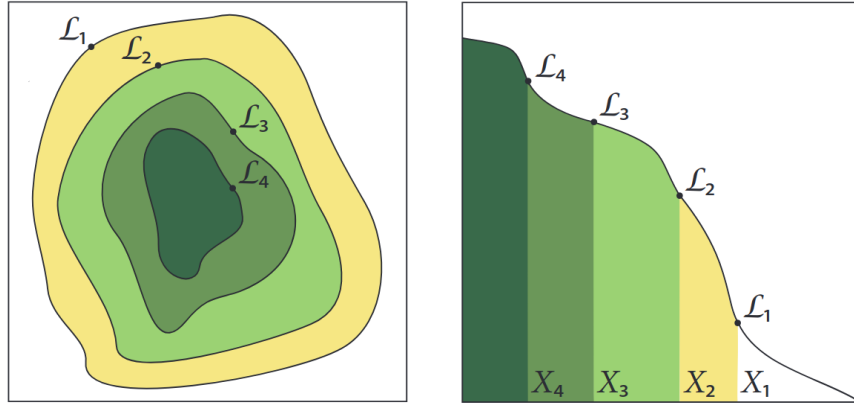


Figure 4.1: *Conceptual picture behind how Nested Sampling works. Left: contours in prior space of equal likelihood. Right: $\mathcal{L}(X)$ as a function of X , the integrated area within a particular contour. Taken from [19]*

determine the Bayesian evidence, it also gives a sample of the posterior probability as a convenient byproduct. Considering that we want to find the SMEFT-coefficients in a region close to maximum likelihood, we apply NS with this particular goal in mind.

The key idea underlying NS is to map a high-dimensional problem onto an easy one-dimensional one. It sorts nested likelihood contours by their enclosed prior mass, which subsequently allows MC integration methods to determine \mathcal{Z} . Let us go through these steps in more detail. First, we introduce the survival function $X(\lambda)$, corresponding to the integrated region in prior space such that its associated likelihood is greater than λ :

$$X(\lambda) = \int_{\{\theta: \mathcal{L}(\theta) > \lambda\}} \pi(\theta) d\theta. \quad (4.1.3)$$

Note that $X(\infty) = 0$ and $X(0) = 1$. In general, a higher λ results in a smaller prior volume. Given the survival function, we can recover \mathcal{Z} by recalling that an expectation value of a non-negative random variable can be found by integrating its associated survival function. This specifically applies here, since the Bayesian evidence \mathcal{Z} can be thought of as the likelihood averaged over the prior space. Hence,

$$\mathcal{Z} = \int_0^\infty X(\lambda) d\lambda \quad (4.1.4)$$

Assuming the likelihood function $\mathcal{L}(\theta)$ is continuous, we can define $\mathcal{L}(X)$ as the inverse of $X(\lambda)$. With this, equation (4.1.4) can be equivalently written as

$$\mathcal{Z} = \int_0^1 \mathcal{L}(X) dX. \quad (4.1.5)$$

Before continuing, let us pause to see what is going on visually. Figure 4.1 (left) shows a cartoon of the sampling space with several contours of the likelihood. Consider the contour $\mathcal{L} = \mathcal{L}_1$, which

encloses the prior volume X_1 . As we move to regions of higher likelihood, i.e. from \mathcal{L}_1 to \mathcal{L}_2 , the enclosed prior space decreases from X_1 to X_2 . So nested shells of prior volume get sorted by their likelihood, see figure 4.1 (right).

In principle, if the likelihood is known exactly, we can approximate \mathcal{Z} from equation 4.1.5 by evaluating $\mathcal{L}(X_i)$ for the sequence

$$X_N < \dots < X_2 < X_1 < X_0 = 1, \quad (4.1.6)$$

and writing

$$\mathcal{Z} \approx \tilde{\mathcal{Z}} = \sum_i^N \mathcal{L}(X_i) w_i, \quad (4.1.7)$$

where the weights w_i are given by an appropriate quadrature method and thus depend on X_i . In practice, however, we cannot find X_i exactly and the above method will not be applicable. Instead, we employ the following iterative procedure. We start by drawing N_{live} points from the prior distribution $\pi(\boldsymbol{\theta})$, known as *live points* and evaluate their corresponding likelihoods. In the next iteration, say iteration i , we drop the sample with the smallest likelihood, denoted \mathcal{L}_i , and draw a new one from the prior distribution under the constraint that its corresponding likelihood is higher than \mathcal{L}_i . This procedure is repeated until the entire prior space has been covered, and each time the live points get replaced by samples of higher likelihood. So the algorithm ends by giving a set $\{\boldsymbol{\theta}^{(k)}\}$, where $k = 1, \dots, N_{live}$, that corresponds to the region of maximum-likelihood. In this respect, Nested Sampling is not different from the MC fit method. That is, both end up with samples that either maximize the likelihood, or minimize a cost-function. However, Nested Sampling achieves this by pure sampling techniques, without doing any fits, as opposed to MC fit. This makes them two orthogonal methods that can be compared in order to yield useful cross-checks of the Wilson-coefficients at 95% confidence level.

4.2 Operator Definitions and Experiments

In this last section, we introduce the notation that is used throughout this work to denote the SMEFT operators. We then classify the different experiments that have been used to constrain the SMEFT degrees of freedom.

Operators

We can distinguish between three different classes of operators: four heavy-quark operators ($QQQQ$), two-heavy-two-light operators ($QQqq$) and operators that couple two heavy-quarks to either the Higgs field or the Gauge fields ($QQ + V, G, \phi$). The complete list of the SMEFT degrees of freedom that enter our fit can be found in Table 4.1. This notation will later also be used in

chapter 5.

Experiments

A total number of 33 experiments have been used to constrain the SMEFT degrees of freedom from Table 4.1. They can be classified by the different processes they describe. Tables 3.1 – 3.3 in ref. [3] provide an exhaustive overview, and we invite the reader to go there for further details. In short, we include the following processes: inclusive $t\bar{t}$ -production, $t\bar{t}$ -production in association with two heavy quarks/the Higgs boson or a weak vector boson, single t -production and single t -production in association with vector bosons.

Class	Notation	Degree of Freedom	Operator Definition
QQQQ	OQQ1	c_{QQ}^1	$2C_{qq}^{1(3333)} - \frac{2}{3}C_{qq}^{3(3333)}$
	OQQ8	c_{QQ}^8	$8C_{qq}^{3(3333)}$
	OQt1	c_{Qt}^1	$C_{qu}^{1(3333)}$
	OQt8	c_{Qt}^8	$C_{qu}^{8(3333)}$
	OQb1	c_{Qb}^1	$C_{qd}^{1(3333)}$
	OQb8	c_{Qb}^8	$C_{qd}^{8(3333)}$
	Ott1	c_{tt}^1	$C_{uu}^{(3333)}$
	Otb1	c_{tb}^1	$C_{ud}^{1(3333)}$
	Otb8	c_{tb}^8	$C_{ud}^{8(3333)}$
	OQtQb1	c_{QtQb}^1	$C_{quqd}^{1(3333)}$
	OQtQb8	c_{QtQb}^8	$C_{quqd}^{8(3333)}$
	QQqq	O81qq	$c_{Qq}^{1,8}$
O11qq		$c_{Qq}^{1,1}$	$C_{qq}^{1(ii33)} + \frac{1}{6}C_{qq}^{1(i33i)} + \frac{1}{2}C_{qq}^{3(i33i)}$
O83qq		$c_{Qq}^{3,8}$	$C_{qq}^{1(i33i)} - C_{qq}^{3(i33i)}$
O13qq		$c_{Qq}^{3,1}$	$C_{qq}^{3(ii33)} + \frac{1}{6}(C_{qq}^{1(i33i)} - C_{qq}^{3(i33i)})$
O8qt		c_{tq}^8	$C_{qu}^{8(ii33)}$
O1qt		c_{tq}^1	$C_{qu}^{1(ii33)}$
O8ut		c_{tu}^8	$2C_{uu}^{(i33i)}$
O1ut		c_{tu}^1	$C_{uu}^{(ii33)} + \frac{1}{3}C_{uu}^{(i33i)}$
O8qu		c_{Qu}^8	$C_{qu}^{8(33ii)}$
O1qu		c_{Qu}^1	$C_{qu}^{1(33ii)}$
O8dt		c_{td}^8	$C_{ud}^{8(33ii)}$
O1dt		c_{td}^1	$C_{ud}^{1(33ii)}$
O8qd		c_{Qd}^8	$C_{qd}^{8(33ii)}$
O1qd		c_{Qd}^1	$C_{qd}^{1(33ii)}$
QQ + V, G, φ	OtG	c_{tG}	$\text{Re}\{C_{uG}^{(33)}\}$
	OtW	c_{tW}	$\text{Re}\{C_{uW}^{(33)}\}$
	ObW	c_{bW}	$\text{Re}\{C_{dW}^{(33)}\}$
	OtZ	c_{tZ}	$\text{Re}\{-s_W C_{uB}^{(33)} + c_W C_{uW}^{(33)}\}$
	Off	$c_{\varphi tb}$	$\text{Re}\{C_{\varphi ud}^{(33)}\}$
	Ofq3	$c_{\varphi Q}^3$	$C_{\varphi q}^{3(33)}$
	OpQM	$c_{\varphi Q}^-$	$C_{\varphi q}^{1(33)} - C_{\varphi q}^{3(33)}$
	Opt	$c_{\varphi t}$	$C_{\varphi u}^{(33)}$
	Otp	$c_{t\varphi}$	$\text{Re}\{C_{u\varphi}^{(33)}\}$

Table 4.1: The notation that will be used to present results in this work. The operators are divided into three classes: four heavy-quark operators (QQQQ), two-heavy-two-light operators (QQqq) and operators that couple two heavy-quarks to either the Higgs field or the Gauge fields (QQ + V, G, ϕ). The operator definition is given in the last column and should be read alongside Tables A.1 and A.2 in appendix A. Table taken from [3].

Chapter 5

Dimensional Reduction: Sensitivity

So far, in order to retain a model independent description of new physics beyond the standard model, we have adopted the framework of effective field theory. Following a bottom-up approach, we have parameterised deviations from the standard model by the addition of dimension-six operators expressed in terms of SM fields. Since the full UV-theory is not known a priori, the Wilson coefficients can only be determined from experimental data. However, already within the top-quark sector alone, we are faced with 34 dimension-six operators. Therefore, a fit to experimental data is a high dimensional problem. Considering our future wish to not only include processes that involve the top-quark sector, but also include processes within the Higgs-sector for example, the high dimension of the parameter space will soon become a significant problem. This motivates the search for methods that reduce the dimension of this parameter space. With this in mind, we explore a new statistical measure, called the sensitivity [20], that measures the influence of empirical information on the SMEFT-parameters. More specifically, the sensitivity puts a quantitative measure on the degree to which a SMEFT-parameter can be constrained by a given data set. Even though many operators do in principle enter a particular process, not all of these will be equally ‘sensitive’ to the data. That is, some SMEFT degrees are more sensitive to processes of a particular kind than others, where ‘sensitive’ will be given a precise quantitative meaning in the upcoming sections. Let us start by outlining some necessary preliminaries.

5.1 Preliminaries

Using Nested Sampling, as described in section 4.1, we can obtain a collection $\{c_l^{(k)}\}$ that consists of N_{rep} samples, labeled by k , of the SMEFT-parameter c_l . This allows for the introduction of various statistics. Let us define these using a generic collection $\{X^{(k)}\}$ that consists of N_{rep} samples. Firstly,

the expectation value $\langle X \rangle$ is defined by

$$\langle X \rangle \equiv \frac{1}{N_{rep}} \sum_{k=1}^{N_{rep}} X^{(k)}. \quad (5.1.1)$$

Secondly, we define the resulting Monte-Carlo uncertainty on X as

$$\Delta_{MC} X \equiv \left(\frac{1}{N_{rep} - 1} \sum_{k=1}^{N_{rep}} \left(X^{(k)} - \langle X \rangle \right)^2 \right)^{1/2}. \quad (5.1.2)$$

Lastly, the correlation between X and another collection Y of N_{rep} samples can be constructed as

$$\text{Corr}[X, Y] \equiv \frac{\langle XY \rangle - \langle X \rangle \langle Y \rangle}{\Delta_{MC} X \Delta_{MC} Y}. \quad (5.1.3)$$

Given the SMEFT-parameters $\{c_i^{(k)}\}$, we can compute theoretical predictions beyond the standard model. Denoting the i^{th} theoretical prediction of data point D_i by T_i , we define the residual r_i , or fitting deviation, as

$$r_i(\{c_i^{(k)}\}) \equiv \frac{T_i(\{c_i^{(k)}\}) - D_i}{\sigma_i}, \quad (5.1.4)$$

where σ_i is the total uncorrelated uncertainty, obtained by adding the systematic and statistical uncertainties in quadrature.

5.2 The Sensitivity

In this section, we develop the statistical measure, called the sensitivity $S_E(c_l)$, that quantifies to which degree a SMEFT degree of freedom c_l is sensitive for experiment E . Rather than giving its full definition now, we will first introduce its various parts and see what each of these tell us separately.

Continuing from section 5.1, let us apply equation (5.1.3) and consider the correlation between a SMEFT degree of freedom c_l and the residual r_i for data point i :

$$\text{Corr}[c_l, r_i] = \frac{\langle c_l \cdot r_i \rangle - \langle c_l \rangle \langle r_i \rangle}{\Delta_{c_l} \cdot \Delta_{r_i}}. \quad l = 1, \dots, N_{ops} \quad (5.2.1)$$

This measures whether there may be a predictive relationship between the SMEFT coefficient c_l and the goodness of fit of the i^{th} point. It can also be thought as measuring the response of $r_i(\{c_l^{(k)}\})$ to the variations in the SMEFT coefficients. Whenever the correlation is close to zero, the coefficient c_l has little effect on the goodness of fit. In contrast, if the correlation is close to one, or minus one, the coefficient has a large impact on the goodness of fit. This already gets across the intuitive notion of what we mean by sensitivity. However, as it stands, equation (5.2.1) is insensitive to experimental uncertainties. Even when the correlation in (5.2.1) comes out high, the experimental

data point might not result in a significant contribution to the χ^2 if the errors are large. However, if new measurements were to be reported with fairly tight uncertainties, we would typically want the sensitivity of theoretical predictions for this measurement to increase. To remedy this issue, we modify equation (5.2.1) by multiplying with a factor that takes the experimental uncertainties into account, which will be our working definition of sensitivity:

$$S_i(c_l) \equiv \Delta r_i \cdot \text{Corr}[c_l, r_i]. \quad (5.2.2)$$

Here, Δr_i is the MC-uncertainty on the residual of the i^{th} data point:

$$\Delta r_i = \frac{\Delta T_i(\{c_l^{(k)}\})}{\sigma_i}. \quad (5.2.3)$$

So if the experimental uncertainties σ_i are small compared to the theory error $\Delta T_i(\{c_l^{(k)}\})$, these data points will have a high associated sensitivity according to definition (5.2.2).

5.3 Results

In this section, we present our results for the correlation and sensitivity, defined in (5.2.1) and (5.2.2) respectively. As we mentioned before in section 4.2, we use the experiments listed in Tables 3.1-3.3 of ref. [3]. We consider two separate cases:

1. Single data set results: NS is only run for one data set at a time. The coefficients thus obtained are data set dependent.
2. Global data set results: NS is run for all data sets simultaneously. Extra care was taken to make sure the final samples had smooth distributions, see figures 5.6 up to 5.8. These shows all the 34 SMEFT degrees of freedom that enter the global analysis and together with their associated distributions as obtained by NS. It is important that the distributions have smooth tails in order to make sure enough statistics enter the analysis.

Let us first present the single data set results. Figure 5.1 shows the absolute value of the correlation in (5.2.1) averaged over the data points. Any area in white indicates that those operators do not enter that particular data set. For instance, the `0tp`-operator can only be constrained by $t\bar{t}H$ -processes, and hence only shows up in the experiments `ATLSTTBARHTOT13TEV` and `CMSTTBARHMU13TEV`. Figure 5.2 shows the absolute value of the sensitivity from equation (5.2.2), averaged over the data points. In both cases we used theory predictions at order Λ^{-2} .

We now move on to presenting the global results. Here, we used NS results whose mutual correlation is shown in figure 5.3. The analogue of figures 5.1 and 5.2 in the global case are shown in figures 5.4 and 5.5 respectively.

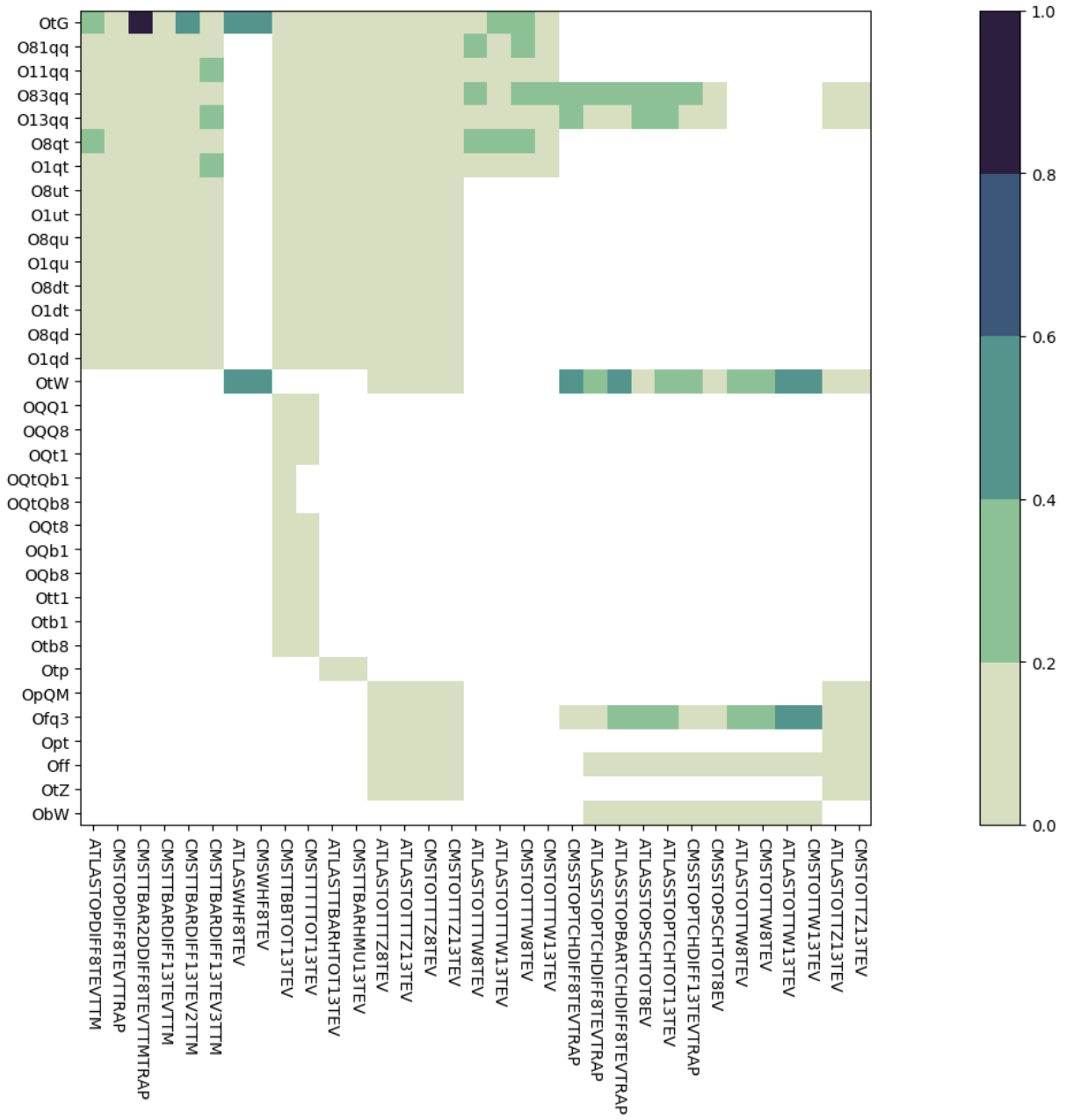


Figure 5.1: *The average absolute correlation $\langle |Corr[c_l, r_i]| \rangle$ between the SMEFT parameter c_l and the residual r_i for the i^{th} data point in experiment E in case of single data set NS results at order $\mathcal{O}(\Lambda^{-2})$. Any region in white indicates that that particular SMEFT parameter does not enter the theory prediction of data set E .*

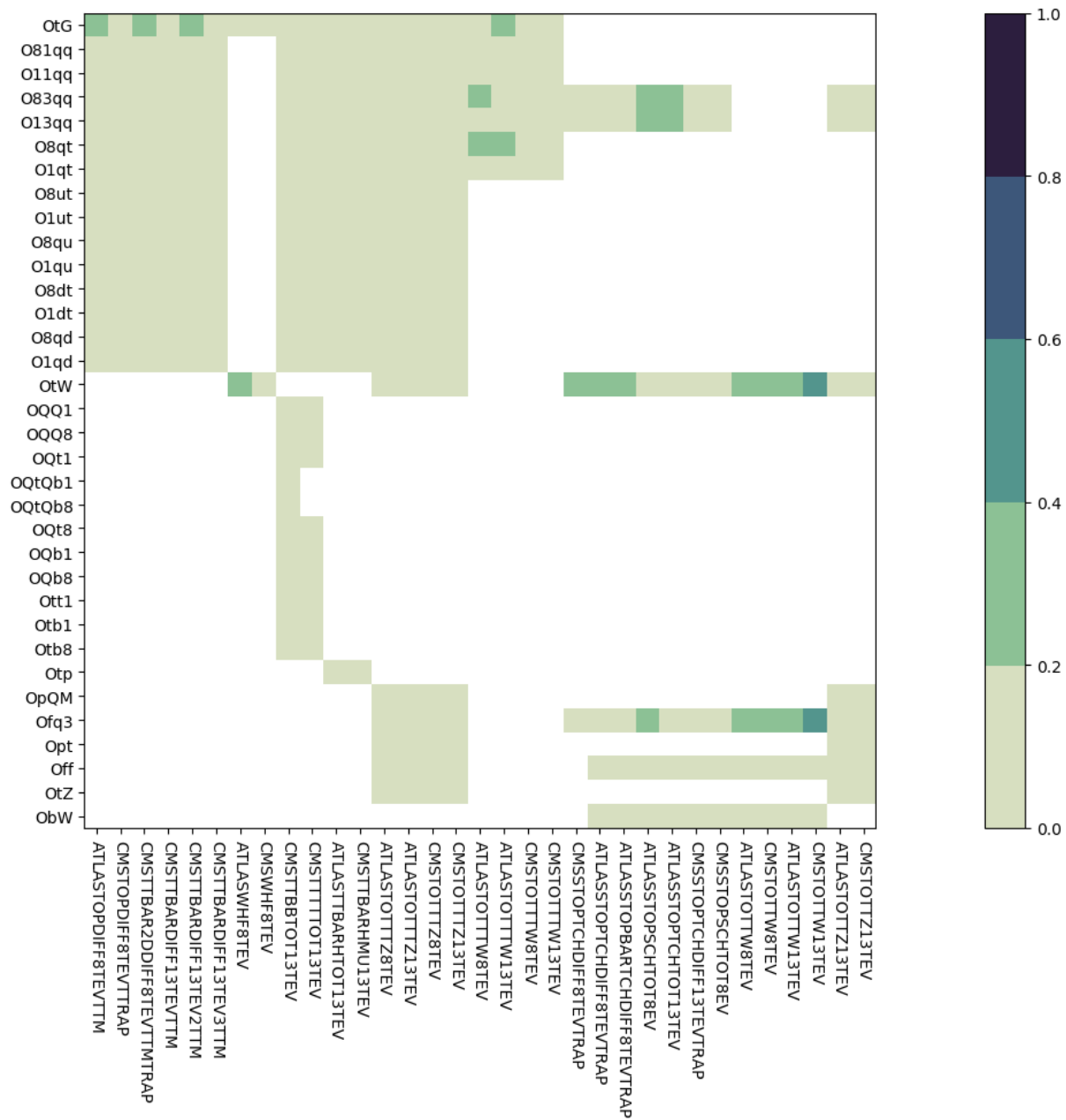


Figure 5.2: The average absolute sensitivity $\langle |S_i(c_i)| \rangle$ as defined in equation (5.2.2) between the SMEFT parameter c_i and the residual r_i for the i^{th} data point in experiment E in case of single data set NS results at $\mathcal{O}(\Lambda^{-2})$.

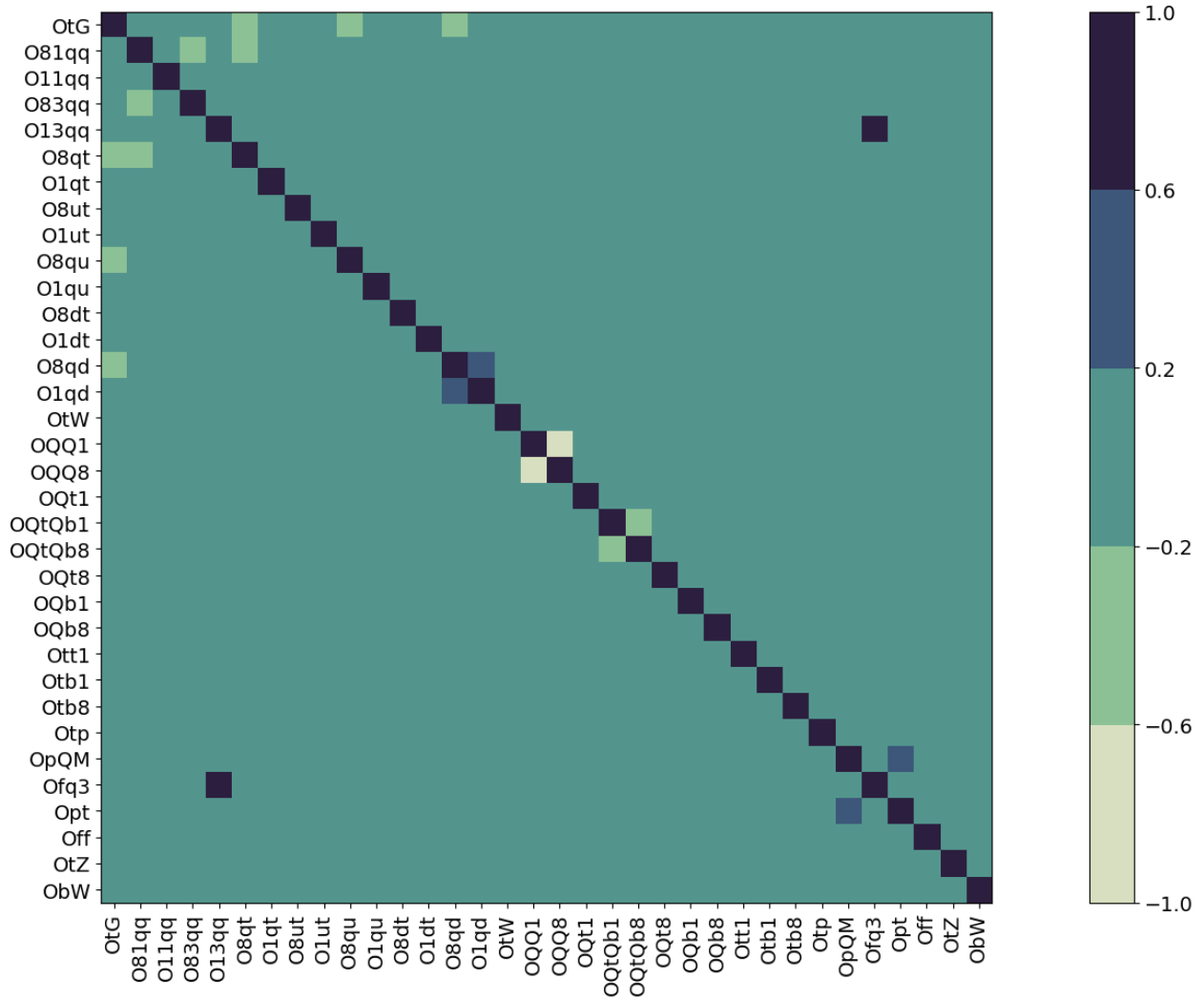


Figure 5.3: The values of the correlation coefficient between the SMEFT-parameters c_i , as obtained from a global NS run at $\mathcal{O}(\Lambda^{-4})$.

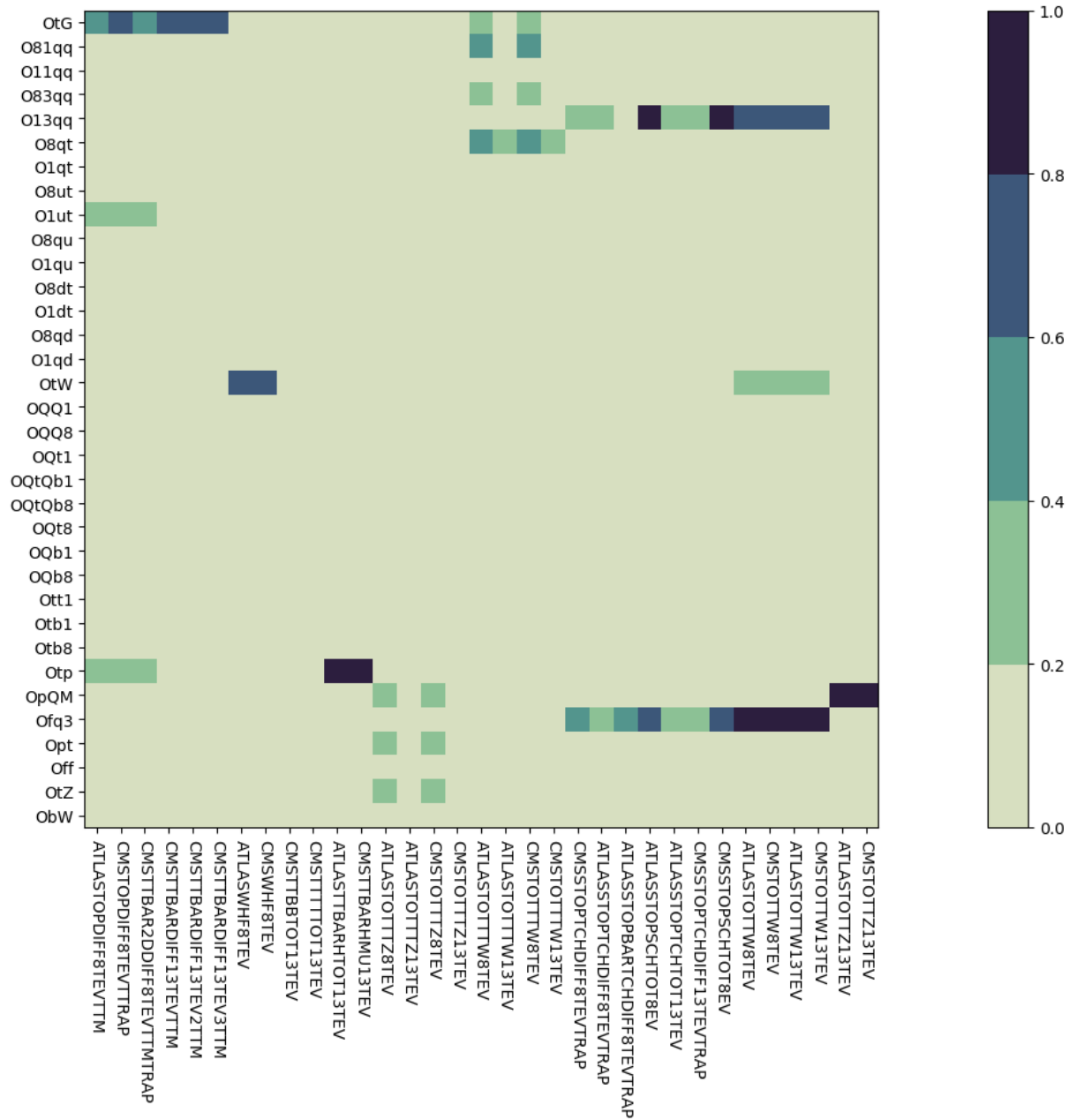


Figure 5.4: The average absolute correlation $\langle |Corr[c_i, r_i]| \rangle$ between the SMEFT parameter c_i and the residual r_i for the i^{th} data point in experiment E in case of global data set NS results at $\mathcal{O}(\Lambda^{-4})$. The theory predictions are also at $\mathcal{O}(\Lambda^{-4})$.

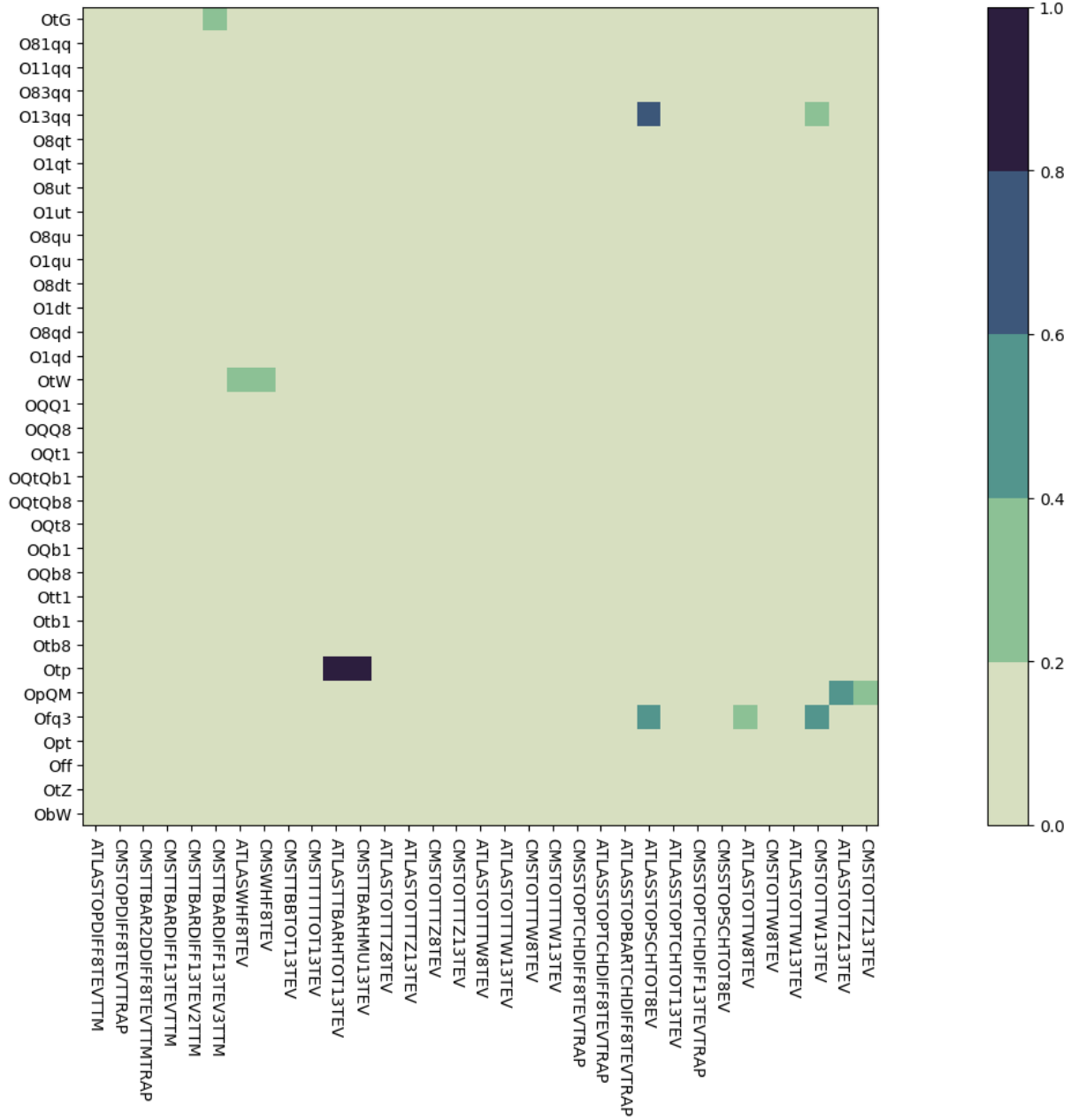


Figure 5.5: The average absolute sensitivity $\langle |S_i(c_i)| \rangle$ as defined in equation (5.2.2) between the SMEFT parameter c_i and the residual r_i for the i^{th} data point in experiment E in case of global data set NS results at $\mathcal{O}(\Lambda^{-4})$. The theory predictions are also at $\mathcal{O}(\Lambda^{-4})$.

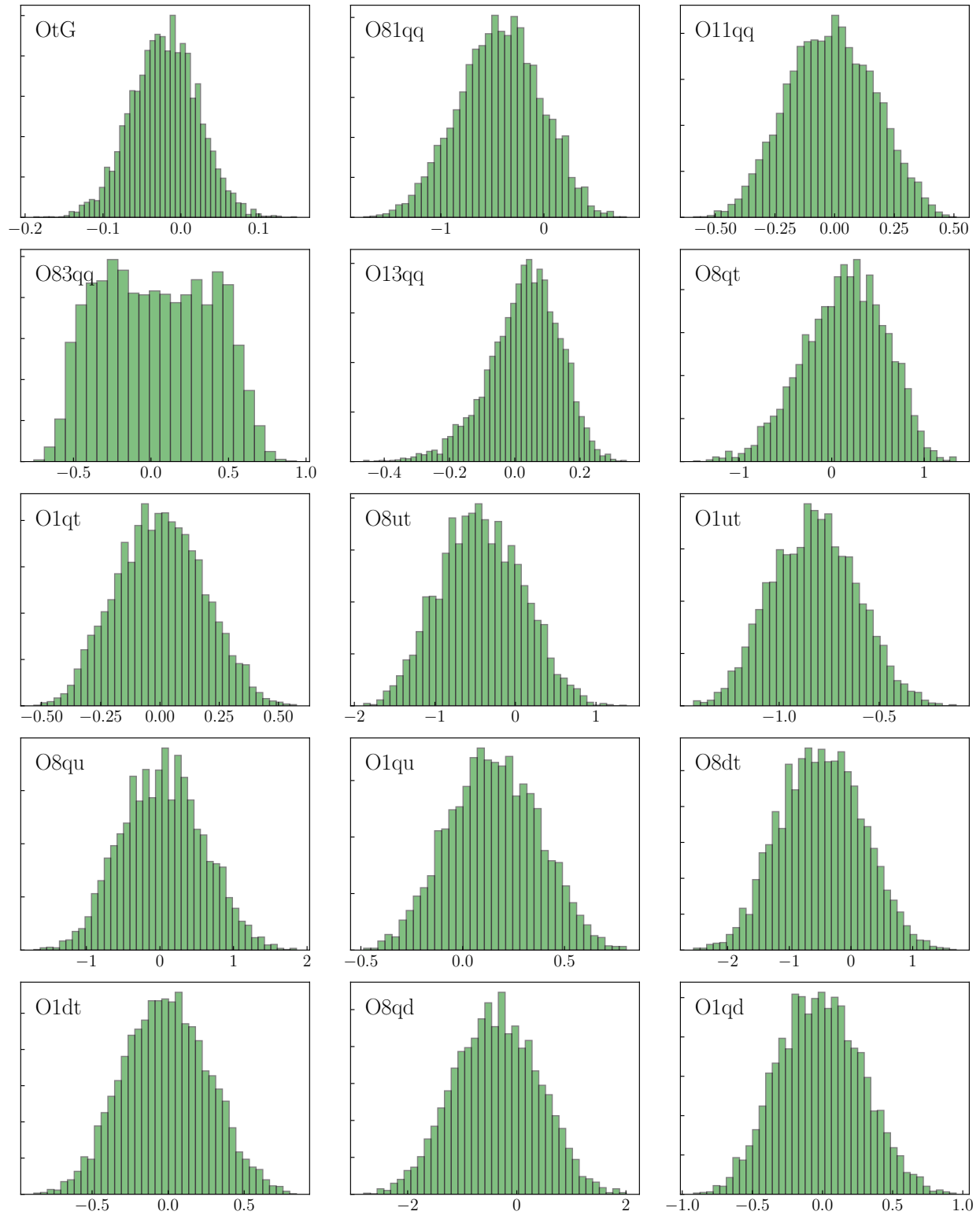


Figure 5.6: Histograms of the SMEFT-parameters $\text{O}t\text{G}$ up to $\text{O}1\text{q}d$ that were sampled using a global NS run. Note that $\text{O}t\text{G}$ is relatively well constrained due to the fact that it enters in all top-quark production processes except for single-top and single-top in association with a W -boson.

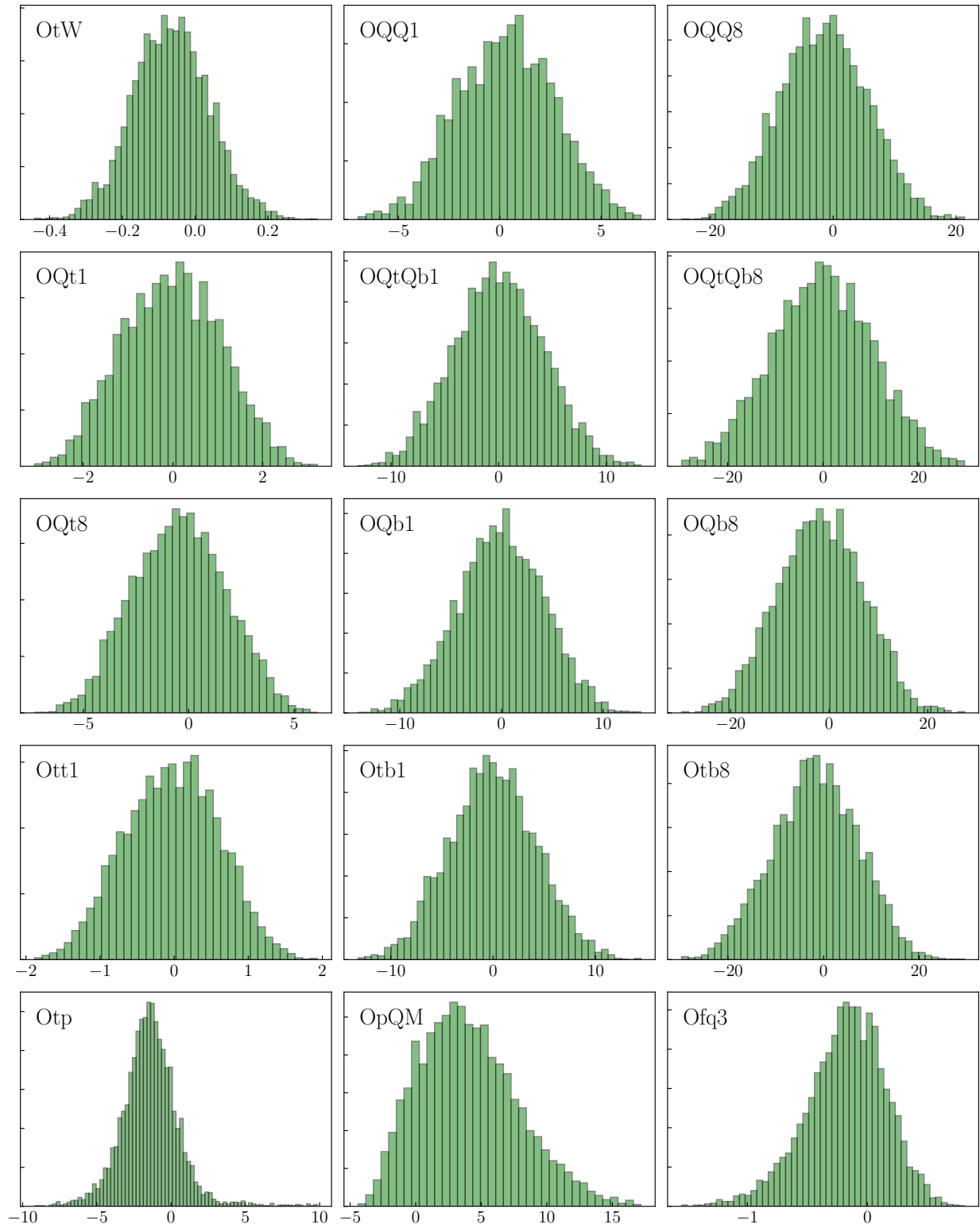


Figure 5.7: Continued from figure 5.6. Histograms of the SMEFT-parameters O_{tW} up to O_{f_3} that were sampled using a global NS run.

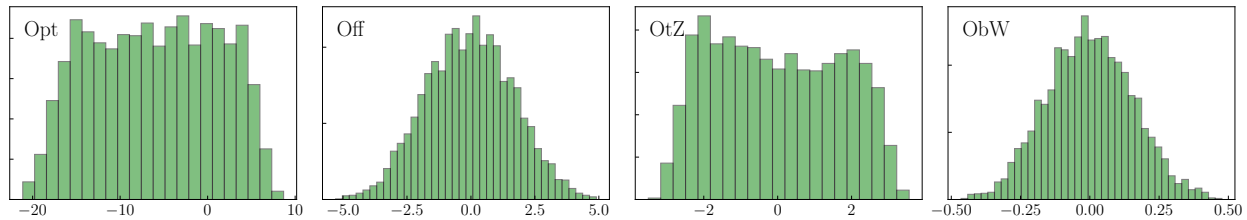


Figure 5.8: Continued from figure 5.7. Histograms of the SMEFT-parameters Opt up to ObW that were sampled using a global NS run.

5.4 Discussion

It is good to make a few remarks regarding the results we presented in figures 5.1-5.5.

- From figure 5.3 we observe that Ofq3 is strongly correlated with O13qq with a correlation coefficient of at least 0.6. This means that experiments that are sensitive for Ofq3 in a single data set fit, are likely to also be sensitive for O13qq in case of a global fit. Indeed, from figure 5.4 we observe that the $t\bar{t}W$ -experiments ATLASTOTTW8TEV , CMSTOTTW8TEV , ATLASTOTTW13TEV and CMSTOTTW13TEV are sensitive for both Ofq3 as well as O13qq , even though these data sets cannot constrain O13qq in case of an individual (single data set) fit.
- Experiments with a high averaged absolute correlation $\langle |\text{Corr}[c_l, r_i]| \rangle$, can nonetheless have a low sensitivity if its uncertainties are high compared to the theory error. If this is the case, the factor Δr_i is small, and thus suppresses the large contribution coming from $\text{Corr}[c_l, r_i]$. This explains how figure 5.5 is related to figure 5.4. For instance, the operator OtG has a relatively large correlation in the inclusive $t\bar{t}$ -production data sets, whereas figure 5.5 shows that it is almost insensitive for these data sets. Intuitively, it means that data sets with large experimental uncertainties will do a poor job at constraining its associated SMEFT degrees of freedom.
- The $t\bar{t}H$ -experiments $\text{ATLASTTBARHTOT13TEV}$ and CMSTTBARHMU13TEV are highly sensitive for the operator Otp , as can be seen from figure 5.5. This is to be expected, since Otp constrains $t\bar{t}$ -production in association with the Higgs boson.

As written, equation (5.2.2) does not take into account the number of data points that are present in the experiment. However, all of the $t\bar{t}W$, $t\bar{t}Z$, $t\bar{t}H$ and $t\bar{t}$ in association with two heavy quarks data sets contribute by only one data point. Therefore, their contribution to the overall χ^2 of the global SMEFiT analysis is small and can fluctuate by a lot. Therefore, if new experiments with more data points were to be reported, we would typically want the SMEFT degrees of freedom to be relatively sensitive for these. In future studies, we should therefore accommodate for the number of data points and its associated spreading.

Chapter 6

Top-quark Matching

In this chapter, we study several explicit extensions of the SM and match these onto the SMEFT. We start with a relatively simple extension, in which a heavy scalar particle S is coupled to the SM quarks. By integrating out S , we obtain an effective theory that lets us relate the Wilson coefficients to the UV parameters. Here, the UV parameters are typically either masses or couplings of the heavy particle. It turns out that the matching procedure generates higher dimensional operators that are not part of the Warsaw basis. Therefore, a large part of the upcoming sections is devoted to re-expressing the generated operators in the Warsaw basis. Next, we move on to a slightly more complex model, the heavy vector model, and perform the same exercise there. That is, we integrate out the heavy vector boson from the UV theory and match it to the SMEFT. This is part of section 6.2. In both cases, our goal is to translate the SMEFT bounds to the UV parameters in order to constrain these specific models.

Alternatively, we can choose to work with the SM extensions directly and compare its predictions to experiment. This can become a tedious route to finding new physics, since it requires computing numerous cross sections and decay widths. Although this is a straightforward exercise in principle, the model-independent nature of effective field theories makes them the method of choice in the search for new physics. Nevertheless, chapter 7 presents a detailed analysis of this alternative, more direct, approach.

Zooming out, we can thus distinguish between two different ways of finding constraints on new physics. On the one hand, we can use the bounds on the Wilson coefficients to look for new physics, which is much more efficient due to the model independence nature of SMEFT. That is, single bounds on the Wilson coefficients can constrain a plethora of SM extensions. On the other hand, UV-completions can also be constrained by comparing to experimental data directly.

After these introductory remarks, let us move on the first SM extension: the heavy scalar.

6.1 Model: Heavy Scalar

In this section, we match a heavy scalar to the SMEFT. Not only will this prove useful later on in chapter 7, it also gives us the opportunity to discuss the matching procedure in a concrete setting.

We extend the SM by a complex heavy scalar S that transforms under the SM gauge group as

$$S \sim (1, 2)_{1/2}, \quad (6.1.1)$$

where $(R_c, R_L)_Y$ denote the representation R_c under $SU(3)_c$, the representation R_L under $SU(2)_L$ and the hypercharge Y respectively. In other words, the scalar S transforms as a doublet under $SU(2)$. This is the simplest scalar extension of the SM that can couple to the SM quarks while preserving gauge invariance [21]. The associated Lagrangian is given by

$$\mathcal{L}_{UV} = \mathcal{L}_{SM} + \partial_\mu S^\dagger \partial^\mu S + m_S^2 S^\dagger S - J_S^\dagger S - S^\dagger J_S, \quad (6.1.2)$$

where

$$\begin{aligned} J_S &\equiv c_S \bar{b}_R q_L^3 + c_S i \sigma_2 \bar{q}_L^{3T} t_R \\ &= c_S \bar{b}_R \begin{pmatrix} t_L \\ b_L \end{pmatrix} + c_S \begin{pmatrix} 0 & 1 \\ -1 & 0 \end{pmatrix} \begin{pmatrix} \bar{t}_L \\ \bar{b}_L \end{pmatrix} t_R \\ &= c_S \bar{b}_R \begin{pmatrix} t_L \\ b_L \end{pmatrix} + c_S \begin{pmatrix} \bar{b}_L \\ -\bar{t}_L \end{pmatrix} t_R \end{aligned} \quad (6.1.3)$$

defines the scalar current. For now, we have chosen to couple the heavy scalar to only one generation in order to simplify our notation. We generalise this later to also include the light generations. In the unitary gauge we can write $S^\dagger = \begin{pmatrix} 0 & S \end{pmatrix}$, and the interaction part of the Lagrangian then takes the following simple form:

$$\begin{aligned} S^\dagger J_S + \text{h.c.} &= S^\dagger c_S \bar{b}_R \begin{pmatrix} t_L \\ b_L \end{pmatrix} + S^\dagger c_S \begin{pmatrix} \bar{b}_L \\ -\bar{t}_L \end{pmatrix} t_R + \text{h.c.} \\ &= c_S \bar{b}_R b_L S - c_S \bar{t}_L t_R S + \text{h.c.} \\ &= -c_S S (\bar{t}t - \bar{b}b). \end{aligned} \quad (6.1.4)$$

Hence, we see that the scalar particle contributes to top-quark production. Our Feynman rule is to simply associate a factor $\pm i c_S$ to the $\bar{q}_f q_f S$ -vertices:

$$\begin{array}{c}
 \bar{t} \\
 \nearrow \\
 \text{---} S \text{---} \bullet \\
 \searrow \\
 t
 \end{array}
 = i c_S.$$

Next, we derive the effective theory by integrating out S . To this end, we first determine its EOM via the Euler-Lagrange equations:

$$\frac{\partial \mathcal{L}}{\partial S^\dagger} = \partial_\mu \frac{\partial \mathcal{L}}{\partial(\partial_\mu S^\dagger)} \quad \Longrightarrow \quad m_S^2 S - J_S = \partial^2 S. \quad (6.1.5)$$

Hence,

$$S = -\frac{J_S}{\partial^2 - m_S^2} \quad \text{and} \quad S^\dagger = -\frac{J_S^\dagger}{\partial^2 - m_S^2}. \quad (6.1.6)$$

By substituting the classical solution (6.1.6) back into \mathcal{L}_{UV} , we eliminate S to obtain

$$\begin{aligned} \mathcal{L}_{UV} &= \mathcal{L}_{SM} - S^\dagger(\partial^2 - m_S^2)S - J_S^\dagger S - S^\dagger J_S \\ &= \mathcal{L}_{SM} - \frac{J_S^\dagger J_S}{\partial^2 - m_S^2} + \frac{J_S^\dagger J_S}{\partial^2 - m_S^2} + \frac{J_S^\dagger J_S}{\partial^2 - m_S^2} \\ &= \mathcal{L}_{SM} + \frac{J_S^\dagger J_S}{\partial^2 - m_S^2}. \end{aligned} \quad (6.1.7)$$

In the EFT-regime, we have $p_S^2 \ll m_S^2$, with p_S the scalar particle's momentum. Consequently, we can expand the scalar propagator as follows:

$$\frac{1}{\partial^2 - m_S^2} = -\frac{1}{m_S^2} \left(1 - \frac{\partial^2}{m_S^2} \right) + \mathcal{O} \left(\frac{1}{m_S^4} \right).$$

The UV-Lagrangian (6.1.7) can thus be written as

$$\mathcal{L}_{\text{eff}} = \mathcal{L}_{SM} - \frac{1}{m_S^2} J_S^\dagger J_S + \mathcal{O} \left(\frac{1}{m_S^4} \right). \quad (6.1.8)$$

Let us now substitute the scalar current (6.1.3) in order to express $J_S^\dagger J_S$ in terms of the SM-fields:

$$\begin{aligned} J_S^\dagger J_S &= c_S^2 \left((\bar{t}_L \quad \bar{b}_L) b_R + \bar{t}_R (b_L \quad -t_L) \right) \left(\bar{b}_R \begin{pmatrix} t_L \\ b_L \end{pmatrix} + c_S \begin{pmatrix} \bar{b}_L \\ -\bar{t}_L \end{pmatrix} t_R \right) \\ &= c_S^2 \left((\bar{t}_L \quad \bar{b}_L) b_R \bar{b}_R \begin{pmatrix} t_L \\ b_L \end{pmatrix} + (\bar{t}_L \quad \bar{b}_L) b_R \begin{pmatrix} \bar{b}_L \\ -\bar{t}_L \end{pmatrix} t_R + \bar{t}_R (b_L \quad -t_L) \bar{b}_R \begin{pmatrix} t_L \\ b_L \end{pmatrix} \right. \\ &\quad \left. + \bar{t}_R (b_L \quad -t_L) \begin{pmatrix} \bar{b}_L \\ -\bar{t}_L \end{pmatrix} t_R \right) \\ &= c_S^2 \left(\bar{t}_L b_R \bar{b}_R t_L + \bar{b}_L b_R \bar{b}_R b_L + \bar{t}_L b_R \bar{b}_L t_R - \bar{b}_L b_R \bar{t}_L t_R \right. \\ &\quad \left. - \bar{t}_R t_L \bar{b}_R b_L + \bar{t}_R b_L \bar{b}_R t_L + \bar{t}_R t_L \bar{t}_L t_R + \bar{t}_R b_L \bar{b}_L t_R \right) \end{aligned} \quad (6.1.9)$$

Therefore, at leading order in the EFT-expansion, we have

$$\begin{aligned} \mathcal{L}_{\text{eff}} &= \mathcal{L}_{SM} - \frac{c_S^2}{m_S^2} \left(\bar{t}_L b_R \bar{b}_R t_L + \bar{b}_L b_R \bar{b}_R b_L + \bar{t}_L b_R \bar{b}_L t_R - \bar{b}_L b_R \bar{t}_L t_R \right. \\ &\quad \left. - \bar{t}_R t_L \bar{b}_R b_L + \bar{t}_R b_L \bar{b}_R t_L + \bar{t}_R t_L \bar{t}_L t_R + \bar{t}_R b_L \bar{b}_L t_R \right). \end{aligned} \quad (6.1.10)$$

As it stands, the coefficients in front of the operators appearing in (6.1.10) cannot yet be matched to the SMEFT coefficients. We first have to convert these operators to the Warsaw basis, since the SMEFT results in [3] are presented with this choice of basis. A list of definitions of operators in the Warsaw basis is provided in appendix A. We use this notation.

It is convenient to take a backwards approach here and start by simply giving the effective Lagrangian in the Warsaw basis. We then prove its correctness by showing that it equals the original effective Lagrangian (6.1.10). Expressed in the Warsaw basis, we have [22]

$$\mathcal{L}_{\text{eff}} = \mathcal{L}_{\text{SM}} - \frac{c_S^2}{6m_S^2} \left(\mathcal{Q}_{qd}^{(1)} + \mathcal{Q}_{qu}^{(1)} \right) - \frac{c_S^2}{m_S^2} \left(\mathcal{Q}_{qd}^{(8)} + \mathcal{Q}_{qu}^{(8)} \right) + \frac{c_S^2}{m_S^2} \left(\mathcal{Q}_{quqd}^{(1)} + \text{h.c.} \right). \quad (6.1.11)$$

Proof of (6.1.11)

Our strategy is to consider the operators in (6.1.11) in turn, and show, after a little manipulation, that they give the operators in (6.1.10). Let us start with the operator $\mathcal{Q}_{qd}^{(1)}$. Making the colour indices (α, β) explicit, we have

$$\begin{aligned} \mathcal{Q}_{qd}^{(1)} &= (\bar{q}_L \gamma_\mu q_L) (\bar{b}_R \gamma^\mu b_R) \\ &= (\bar{t}_L^\alpha \gamma_\mu t_L^\alpha) (\bar{b}_R^\beta \gamma^\mu b_R^\beta) + (\bar{b}_L^\alpha \gamma_\mu b_L^\alpha) (\bar{t}_R^\beta \gamma^\mu t_R^\beta) \\ &= 2\bar{t}_L^\alpha b_R^\beta \bar{b}_R^\beta t_L^\alpha + 2\bar{b}_L^\alpha t_R^\beta \bar{t}_R^\beta b_L^\alpha, \end{aligned} \quad (6.1.12)$$

where on the last line we used the following Fierz identity:

$$[\bar{\psi}_{L_1} \psi_{R_2}] [\bar{\psi}_{R_3} \psi_{L_4}] = \frac{1}{2} [\bar{\psi}_{L_1} \gamma^\mu \psi_{L_4}] [\bar{\psi}_{R_3} \gamma_\mu \psi_{R_2}]. \quad (6.1.13)$$

We refer to appendix B for a derivation here. Similarly to $\mathcal{Q}_{qd}^{(1)}$, we can show that

$$\mathcal{Q}_{qu}^{(1)} = 2\bar{t}_L^\alpha t_R^\beta \bar{t}_R^\beta t_L^\alpha + 2\bar{b}_L^\alpha t_R^\beta \bar{t}_R^\beta b_L^\alpha. \quad (6.1.14)$$

The operators $\mathcal{Q}_{qd}^{(8)}$ and $\mathcal{Q}_{qu}^{(8)}$ are less straightforward to convert. We first need that

$$T_{\alpha\beta}^A T_{\kappa\lambda}^A = \frac{1}{2} \delta_{\alpha\lambda} \delta_{\kappa\beta} - \frac{1}{6} \delta_{\alpha\beta} \delta_{\kappa\lambda}.$$

With this, we obtain:

$$\begin{aligned} \mathcal{Q}_{qd}^{(8)} &= (\bar{q}_L \gamma_\mu T_A q_L) (\bar{b}_R \gamma^\mu T_A b_R) \\ &= (\bar{t}_L \gamma_\mu T_A t_L) (\bar{b}_R \gamma^\mu T_A b_R) + (\bar{b}_L \gamma_\mu T_A b_L) (\bar{t}_R \gamma^\mu T_A t_R) \\ &= \left(\bar{t}_L^\alpha \gamma_\mu t_L^\beta \right) \left(\bar{b}_R^\kappa \gamma_\mu b_R^\lambda \right) \left(\frac{1}{2} \delta_{\alpha\lambda} \delta_{\kappa\beta} - \frac{1}{6} \delta_{\alpha\beta} \delta_{\kappa\lambda} \right) \\ &\quad + \left(\bar{b}_L^\alpha \gamma_\mu b_L^\beta \right) \left(\bar{t}_R^\kappa \gamma_\mu t_R^\lambda \right) \left(\frac{1}{2} \delta_{\alpha\lambda} \delta_{\kappa\beta} - \frac{1}{6} \delta_{\alpha\beta} \delta_{\kappa\lambda} \right) \\ &= \frac{1}{2} \left(\bar{t}_L^\alpha \gamma_\mu t_L^\beta \right) \left(\bar{b}_R^\beta \gamma^\mu b_R^\alpha \right) - \frac{1}{6} \left(\bar{t}_L^\alpha \gamma_\mu t_L^\alpha \right) \left(\bar{b}_R^\beta \gamma^\mu b_R^\beta \right) \\ &\quad - \frac{1}{2} \left(\bar{b}_L^\alpha \gamma_\mu b_L^\beta \right) \left(\bar{t}_R^\beta \gamma^\mu t_R^\alpha \right) + \frac{1}{6} \left(\bar{b}_L^\alpha \gamma_\mu b_L^\alpha \right) \left(\bar{t}_R^\beta \gamma^\mu t_R^\beta \right). \end{aligned}$$

Finally, using again the Fierz identity (6.1.13) to remove the gamma-matrices, we find

$$\mathcal{Q}_{qd}^{(8)} = \bar{t}_L b_R \bar{b}_R t_L - \frac{1}{3} \bar{t}_L^\alpha b_R^\beta \bar{b}_R^\beta t_L^\alpha + \bar{b}_L b_R \bar{b}_R b_L - \frac{1}{3} \bar{b}_L^\alpha b_R^\beta \bar{b}_R^\beta b_L^\alpha. \quad (6.1.15)$$

Similarly, we obtain

$$\mathcal{Q}_{qu}^{(8)} = \bar{t}_L t_R \bar{t}_R t_L - \frac{1}{3} \bar{t}_L^\alpha t_R^\beta \bar{t}_R^\beta t_L^\alpha + \bar{b}_L t_R \bar{t}_R b_L - \frac{1}{3} \bar{b}_L^\alpha t_R^\beta \bar{t}_R^\beta b_L^\alpha \quad (6.1.16)$$

Now, what remains is to convert the operator $\mathcal{Q}_{quqd}^{(1)}$. Carrying out the multiplication, gives

$$\mathcal{Q}_{quqd}^{(1)} = \left(\bar{q}_L^j t_R \right) \epsilon_{jk} \left(\bar{q}_L^k b_R \right) = \bar{t}_L t_R \bar{b}_L b_R - \bar{b}_L t_R \bar{t}_L b_R. \quad (6.1.17)$$

Having converted all the Warsaw operators to a form that resembles the operators in (6.1.10), we can now plug our results (6.1.12)-(6.1.17) into the effective Lagrangian from (6.1.11) to find

$$\begin{aligned} \mathcal{L}_{\text{eff}} = \mathcal{L}_{\text{SM}} - \frac{c_S^2}{m_S^2} & \left(\frac{1}{3} \bar{t}_L^\alpha b_R^\beta \bar{b}_R^\beta t_L^\alpha + \frac{1}{3} \bar{b}_L^\alpha b_R^\beta \bar{b}_R^\beta b_L^\alpha + \frac{1}{3} \bar{t}_L^\alpha t_R^\beta \bar{t}_R^\beta t_L^\alpha + \frac{1}{3} \bar{b}_L^\alpha t_R^\beta \bar{t}_R^\beta b_L^\alpha \right. \\ & + (\bar{t}_L b_R \bar{b}_R t_L) - \frac{1}{3} \bar{t}_L^\alpha b_R^\beta \bar{b}_R^\beta t_L^\alpha + (\bar{b}_L b_R \bar{b}_R b_L) - \frac{1}{3} \bar{b}_L^\alpha b_R^\beta \bar{b}_R^\beta b_L^\alpha + (\bar{t}_L t_R \bar{t}_R t_L) \\ & \left. - \frac{1}{3} \bar{t}_L^\alpha t_R^\beta \bar{t}_R^\beta t_L^\alpha + (\bar{b}_L t_R \bar{t}_R b_L) - \frac{1}{3} \bar{b}_L^\alpha t_R^\beta \bar{t}_R^\beta b_L^\alpha - (\bar{t}_L t_R \bar{b}_L b_R - \bar{b}_L t_R \bar{t}_L b_R + \text{h.c.}) \right). \quad (6.1.18) \end{aligned}$$

Finally, canceling common terms and writing out the hermitean conjugate leaves us with

$$\begin{aligned} \mathcal{L}_{\text{eff}} = \mathcal{L}_{\text{SM}} - \frac{c_S^2}{m_S^2} & (\bar{t}_L b_R \bar{b}_R t_L + \bar{b}_L b_R \bar{b}_R b_L + \bar{t}_L t_R \bar{t}_R t_L + \bar{b}_L t_R \bar{t}_R b_L \\ & - \bar{t}_L t_R \bar{b}_L b_R + \bar{b}_L t_R \bar{t}_L b_R - \bar{b}_R b_L \bar{t}_R t_L + \bar{b}_R t_L \bar{t}_R b_L), \quad (6.1.19) \end{aligned}$$

which is seen to equal (6.1.10) and thus proves (6.1.11). **End of proof.**

We would like to generalise our model to include other fermionic families as well. This can be straightforwardly done by carefully keeping track of the generation-indices. The coupling c_S now gets replaced by a 3×3 -matrix $(c_S)_{ij}$ in generation space:

$$\begin{aligned} \mathcal{L}_{\text{eff}} = \mathcal{L}_{\text{SM}} - \sum_{ijkl} \frac{(c_S)_{kj} (c_S)_{il}}{6m_S^2} & \left(\mathcal{Q}_{qd}^{(1)ijkl} + \mathcal{Q}_{qu}^{(1)ijkl} \right) - \sum_{ijkl} \frac{(c_S)_{kj} (c_S)_{il}}{m_S^2} \left(\mathcal{Q}_{qd}^{(8)ijkl} + \mathcal{Q}_{qu}^{(8)ijkl} \right) \\ & + \sum_{ijkl} \frac{(c_S)_{ij} (c_S)_{kl}}{m_S^2} \left(\mathcal{Q}_{qud}^{(1)ijkl} + \text{h.c.} \right). \quad (6.1.20) \end{aligned}$$

If we furthermore impose that the scalar particle S couples with equal strength only to quarks that have the same flavour, we get that $(c_S)_{ij} = c_S \delta_{ij}$ and (6.1.20) simplifies to

$$\begin{aligned} \mathcal{L}_{\text{eff}} = \mathcal{L}_{\text{SM}} - c_S^2 \sum_{ijkl} \frac{\delta_{kj} \delta_{il}}{6m_S^2} & \left(\mathcal{Q}_{qd}^{(1)ijkl} + \mathcal{Q}_{qu}^{(1)ijkl} \right) - c_S^2 \sum_{ijkl} \frac{\delta_{kj} \delta_{il}}{m_S^2} \left(\mathcal{Q}_{qd}^{(8)ijkl} + \mathcal{Q}_{qu}^{(8)ijkl} \right) \\ & + c_S^2 \sum_{ijkl} \frac{\delta_{ij} \delta_{kl}}{m_S^2} \left(\mathcal{Q}_{qud}^{(1)ijkl} + \text{h.c.} \right). \quad (6.1.21) \end{aligned}$$

The correct generalisation of the current J_S (6.1.3) to all generations can be written as

$$J_S \equiv c_S \sum_{i,j} \bar{d}_R^i q_L^j \delta_{ij} + c_S i \sigma_2 \sum_{i,j} \bar{q}_L^{iT} u_R^j \delta_{ij}, \quad (6.1.22)$$

where we have taken again $(c_S)_{ij} = c_S \delta_{ij}$. The current (6.1.22) then leads to

$$S^\dagger J_S + \text{h.c.} = -c_S S (\bar{u}u - \bar{d}d + \bar{c}c - \bar{s}s + \bar{t}t - \bar{b}b), \quad (6.1.23)$$

which shows that the $\bar{q}_f q_f S$ -vertices again get associated a factor $\pm i c_S$.

As becomes apparent from the effective Lagrangian in (6.1.21), we generate two different kinds of four fermionic operators upon going to the EFT. For $i, j, k, l = 3$, we have the four-heavy quark operators, and when exactly two generation indices equal three, we get the two-light-two-heavy (2L2H) operators. As for the latter, they come in the pattern $(i33i)$ or $(3ii3)$, where $i = 1, 2$ refers to a light quark. However, the SMEFT fitting basis used in ref. [3] (see Table 4.1 in chapter 4) only includes 2L2H operators of the kind $(ii33)$ or $(i33i)$. This can be traced back to the flavour assumptions that were made in [3]. They assume a $U(2)_q \times U(2)_u \times U(2)_d$ flavour symmetry among the first two generations, which excludes four-fermionic operators of the kind $(i33i)$ and $(3ii3)$ [23]. The bottom line of this observation is that we cannot use the 2L2H bounds from SMEFiT to constrain the UV-parameters c_S and m_S .

What about the four-heavy quark operators? In the effective Lagrangian (6.1.21), the contribution with generation indices $i, j, k, l = 3$ results in the operators $\mathcal{O}_{qd}^{(1)3333}$, $\mathcal{O}_{qu}^{(1)3333}$, $\mathcal{O}_{qd}^{(8)3333}$ and $\mathcal{O}_{qu}^{(8)3333}$. In contrast to the 2L2H operators, we now do generate operators that are part of our SMEFT fitting basis. This therefore allows us to study how the SMEFT bounds carry over to the BSM parameters.

Using Nested Sampling (NS, chapter 4), we construct 95% CL bounds for the above mentioned four-heavy quark operators. The operators are fit individually, i.e. constrained one at a time, since this leads to more stringent bounds due to the absence of cross-correlations. The results, at SMEFT order $\mathcal{O}(\Lambda^{-4})$ are shown in Table 6.1. For completeness, we also present the SMEFT bounds for the 2L2H operators in Table 6.2, although these will not be used for the above-mentioned reason. Here, results are shown at both order $\mathcal{O}(\Lambda^{-2})$ and $\mathcal{O}(\Lambda^{-4})$.

Let us now use the bounds on the four-heavy operators to constrain the ratio c_S^2/m_S^2 . Identifying the coefficients appearing in front of the operators in (6.1.21) with the SMEFT coefficients in Table 6.1, results in the following constraints:

$$\begin{aligned}
-0.595 &< -\frac{c_S^2}{6m_S^2} < -0.0448 \quad \text{TeV}^{-2} \\
-0.0150 &< -\frac{c_S^2}{6m_S^2} < 0.145 \quad \text{TeV}^{-2} \\
-3.128 &< -\frac{c_S^2}{m_S^2} < -1.982 \quad \text{TeV}^{-2} \\
-0.802 &< -\frac{c_S^2}{m_S^2} < -0.473 \quad \text{TeV}^{-2}.
\end{aligned} \tag{6.1.24}$$

Keeping only the upper bounds on c_S^2/m_S^2 , we can write (6.1.24) as:

$$\begin{aligned}
\frac{c_S^2}{m_S^2} &< 3.570 \quad \text{TeV}^{-2} \\
\frac{c_S^2}{m_S^2} &< 0.0900 \quad \text{TeV}^{-2} \\
\frac{c_S^2}{m_S^2} &< 3.128 \quad \text{TeV}^{-2} \\
\frac{c_S^2}{m_S^2} &< 0.802 \quad \text{TeV}^{-2},
\end{aligned} \tag{6.1.25}$$

where we have kept the same order as in (6.1.24). Therefore, the most stringent bound, or best bound, is given by

$$\frac{c_S^2}{m_S^2} < 0.0900 \quad \text{TeV}^{-2} \quad (\text{Best}). \tag{6.1.26}$$

This concludes the discussion about the heavy scalar model for now. We return to this model in chapter 7, where it is used in the context of BSM phenomenology.

QQQQ	$\mathcal{O}(\Lambda^{-4})$
0Qb1 = $C_{qd}^{(1)3333}$	[-0.595, -0.0448]
0Qt1 = $C_{qu}^{(1)3333}$	[-0.0150, 0.145]
0Qb8 = $C_{qd}^{(8)3333}$	[-3.128, -1.982]
0Qt8 = $C_{qu}^{(8)3333}$	[-0.802, -0.473]

Table 6.1: *The 95% confidence level intervals (in units of TeV^{-2} , with $\Lambda = 1 \text{ TeV}$) for the four-heavy operators appearing in the effective Lagrangian (6.1.20).*

2L2H	$\mathcal{O}(\Lambda^{-2})$	$\mathcal{O}(\Lambda^{-4})$
$01\text{qd} = C_{qd}^{(1)33ii}$	[0.919, 1.037]	[0.0281, 0.0475]
$01\text{qu} = C_{qu}^{(1)33ii}$	[0.951, 1.002]	[0.0807, 0.0951]
$01\text{qt} = C_{qu}^{(1)ii33}$	[0.090, 0.191]	[0.00268, 0.0144]
$08\text{qd} = C_{qd}^{(8)33ii}$	[-1.261, -1.163]	[-0.394, -0.342]
$08\text{qt} = C_{qu}^{(8)ii33}$	[0.047, 0.091]	[-0.0293, -0.00176]
$08\text{qu} = C_{qu}^{(8)33ii}$	[-1.627, -1.528]	[-0.240, -0.202]

Table 6.2: The 95% confidence level intervals (in units of TeV^{-2} , with $\Lambda = 1 \text{ TeV}$) for the two-light-two-heavy (2L2H) operators appearing in the effective Lagrangian (6.1.20). at order $\mathcal{O}(\Lambda^{-2})$ and $\mathcal{O}(\Lambda^{-4})$.

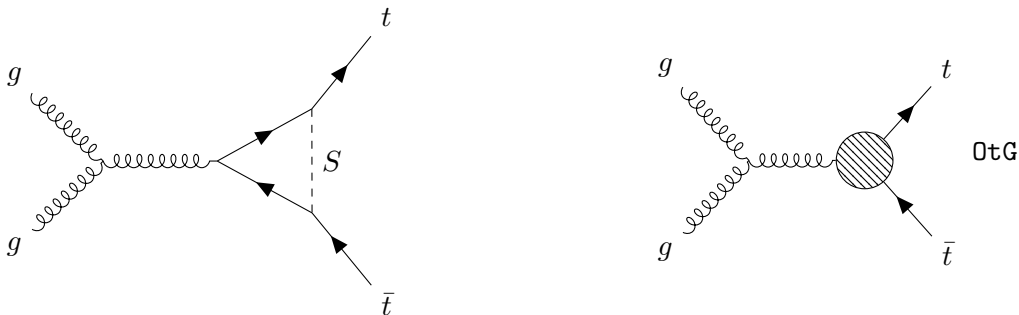


Figure 6.1: In the heavy scalar model, the chromomagnetic operator 0tG is generated in the EFT (right) at NLO in QCD (left).

6.1.1 NLO Effects

In the previous section we matched a heavy scalar extension of the SM onto the SMEFT at leading order (LO) in QCD. That is, we only considered diagrams in the full theory that did not include any loops. However, the heavy scalar S also contributes to $t\bar{t}$ -production at next-to-leading order (NLO) in QCD, as can be understood from figure 6.1. If we were now to integrate out S here, we would additionally also generate the chromomagnetic operator 0tG [24], which contributes to $t\bar{t}$ -production at LO in the EFT. Considering that 0tG is constrained by many different processes (i.e. all the top-quark production mechanisms except for single top production and single top production in association with a Z -boson), it is relatively tightly constrained [3]. Therefore, matching at NLO would possibly give more stringent constraints on the UV parameters c_S and m_S .

6.2 Model: Heavy Vector Boson

Having extended the SM with a heavy scalar particle S in section 6.1, we now consider a slightly more complex BSM theory. Following [25], let us add a heavy vector boson B_μ to the SM with the following representation under the SM gauge group:

$$B_\mu \sim (1, 1)_0.$$

Here, $(R_c, R_L)_Y$ again denote the representation R_c under $SU(3)_c$, the representation R_L under $SU(2)_L$ and the hypercharge Y respectively. Note that $Y = 0$ implies that we are dealing with a real representation. The associated Lagrangian is given by

$$\mathcal{L}_{\text{UV}} = \mathcal{L}_{\text{SM}} + \mathcal{L}_B + \mathcal{L}_{B-SM} + \text{nonlinear}, \quad (6.2.1)$$

where \mathcal{L}_B contains terms quadratic in the vector boson B_μ (i.e. the kinetic term and the mass term), and \mathcal{L}_{B-SM} contains terms involving B_μ that are linearly coupled to the SM. To be explicit,

$$\mathcal{L}_B = -\frac{1}{2}D_\mu B_\nu^\dagger D^\mu B^\nu - \frac{1}{2}D_\mu B_\nu^\dagger D^\nu B^\mu + \frac{1}{2}M_B^2 B_\mu^\dagger B^\mu \quad (6.2.2)$$

$$\mathcal{L}_{B-SM} = -\frac{1}{2}(B^{\mu\dagger} J_\mu^B + \text{h.c.}). \quad (6.2.3)$$

Here, J_μ^B defines the vector current, which couples the heavy vector boson to the quarks according to

$$J_\mu^B = (g_B^q)_{ij} \bar{q}_L^i \gamma_\mu q_L^j + (g_B^u)_{ij} \bar{u}_R^i \gamma_\mu u_R^j + (g_B^d)_{ij} \bar{d}_R^i \gamma_\mu d_R^j. \quad (6.2.4)$$

Let us now derive the effective Lagrangian. Similarly to the scalar case in (6.1.8), we integrate out the heavy vector B_μ . This gives

$$\mathcal{L}_{\text{eff}} = \mathcal{L}_{\text{SM}} - \frac{1}{2M_B^2} (J_\mu^B)^\dagger J^{B\mu} + \mathcal{O}\left(\frac{1}{M_B^4}\right).$$

Working at leading order, and substituting the vector current (6.2.4) into the above, we thus obtain

$$\begin{aligned} \mathcal{L}_{\text{eff}} &= \mathcal{L}_{\text{SM}} - \frac{1}{2M_B^2} \left((g_B^q)_{ij} \bar{q}_L^i \gamma_\mu q_L^j + (g_B^u)_{ij} \bar{u}_R^i \gamma_\mu u_R^j + (g_B^d)_{ij} \bar{d}_R^i \gamma_\mu d_R^j \right) \\ &\quad \left((g_B^q)_{kl} \bar{q}_L^k \gamma_\mu q_L^l + (g_B^u)_{kl} \bar{u}_R^k \gamma_\mu u_R^l + (g_B^d)_{kl} \bar{d}_R^k \gamma_\mu d_R^l \right) \\ &\equiv \mathcal{L}_{\text{SM}} + \sum_i \frac{\alpha_i}{M_B^2} \mathcal{O}_i, \end{aligned} \quad (6.2.5)$$

where the operators \mathcal{O}_i are in the ‘‘Buchmüller’’-basis [26] (not the Warsaw-basis!). The coefficients α_i are collected in appendix B of ref. [25]. From there we deduce that

$$\begin{aligned} \sum_i \frac{\alpha_i}{M_B^2} \mathcal{O}_i &= -\frac{(g_B^q)_{ij} (g_B^q)_{kl}}{M_B^2} \mathcal{O}_{qq}^{(1,1)ijkl} - \frac{(g_B^u)_{ij} (g_B^u)_{kl}}{M_B^2} \mathcal{O}_{uu}^{(1)ijkl} - \frac{(g_B^d)_{ij} (g_B^d)_{kl}}{M_B^2} \mathcal{O}_{dd}^{(1)ijkl} \\ &\quad - \frac{2(g_B^d)_{ij} (g_B^u)_{kl}}{M_B^2} \mathcal{O}_{du}^{(1)ijkl} + \frac{2(g_B^q)_{il} (g_B^u)_{kj}}{3M_B^2} \mathcal{O}_{qu}^{(1)ijkl} + \frac{(g_B^q)_{il} (g_B^u)_{kj}}{M_B^2} \mathcal{O}_{qu}^{(8)ijkl} \\ &\quad + \frac{2(g_B^q)_{il} (g_B^d)_{kj}}{3M_B^2} \mathcal{O}_{qd}^{(1)ijkl} + \frac{(g_B^q)_{il} (g_B^d)_{kj}}{M_B^2} \mathcal{O}_{qd}^{(8)ijkl}. \end{aligned} \quad (6.2.6)$$

So we have generated eight dimension-six operators in total by integrating out the heavy vector boson. The operators \mathcal{O}_i in (6.2.6) are defined in Table 6.3. Some of these are already in the Warsaw basis, in which case this is indicated by a tick in the second column together with the relevant operator. Here, generation indices i, j, k, l are left implicit, and can be easily restored. For example, $\mathcal{O}_{qq}^{(1,1)ijkl} = \frac{1}{2}(\bar{q}_L^i \gamma_\mu q_L^j)(\bar{q}_L^k \gamma^\mu q_L^l)$. The notation $\mathcal{O}_{ud}^{(1)}$ and $\mathcal{O}_{du}^{(1)}$ is used interchangeably, since they refer to the same operator.

	Operator (“Buchmüller”-basis)	Warsaw
1.	$\mathcal{O}_{qq}^{(1,1)} \equiv \frac{1}{2}(\bar{q}_L \gamma_\mu q_L)(\bar{q}_L \gamma^\mu q_L)$	✓ $\frac{1}{2} \mathcal{Q}_{qq}^{(1)}$
2.	$\mathcal{O}_{uu}^{(1)} \equiv \frac{1}{2}(\bar{u}_R \gamma_\mu u_R)(\bar{u}_R \gamma^\mu u_R)$	✓ $\frac{1}{2} \mathcal{Q}_{uu}$
3.	$\mathcal{O}_{dd}^{(1)} \equiv \frac{1}{2}(\bar{d}_R \gamma_\mu d_R)(\bar{d}_R \gamma^\mu d_R)$	✓ $\frac{1}{2} \mathcal{Q}_{dd}$
4.	$\mathcal{O}_{ud}^{(1)} \equiv (\bar{u}_R \gamma_\mu u_R)(\bar{d}_R \gamma^\mu d_R)$	✓ $\mathcal{Q}_{ud}^{(1)}$
5.	$\mathcal{O}_{qu}^{(1)} \equiv (\bar{q}_L u_R)(\bar{u}_R q_L)$	×
6.	$\mathcal{O}_{qu}^{(8)} \equiv (\bar{q}_L T_A u_R)(\bar{u}_R T_A q_L)$	×
7.	$\mathcal{O}_{qd}^{(1)} \equiv (\bar{q}_L d_R)(\bar{d}_R q_L)$	×
8.	$\mathcal{O}_{qd}^{(8)} \equiv (\bar{q}_L T_A d_R)(\bar{d}_R T_A q_L)$	×

Table 6.3: *Dimension-six operators generated in the heavy vector boson EFT (6.2.5). The Warsaw operators are denoted by \mathcal{Q} to distinguish them from the “Buchmüller” operators \mathcal{O}_i . We refer the reader to appendix A for a definition of the Warsaw operators. Generation indices i, j, k, l are left implicit.*

The idea is now to convert operators 5 – 8 to the Warsaw basis. Let us start with operators 5 and 7. Applying the Fierz identity from equation (6.1.13), we find

$$\begin{aligned}
\mathcal{O}_{qu}^{(1)ijkl} &= (\bar{q}_L^i u_R^j)(\bar{u}_R^k q_L^l) = \frac{1}{2}(\bar{q}_L^i \gamma_\mu q_L^l)(\bar{u}_R^k \gamma^\mu u_R^j) = \frac{1}{2} \mathcal{Q}_{qu}^{(1)ilkj} \\
\mathcal{O}_{qd}^{(1)ijkl} &= (\bar{q}_L^i d_R^j)(\bar{d}_R^k q_L^l) = \frac{1}{2}(\bar{q}_L^i \gamma_\mu q_L^l)(\bar{d}_R^k \gamma^\mu d_R^j) = \frac{1}{2} \mathcal{Q}_{qd}^{(1)ilkj}.
\end{aligned} \tag{6.2.7}$$

Next, we convert operator 6:

$$\begin{aligned}
\mathcal{O}_{qu}^{(8)ijkl} &= (\bar{q}_L^i T_A u_R^j)(\bar{u}_R^k T_A q_L^l) \\
&= (\bar{q}_L^\alpha T_{\alpha\beta}^A u_R^\beta)(\bar{u}_R^\kappa T_{\kappa\lambda}^A q_L^\lambda) \\
&= (\bar{q}_L^\alpha u_R^\beta)(\bar{u}_R^\kappa q_L^\lambda) \left(\frac{1}{2} \delta_{\alpha\lambda} \delta_{\kappa\beta} - \frac{1}{6} \delta_{\alpha\beta} \delta_{\kappa\lambda} \right) \\
&= \frac{1}{2} (\bar{q}_L^\alpha u_R^\beta)(\bar{u}_R^\beta q_L^\alpha) - \frac{1}{6} (\bar{q}_L^\alpha u_R^\alpha)(\bar{u}_R^\beta q_L^\beta) \\
&= -\frac{1}{6} (\bar{q}_L u_R)(\bar{u}_R q_L) \\
&= -\frac{1}{12} (\bar{q}_L \gamma_\mu q_L)(\bar{u}_R \gamma^\mu u_R) \\
&= -\frac{1}{12} \mathcal{Q}_{qu}^{(1)ilkj}. \tag{6.2.8}
\end{aligned}$$

Let us comment on the various steps we take in (6.2.8). We leave the generation indices implicit in going from the first to the second line and the colour indices are denoted by the Greek-letters $\alpha, \beta, \kappa, \lambda$. We furthermore use on the third line that

$$T_{\alpha\beta}^A T_{\kappa\lambda}^A = \frac{1}{2} \delta_{\alpha\lambda} \delta_{\kappa\beta} - \frac{1}{6} \delta_{\alpha\beta} \delta_{\kappa\lambda}$$

and the first term on the fourth line in (6.2.8) vanishes, because $\bar{q}_L^\alpha q_L^\alpha$ projects to zero. Also, in order to remove the gamma-matrices we apply the Fierz identity from (6.1.13) on the second to last line. Finally, we restore the generation indices again on the last line.

Converting operator 8 proceeds analogously, and so we find

$$\mathcal{O}_{qd}^{(8)ijkl} = -\frac{1}{12} \mathcal{Q}_{qd}^{(1)ilkj}. \tag{6.2.9}$$

Having converted all the operators to the Warsaw basis, let us give an overview of our results in Table 6.4. It is a conversion Table that shows how to go from the ‘‘Buchmüller’’-basis to the Warsaw-basis.

Continuing, we substitute operators (6.2.7) – (6.2.9) into the effective Lagrangian from (6.2.5) together with (6.2.6), to obtain

$$\begin{aligned}
\mathcal{L}_{\text{eff}} = \mathcal{L}_{\text{SM}} &- \frac{(g_B^q)_{ij}(g_B^q)_{kl}}{2M_B^2} \mathcal{Q}_{qq}^{(1)ijkl} - \frac{(g_B^u)_{ij}(g_B^u)_{kl}}{2M_B^2} \mathcal{Q}_{uu}^{ijkl} - \frac{(g_B^d)_{ij}(g_B^d)_{kl}}{2M_B^2} \mathcal{Q}_{dd}^{ijkl} \\
&- \frac{2(g_B^d)_{ij}(g_B^u)_{kl}}{M_B^2} \mathcal{Q}_{du}^{(1)ijkl} + \frac{(g_B^q)_{il}(g_B)_{kj}}{3M_B^2} \mathcal{Q}_{qu}^{(1)ilkj} - \frac{(g_B^q)_{il}(g_B^u)_{kj}}{12M_B^2} \mathcal{Q}_{qu}^{(1)ilkj} \\
&+ \frac{(g_B^q)_{il}(g_B^d)_{kj}}{3M_B^2} \mathcal{Q}_{qd}^{(1)ilkj} - \frac{(g_B^q)_{il}(g_B^d)_{kj}}{12M_B^2} \mathcal{O}_{qd}^{(1)ilkj}. \tag{6.2.10}
\end{aligned}$$

Gathering common terms, and relabeling generation-indices, finally gives

$$\begin{aligned}
\mathcal{L}_{\text{eff}} = \mathcal{L}_{\text{SM}} &- \frac{(g_B^q)_{ij}(g_B^q)_{kl}}{2M_B^2} \mathcal{Q}_{qq}^{(1)ijkl} - \frac{(g_B^u)_{ij}(g_B^u)_{kl}}{2M_B^2} \mathcal{Q}_{uu}^{ijkl} - \frac{(g_B^d)_{ij}(g_B^d)_{kl}}{2M_B^2} \mathcal{Q}_{dd}^{ijkl} \\
&- \frac{2(g_B^d)_{ij}(g_B^u)_{kl}}{M_B^2} \mathcal{Q}_{du}^{(1)ijkl} + \frac{(g_B^q)_{ij}(g_B^u)_{kl}}{4M_B^2} \mathcal{Q}_{qu}^{(1)ijkl} + \frac{(g_B^q)_{ij}(g_B^d)_{kl}}{4M_B^2} \mathcal{Q}_{qd}^{(1)ijkl}. \tag{6.2.11}
\end{aligned}$$

	Operator (“Buchmüller”-basis)	Warsaw
1.	$\mathcal{O}_{qq}^{(1,1)ijkl}$	$\frac{1}{2}\mathcal{Q}_{qq}^{(1)ijkl}$
2.	$\mathcal{O}_{uu}^{(1)ijkl}$	$\frac{1}{2}\mathcal{Q}_{uu}^{ijkl}$
3.	$\mathcal{O}_{dd}^{(1)ijkl}$	$\frac{1}{2}\mathcal{Q}_{dd}^{ijkl}$
4.	$\mathcal{O}_{ud}^{(1)ijkl}$	$\mathcal{Q}_{ud}^{(1)ijkl}$
5.	$\mathcal{O}_{qu}^{(1)ijkl}$	$\frac{1}{2}\mathcal{Q}_{qu}^{(1)ilkj}$
6.	$\mathcal{O}_{qu}^{(8)ijkl}$	$-\frac{1}{12}\mathcal{Q}_{qu}^{(1)ilkj}$
7.	$\mathcal{O}_{qd}^{(1)ijkl}$	$\frac{1}{2}\mathcal{Q}_{qd}^{(1)ilkj}$
8.	$\mathcal{O}_{qd}^{(8)ijkl}$	$-\frac{1}{12}\mathcal{Q}_{qd}^{(1)ilkj}$

Table 6.4: *Conversion Table that shows how to the conversion from the “Buchmüller”-operators to the Warsaw operators. The generation-indices i, j, k, l are written explicitly.*

The effective Lagrangian (6.2.11) then defines our final working expression in the Warsaw-basis.

We can now use the SMEFiT bounds to put bounds on the UV-parameters in the heavy vector model. From the operators appearing in equation (6.2.11), the ones that have corresponding SMEFiT bounds are presented in Table 6.5. Note how we are able to use the 2L2H operators in this case, as opposed to before in the heavy scalar model from section 6.1. This will lead to more stringent bounds on the UV-parameters, since the 2L2H operators are sensitive to more top-quark processes than the four-heavy quark operators. Again, The SMEFiT bounds are obtained by a NS-run (see Chapter 4) when only one operator is constrained at a time¹.

Identifying the coefficients in equation (6.2.11) with the coefficients in Table 6.5, therefore results in the following bounds on the UV-parameters g_B^q, g_B^u, g_B^d and M_B at order $\mathcal{O}(\Lambda^{-2})$:

¹When the Warsaw operators are linear combinations of the SMEFT degrees of freedom, we have propagated the 95% CL by the standard formula $\text{Var}(z) = \left(\frac{\partial f(x,y)}{\partial x}\right)^2 \text{Var}(x) + \left(\frac{\partial f(x,y)}{\partial y}\right)^2 \text{Var}(y)$, with $z \equiv f(x, y)$. In general, the 95% CL for operator X is determined from the NS samples by computing $\bar{X} \pm 1.96 \cdot \hat{\sigma}/\sqrt{n}$, where \bar{X} is the sample mean, $\hat{\sigma}$ the estimator of the standard deviation of the sample mean and n the number of NS samples.

2L2H	$\mathcal{O}(\Lambda^{-2})$	$\mathcal{O}(\Lambda^{-4})$
$\frac{1}{4}(081\text{qq} + 3083\text{qq}) = C_{qq}^{(1)i33i}$	$[-1.415, -1.341]$	$[-0.205, -0.185]$
$011\text{qq} - \frac{1}{6}081\text{qq} = C_{qq}^{(1)ii33}$	$[-0.732, -0.645]$	$[0.0371, 0.0498]$
$\frac{1}{2}08\text{ut} = C_{uu}^{i33i}$	$[-0.441, -0.421]$	$[-0.374, -0.354]$
$01\text{ut} - \frac{1}{6}08\text{ut} = C_{uu}^{ii33}$	$[-0.00317, 0.00643]$	$[-1.223, -1.200]$
$01\text{dt} = C_{ud}^{(1)33ii}$	$[-1.311, -1.188]$	$[-0.0338, -0.0152]$
$01\text{qu} = C_{qu}^{(1)33ii}$	$[0.951, 1.002]$	$[0.0807, 0.0951]$
$01\text{qt} = C_{qu}^{(1)ii33}$	$[0.090, 0.191]$	$[0.00268, 0.0144]$
$01\text{qd} = C_{qd}^{(1)33ii}$	$[0.919, 1.037]$	$[0.0282, 0.0475]$

Table 6.5: The 95% confidence level intervals (in units of TeV^{-2} , with $\Lambda = 1 \text{ TeV}$) for the dimension-six operators appearing in the effective Lagrangian (6.2.11) at order $\mathcal{O}(\Lambda^{-2})$ and $\mathcal{O}(\Lambda^{-4})$. The bounds are obtained by a NS-run when only a single operator is constrained at a time.

$$\begin{aligned}
-1.415 &< -\frac{(g_B^q)_{i3}(g_B^q)_{3i}}{2M_B^2} < -1.341 \quad \text{TeV}^{-2} \\
-0.732 &< -\frac{(g_B^q)_{ii}(g_B^q)_{33}}{2M_B^2} < -0.645 \quad \text{TeV}^{-2} \\
-0.441 &< -\frac{(g_B^u)_{i3}(g_B^u)_{3i}}{2M_B^2} < -0.421 \quad \text{TeV}^{-2} \\
-0.00317 &< -\frac{(g_B^u)_{ii}(g_B^u)_{33}}{2M_B^2} < 0.00643 \quad \text{TeV}^{-2} \\
-1.311 &< -\frac{2(g_B^u)_{33}(g_B^d)_{ii}}{M_B^2} < -1.188 \quad \text{TeV}^{-2} \\
0.951 &< \frac{(g_B^q)_{33}(g_B^u)_{ii}}{4M_B^2} < 1.002 \quad \text{TeV}^{-2} \\
0.090 &< \frac{(g_B^q)_{ii}(g_B^u)_{33}}{4M_B^2} < 0.191 \quad \text{TeV}^{-2} \\
0.919 &< \frac{(g_B^q)_{33}(g_B^d)_{ii}}{4M_B^2} < 1.037 \quad \text{TeV}^{-2}.
\end{aligned} \tag{6.2.12}$$

Note how the signs work out consistently here in all cases, so that the ratio g_B^2/M_B^2 always has a positive upper bound (as is required for obvious reasons). As in the scalar case, we now specify to the case $(g_B^q)_{ij} = (g_B^u)_{ij} = (g_B^d)_{ij} \equiv g_B \delta_{ij}$. That is, we assume diagonal couplings of equal strength

g_B . Writing only the upper bounds, (6.2.12) then becomes

$$\begin{aligned} \frac{g_B^2}{M_B^2} &< 2 \cdot 1.415 = 2.829 \quad \text{TeV}^{-2} \\ \frac{g_B^2}{M_B^2} &< 2 \cdot 0.733 = 1.463 \quad \text{TeV}^{-2} \\ \frac{g_B^2}{M_B^2} &< 2 \cdot 0.441 = 0.882 \quad \text{TeV}^{-2} \\ \frac{g_B^2}{M_B^2} &< 2 \cdot 0.00317 = 0.00633 \quad \text{TeV}^{-2} \\ \frac{g_B^2}{M_B^2} &< \frac{1}{2} \cdot 1.311 = 0.656 \quad \text{TeV}^{-2} \\ \frac{g_B^2}{M_B^2} &< 4 \cdot 1.002 = 4.008 \quad \text{TeV}^{-2} \\ \frac{g_B^2}{M_B^2} &< 4 \cdot 0.191 = 0.764 \quad \text{TeV}^{-2} \\ \frac{g_B^2}{M_B^2} &< 4 \cdot 1.037 = 4.148 \quad \text{TeV}^{-2}. \end{aligned}$$

So we get multiple different bounds for the ratio g_B^2/M_B^2 , depending on which SMEFiT bound we use. In order to see how stable the results are, we consider the best, worst, and average upper bound:

$$\frac{g_B^2}{M_B^2} < 0.00633 \quad \text{TeV}^{-2} \quad \text{Best, order } \mathcal{O}(\Lambda^{-2}) \quad (6.2.13)$$

$$\frac{g_B^2}{M_B^2} < 4.148 \quad \text{TeV}^{-2} \quad \text{Worst, order } \mathcal{O}(\Lambda^{-2}) \quad (6.2.14)$$

$$\frac{g_B^2}{M_B^2} < 1.845 \quad \text{TeV}^{-2} \quad \text{Average, order } \mathcal{O}(\Lambda^{-2}). \quad (6.2.15)$$

We can also work at order $\mathcal{O}(\Lambda^{-4})$ if we use the higher order bounds from Table 6.5. Repeating the same steps as at order $\mathcal{O}(\Lambda^{-2})$, we obtain

$$\frac{g_B^2}{M_B^2} < 0.0107 \quad \text{TeV}^{-2} \quad \text{Best, order } \mathcal{O}(\Lambda^{-4}) \quad (6.2.16)$$

$$\frac{g_B^2}{M_B^2} < 2.446 \quad \text{TeV}^{-2} \quad \text{Worst, order } \mathcal{O}(\Lambda^{-4}) \quad (6.2.17)$$

$$\frac{g_B^2}{M_B^2} < 0.581 \quad \text{TeV}^{-2} \quad \text{Average, order } \mathcal{O}(\Lambda^{-4}). \quad (6.2.18)$$

So comparing the results at $\mathcal{O}(\Lambda^{-2})$ and $\mathcal{O}(\Lambda^{-4})$ we conclude that they both give bounds of approximately the same order of magnitude, except for the average bound. Note that the bound on operator $C_{qq}^{(1)ii33}$ at order $\mathcal{O}(\Lambda^{-4})$ leads to an inconsistency, since $0.0371 < -g_B^2/2M_B^2 < 0.0498$ is not allowed for obvious reasons. Therefore, we have decided to drop this contribution and exclude it from the average bound reported here.

Let us conclude this chapter by deriving the Feynman rules for the heavy vector model. We again assume $(g_B^q)_{ij} = (g_B^u)_{ij} = (g_B^d)_{ij} \equiv g_B \delta_{ij}$ and consider

$$\mathcal{L}_{B-SM} = -\frac{1}{2} \left(B^{\mu\dagger} J_\mu^B = \text{h.c.} \right) = -B^\mu J_\mu^B, \quad (6.2.19)$$

with the vector field B^μ taken real. Substituting the vector current (6.2.4), we thus obtain

$$\mathcal{L}_{B-SM} = -g_B B^\mu (\bar{t}\gamma_\mu t + \bar{b}\gamma_\mu b + \bar{c}\gamma_\mu c + \bar{s}\gamma_\mu s + \bar{u}\gamma_\mu u + \bar{d}\gamma_\mu d). \quad (6.2.20)$$

Therefore, the Feynman rule for the $\bar{q}_f q_f B^\mu$ -vertices is given by:

$$= i g_B \gamma^\mu.$$

Finally, the heavy vector boson propagator is given by

$$\mu \overset{p}{\rightsquigarrow} \nu = \frac{i}{p^2 - M_B^2} \left(-g_{\mu\nu} + \frac{p_\mu p_\nu}{M_W^2} \right).$$

Chapter 7

Phenomenology of UV Extensions

In addition to translating the constraints on the Wilson coefficients to bounds on the UV parameters via matching, the latter can also be constrained by experimental data directly. This chapter follows this alternative approach and we study whether it leads to consistent results compared to what we found in chapter 6. We will derive results for both the heavy scalar and the heavy vector boson, introduced in sections 6.1 and 6.2 respectively.

This chapter is structured as follows. We first calculate the differential cross section for $t\bar{t}$ -production in a proton-proton collision at $\sqrt{s} = 13$ TeV in the SM. Later, in section 7.2 we study how this result gets modified by the BSM terms. We are ultimately interested in comparing the BSM prediction to experimental data via a χ^2 -test in section 7.4, which then puts us in the position to find BSM bounds on the UV-parameters c_S , m_S , g_B and M_B that were introduced in sections 6.1 and 6.2. We end this chapter with comparing the resulting BSM bounds and the EFT bounds that we derived in chapter 6.

7.1 Standard Model Contribution

In order to find theoretical predictions for $t\bar{t}$ -production, one starts with considering the relevant subprocesses at the partonic level. These are formed by either two quarks or two gluons in the initial state (see figure 7.1). The first step is to calculate the associated partonic cross section, denoted $\hat{\sigma}$, at leading-order in QCD. In general, partonic variables will carry a hat to distinguish them from their hadronic counterparts. Following this, the partonic cross section will be converted to the hadronic cross section σ by convolution with the parton distribution functions (PDFs):

$$\sigma(p(P_1) + p(P_2) \rightarrow t\bar{t} + X) = \int_0^1 dx_1 \int_0^1 dx_2 \sum_f f_f(x_1) f_{\bar{f}}(x_2) \hat{\sigma}(q_f(x_1 P) + \bar{q}_f(x_2 P) \rightarrow t\bar{t}). \quad (7.1.1)$$

Here, the sum runs over all species of quarks and anti-quarks (that is, $u, d, \bar{u}, \bar{d}, \dots$) except for the top quark, for which there exists no PDF. The PDFs, denoted $f_f(x_i)$, encode the fraction x_i of the

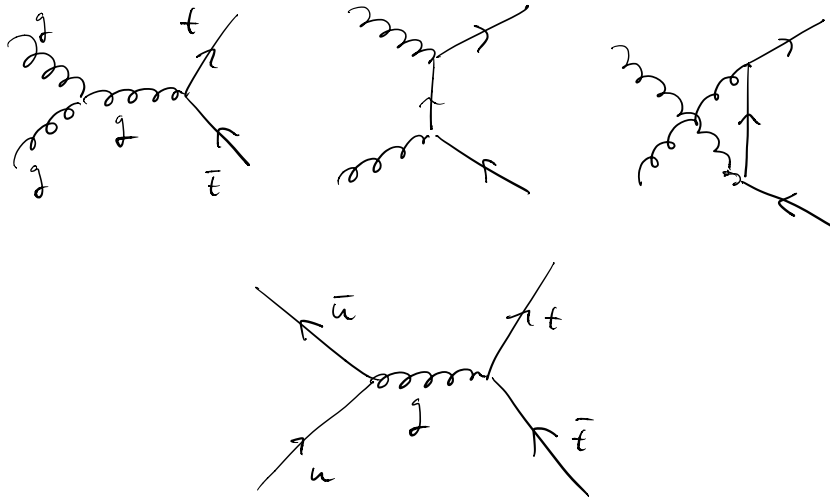


Figure 7.1: Production mechanisms for $t\bar{t}$ -production in the SM at LO. Above: two gluons forming the initial state of $t\bar{t}$ -production. Below: two quarks forming the initial state of $t\bar{t}$ -production. Note that the diagram below has been drawn with an up-quark, but holds in general for any flavour except for the top-quark.

total hadronic momentum that is carried by a parton with flavour f . The X denotes any byproducts resulting from the proton-proton collision. Let us now move on and compute the partonic cross sections of the processes in figure 7.1.

7.1.1 Partonic Cross Sections

Quark-quark initial state

The differential cross section is related to the incoming flux Φ , the matrix element \mathcal{M} and the Lorentz Invariant Phase Space factor (or LIPS for short) as follows:

$$d\hat{\sigma} = \frac{1}{\Phi} |\mathcal{M}|^2 d\Pi_{LIPS}, \quad (7.1.2)$$

where

$$d\Pi_{LIPS} = (2\pi)^4 \delta^4(\Sigma p) \frac{d^3 p_t}{(2\pi)^3} \frac{1}{2E_t} \frac{d^3 p_{\bar{t}}}{(2\pi)^3} \frac{1}{2E_{\bar{t}}} \quad (7.1.3)$$

and

$$\Phi = 4\sqrt{(p_q \cdot p_{\bar{q}})^2 - m_q^2 m_{\bar{q}}^2}. \quad (7.1.4)$$

The delta-function in equation (7.1.3) ensures that 4-momentum is conserved and q denotes one of the incoming quarks. Furthermore, since the masses of the incoming quarks are negligible compared to the top quark's mass, they can be put to zero. With this, the invariant flux Φ simplifies to

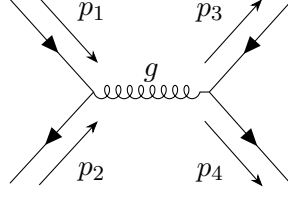


Figure 7.2: Feynman diagram associated to the amplitude in (7.1.10).

$$\Phi = 4p_q \cdot p_{\bar{q}} = 2\hat{s} \quad (\text{massless case}), \quad (7.1.5)$$

where \hat{s} denotes the partonic CM energy squared. The LIPS-factor can also be simplified. Adopting the partonic center of mass (CM) frame, one has $E_t = E_{\bar{t}}$ and $|p_t| = |p_{\bar{t}}|$. Integrating over the 4-momentum $p_{\bar{t}}$ using the delta function, and writing the phase space integral in terms of angular variables, leaves one with

$$\begin{aligned} d\Pi_{LIPS} &= \frac{1}{(2\pi)^2} \delta(E_t + E_{\bar{t}} - E_{CM}) \frac{d^3 p_t}{4E_t^2} \\ &= \frac{1}{16\pi^2} d\Omega \int dp_t \frac{p_t^2}{E_t^2} \delta(2E_t - E_{CM}), \end{aligned} \quad (7.1.6)$$

where $p_t = |p_t|$ for convenience and $E_t = E_{\bar{t}} = \sqrt{p_t^2 + m_t^2}$. In order to evaluate the integral in equation (7.1.6) further, it is convenient to change variables to $x \equiv 2E_t - E_{CM}$. The associated Jacobian of this transformation is

$$\frac{dx}{dp_t} = \frac{d}{dp_t}(2E_t - E_{CM}) = \frac{2p_t}{E_t}. \quad (7.1.7)$$

Hence,

$$\begin{aligned} d\Pi_{LIPS} &= \frac{1}{16\pi^2} d\Omega \int_{2m_t - E_{CM}}^{\infty} dx \frac{p_t}{E_{CM}} \delta(x) \\ &= \frac{1}{16\pi^2} d\Omega \frac{p_t}{E_{CM}} \Theta(E_{CM} - 2m_t), \end{aligned} \quad (7.1.8)$$

where the Heaviside-function Θ ensures that no top-quarks can be produced below threshold. With these simplifications in place, the cross section differential from equation (7.1.2) becomes:

$$d\hat{\sigma} = \frac{1}{2\hat{s}} |\mathcal{M}|^2 \frac{1}{16\pi^2} d\Omega \frac{p_t}{E_{CM}} \theta(E_{CM} - 2m_t). \quad (7.1.9)$$

The last missing piece is to calculate the matrix element \mathcal{M} . Applying the SM Feynman rules to the diagram in figure 7.2, gives:

$$\begin{aligned} i\mathcal{M} &= \bar{v}(p_2) (ig_s \gamma^\mu t_{ij}^A) u(p_1) \left(\frac{-ig_{\mu\nu}}{\hat{s}} \delta^{AB} \right) \bar{u}(p_3) (ig_s \gamma^\nu t_{kl}^B) v(p_4) \\ &= ig_s^2 t_{ij}^A t_{kl}^A \frac{1}{\hat{s}} [\bar{v}(p_2) \gamma^\mu u(p_1) \bar{u}(p_3) \gamma_\mu v(p_4)], \end{aligned} \quad (7.1.10)$$

where A, B label the generators of $SU(3)$ in the fundamental representation of $SU(3)$. Therefore,

$$\mathcal{M} = g_s^2 t_{ij}^A t_{kl}^A \frac{1}{\hat{s}} [\bar{v}(p_2) \gamma^\mu u(p_1) \bar{u}(p_3) \gamma_\mu v(p_4)], \quad (7.1.11)$$

where the product $t_{ij}^A t_{kl}^A$ forms the colour factor. Apart from this factor, the matrix element \mathcal{M} is identical to the corresponding process $e^+ e^- \rightarrow \mu^+ \mu^-$ in QED. Since one cannot observe individual colours, and spin is not measured, the matrix element squared must include the average and sum over incoming and outgoing colours/spins respectively and shall henceforth be denoted $|\bar{\mathcal{M}}|^2$. Explicitly,

$$\begin{aligned} |\bar{\mathcal{M}}|^2 &= \frac{1}{3} \cdot \frac{1}{3} \cdot \frac{1}{2} \cdot \frac{1}{2} \sum_{\text{colour}} \sum_{\text{spin}} |\mathcal{M}|^2 \\ &= \left(\frac{1}{9} \sum_{i,j,k,l} (t_{ij}^A t_{kl}^A) (t_{ij}^B t_{kl}^B)^* \right) \cdot \left(\frac{1}{4} \sum_{\text{spin}} \frac{g_s^4}{\hat{s}^2} |\bar{v}(p_2) \gamma^\mu u(p_1) \bar{u}(p_3) \gamma_\mu v(p_4)|^2 \right) \end{aligned} \quad (7.1.12)$$

Using that the $SU(3)$ generators are Hermitean, the first term in parenthesis (i.e. the colour factor) evaluates to

$$\begin{aligned} \frac{1}{9} \sum_{i,j,k,l} (t_{ij}^A t_{kl}^A) (t_{ij}^B t_{kl}^B)^* &= \frac{1}{9} \sum_{i,j,k,l} t_{ij}^A t_{kl}^A t_{ji}^B t_{lk}^B \\ &= \frac{1}{9} \text{Tr}(t^A t^B) \text{Tr}(t^A t^B) \\ &= \frac{2}{9}. \end{aligned} \quad (7.1.13)$$

The second term in parenthesis in equation (7.1.12), or the QED part, can be evaluated using Dirac traces as will be shown now.

$$\begin{aligned} &\frac{1}{4} \sum_{\text{spin}} \frac{g_s^4}{\hat{s}^2} [\bar{v}(p_2) \gamma^\mu u(p_1) \bar{u}(p_3) \gamma_\mu v(p_4)] \cdot [\bar{v}(p_4) \gamma_\nu u(p_3) \bar{u}(p_1) \gamma^\nu v(p_2)] \\ &= \frac{g_s^4}{4\hat{s}^2} \text{Tr}[(\not{p}_4 - m_4) \gamma_\nu (\not{p}_3 + m_3) \gamma_\mu] \cdot \text{Tr}[(\not{p}_1 + m_1) \gamma^\nu (\not{p}_2 - m_2) \gamma^\mu] \end{aligned}$$

Using that $m_1 = m_2 = 0$ and $m_3 = m_4 = m_t$, gives

$$= \frac{g_s^4}{4\hat{s}^2} \text{Tr}[(\not{p}_4 - m_t) \gamma_\nu (\not{p}_3 + m_t) \gamma_\mu] \cdot \text{Tr}[(\not{p}_1) \gamma^\nu (\not{p}_2) \gamma^\mu]$$

Since the trace over an odd number of gamma matrices vanishes, one obtains

$$= \frac{g_s^4}{4\hat{s}^2} (\text{Tr}[\not{p}_4 \gamma_\nu \not{p}_3 \gamma_\mu] - m_t^2 \text{Tr}[\gamma_\nu \gamma_\mu]) \cdot 4(p_1^\nu p_2^\mu + p_1^\mu p_2^\nu - p_{12} g^{\nu\mu})$$

where we used that $\text{Tr}[\gamma^\rho \gamma^\nu \gamma^\sigma \gamma^\mu] = 4(g^{\rho\nu} g^{\sigma\mu} + g^{\rho\mu} g^{\nu\sigma} - g^{\rho\sigma} g^{\nu\mu})$. The notation p_{ij} is short for $(p_i)^\mu (p_j)_\mu$. Using this identity for the first term as well, and noting that $\text{Tr}[\gamma_\mu \gamma_\nu] = 4g_{\mu\nu}$, results in

$$= \frac{g_s^4}{4\hat{s}^2} (4(p_{4\nu} p_{3\mu} + p_{4\mu} p_{3\nu} - p_{34} g_{\nu\mu}) - 4m_t^2 g_{\mu\nu}) \cdot 4(p_1^\nu p_2^\mu + p_1^\mu p_2^\nu - p_{12} g^{\nu\mu})$$

Expanding terms, performing contractions and cancelling common terms, gives

$$= \frac{8g_s^2}{\hat{s}^2} (p_{14}p_{32} + p_{13}p_{24} + m_t^2 p_{12})$$

In the CM-frame, one has $p_1 = (E, 0, 0, E)$, $p_2 = (E, 0, 0, -E)$, $p_3 = (E, \vec{p}_t)$ and $p_4 = (E, -\vec{p}_t)$.

Substituting these into the above, yields

$$\begin{aligned} &= \frac{8g_s^2}{\hat{s}^2} \left((E^2 + E\sqrt{E^2 - m_t^2} \cos \theta)^2 + (E^2 - E\sqrt{E^2 - m_t^2} \cos \theta)^2 + 2m_t^2 E^2 \right) \\ &= \frac{8g_s^2}{\hat{s}^2} \cdot 2 \left(E^4 + E^2(E^2 - m_t^2) \cos^2 \theta + m_t^2 E^2 \right) \end{aligned}$$

Upon using $4E^2 = \hat{s}$ to rewrite everything in terms of the Mandelstam variable \hat{s} , the above takes the following form:

$$= g_s^2 \left(1 + \frac{4m_t^2}{\hat{s}} + \left(1 - \frac{4m_t^2}{\hat{s}} \right) \cos^2 \theta \right). \quad (7.1.14)$$

So, the following is seen to hold:

$$\frac{1}{4} \sum_{\text{spin}} \frac{g_s^4}{\hat{s}^2} |\bar{v}(p_2) \gamma^\mu u(p_1) \bar{u}(p_3) \gamma_\mu v(p_4)|^2 = g_s^2 \left(1 + \frac{4m_t^2}{\hat{s}} + \left(1 - \frac{4m_t^2}{\hat{s}} \right) \cos^2 \theta \right). \quad (7.1.15)$$

Substituting equations (7.1.15) and (7.1.13) into equation (7.1.12), then finally gives for the squared amplitude

$$|\bar{\mathcal{M}}|^2 = \frac{2}{9} \cdot g_s^2 \left(1 + \frac{4m_t^2}{\hat{s}} + \left(1 - \frac{4m_t^2}{\hat{s}} \right) \cos^2 \theta \right). \quad (7.1.16)$$

Recall equation (7.1.2) for the differential cross section. With the matrix element $|\bar{\mathcal{M}}|^2$ just derived, this becomes:

$$\begin{aligned} d\hat{\sigma} &= \frac{1}{2\hat{s}} \frac{1}{16\pi^2} \frac{p_t}{\sqrt{\hat{s}}} \cdot \frac{2}{9} g_s^2 \left(1 + \frac{4m_t^2}{\hat{s}} + \left(1 - \frac{4m_t^2}{\hat{s}} \right) \cos^2 \theta \right) d\Omega \\ &= \frac{2}{9} \frac{g_s^2}{64\pi^2 \hat{s}} \sqrt{1 - \frac{4m_t^2}{\hat{s}}} \left(1 + \frac{4m_t^2}{\hat{s}} + \left(1 - \frac{4m_t^2}{\hat{s}} \right) \cos^2 \theta \right) d\Omega. \end{aligned} \quad (7.1.17)$$

Lastly, the partonic cross section $\hat{\sigma}$ can now be straightforwardly found by integrating the scattering angle over the full phase space:

$$\begin{aligned} \hat{\sigma} &= \int \frac{d\hat{\sigma}}{d\Omega} d\Omega = 2\pi \int \frac{d\hat{\sigma}}{d\Omega} \sin \theta d\theta \\ &= \frac{2}{9} \cdot \frac{g_s^4}{12\pi \hat{s}} \sqrt{1 - \frac{4m_t^2}{\hat{s}}} \left(1 + \frac{2m_t^2}{\hat{s}} \right). \end{aligned} \quad (7.1.18)$$

Equivalently, one can express the above in terms of the QCD coupling constant $\alpha_s = g_s^2/4\pi$ to end up with

$$\hat{\sigma} = \frac{2}{9} \frac{4\pi \alpha_s^2}{3\hat{s}} \sqrt{1 - \frac{4m_t^2}{\hat{s}}} \left(1 + \frac{2m_t^2}{\hat{s}} \right). \quad (7.1.19)$$

Gluon-gluon initial state

So far only the quark-quark initial state has been considered. However, the process $gg \rightarrow t\bar{t}$ makes up the dominant contribution to top-pair production in fact. It is therefore essential to go through a similar analysis as before, but this time with two gluons forming the initial state. The derivation of the partonic cross section $\hat{\sigma}(gg \rightarrow t\bar{t})$ is quite involved however, so a full derivation will not be given here. Instead, the result is adopted from [27] and reads:

$$\frac{d\hat{\sigma}(gg \rightarrow t\bar{t})}{d\hat{t}} = \frac{\pi\alpha_S^2}{64\hat{s}^2} \left[12M_{ss} + \frac{16}{3}(M_{tt} + M_{uu}) - \frac{2}{3}M_{tu} + 6(M_{st} + M_{su}) \right], \quad (7.1.20)$$

with

$$\begin{aligned} M_{ss} &= \frac{4}{\hat{s}^2}(\hat{t} - m_t^2)(\hat{u} - m_t^2) \\ M_{tt} &= \frac{2}{(\hat{t} - m_t^2)^2} [(\hat{t} - m_t^2)(\hat{u} - m_t^2) - 2m_t^2(\hat{u} + m_t^2)] \\ M_{tu} &= \frac{4m_t^2}{(\hat{t} - m_t^2)(\hat{u} - m_t^2)}(\hat{s} - 4m_t^2) \\ M_{st} &= \frac{4}{\hat{s}(\hat{t} - m_t^2)} [m_t^4 - \hat{t}(\hat{s} + \hat{t})], \end{aligned}$$

and $M_{uu} = M_{tt}\{t \leftrightarrow u\}$, $M_{su} = M_{st}\{t \leftrightarrow u\}$. The conversion of the differential partonic cross section to a total cross section proceeds via an integration over the Mandelstam variable \hat{t} . In order to find its associated integration range, note that

$$\hat{t} = (p_g - p_t)^2 = m_g^2 + m_t^2 - 2p_g \cdot p_t = m_t^2 - 2E^2 + 2\vec{p}_g \cdot \vec{p}_t = m_t^2 - 2E^2 + 2|\vec{p}_g||\vec{p}_t| \cos \theta,$$

Upon using the relativistic dispersion relation we find that \hat{t} lies between t_{min} and t_{max} , with

$$t_{max,min} = m_t^2 - 2E^2 \pm 2E\sqrt{E^2 - m_t^2}. \quad (7.1.21)$$

Hence, the total partonic cross section is given by

$$\hat{\sigma}(gg \rightarrow t\bar{t}) = \int_{t_{min}}^{t_{max}} \frac{d\hat{\sigma}(gg \rightarrow t\bar{t})}{d\hat{t}} d\hat{t}, \quad (7.1.22)$$

with $d\hat{\sigma}(gg \rightarrow t\bar{t})/d\hat{t}$ given by equation (7.1.20).

7.1.2 Differential Hadronic Cross Section

In experiments, hadronic cross sections are often presented as differentials in particular kinematic variables such as the invariant mass, rapidity or transverse momentum. Therefore, equation (7.1.1) needs to be manipulated so as to arrive at a differential cross section instead. Here, the aim is to derive an expression for the hadronic cross section as a differential in the invariant mass of the outgoing parton pair.

Taking equation (7.1.1) as a starting point, the first step is to change variables from x_1, x_2 to \hat{s} and the rapidity Y :

$$x_1 \equiv \sqrt{\frac{\hat{s}}{s}} e^Y \quad \text{and} \quad x_2 \equiv \sqrt{\frac{\hat{s}}{s}} e^{-Y}.$$

The associated Jacobian of the transformation equals

$$\frac{\partial(x_1, x_2)}{\partial(\hat{s}, Y)} = \frac{1}{s} = \frac{x_1 x_2}{\hat{s}}, \quad (7.1.23)$$

where we used that $\hat{s} = x_1 x_2 s$. Hence, equation (7.1.1) can be rewritten as

$$\sigma(pp \rightarrow t\bar{t}) = \sum_f \int d\hat{s} \int dY \frac{\partial(x_1, x_2)}{\partial(\hat{s}, Y)} f_f(x_1) f_{\bar{f}}(x_2) \hat{\sigma}(q_f + \bar{q}_f \rightarrow t\bar{t}),$$

Consequently,

$$\begin{aligned} \frac{d\sigma}{d\hat{s}} &= \int dY \frac{1}{s} \sum_f \hat{\sigma}(q_f + \bar{q}_f \rightarrow t\bar{t}) f_f(x_1) f_{\bar{f}}(x_2) \\ &= \int dY \frac{1}{s} \sum_f \hat{\sigma}\left(q_f\left(\sqrt{\frac{\hat{s}}{s}} e^Y\right) + \bar{q}_f\left(\sqrt{\frac{\hat{s}}{s}} e^{-Y}\right) \rightarrow t\bar{t}\right) f_f\left(\sqrt{\frac{\hat{s}}{s}} e^Y\right) f_{\bar{f}}\left(\sqrt{\frac{\hat{s}}{s}} e^{-Y}\right). \end{aligned} \quad (7.1.24)$$

Since the incoming quarks are taken massless, the partonic $\hat{\sigma}$ is independent of the incoming flavour and can thus be pulled outside the sum. Taking this into account, and presenting the result as a differential in $\sqrt{\hat{s}}$ instead, one arrives at

$$\frac{d\sigma}{d\sqrt{\hat{s}}} = \frac{2\sqrt{\hat{s}}}{s} \int_{-\frac{1}{2}\ln\frac{\hat{s}}{s}}^{\frac{1}{2}\ln\frac{\hat{s}}{s}} dY \hat{\sigma}(q_f + \bar{q}_f \rightarrow t\bar{t}) \sum_f f_f\left(\sqrt{\frac{\hat{s}}{s}} e^Y\right) f_{\bar{f}}\left(\sqrt{\frac{\hat{s}}{s}} e^{-Y}\right), \quad (7.1.25)$$

where the integration limits ensure that the argument of the PDFs do not exceed one, i.e. remain within the physical region. The above did not yet include the gluon-gluon initial state. Adding this contribution, simply gives:

$$\begin{aligned} \frac{d\sigma}{d\sqrt{\hat{s}}} &= \frac{2\sqrt{\hat{s}}}{s} \int dY \hat{\sigma}(q_f + \bar{q}_f \rightarrow t\bar{t}) \sum_f f_f\left(\sqrt{\frac{\hat{s}}{s}} e^Y\right) f_{\bar{f}}\left(\sqrt{\frac{\hat{s}}{s}} e^{-Y}\right) + \\ &\quad \frac{2\sqrt{\hat{s}}}{s} \int dY \hat{\sigma}(gg \rightarrow t\bar{t}) f_g\left(\sqrt{\frac{\hat{s}}{s}} e^Y\right) f_g\left(\sqrt{\frac{\hat{s}}{s}} e^{-Y}\right). \end{aligned} \quad (7.1.26)$$

This concludes the derivation of the hadronic cross section differential in the invariant mass of the outgoing top quarks. The following subsection is devoted to a short discussion about dynamical renormalization scales, a feature carried by the PDFs.

7.1.3 Dynamical Renormalization Scale

The parton distribution functions $f(x_i; \mu_R)$ do not only depend on the fraction of momentum x_i , but also on the renormalization scale μ_R . This can be either set fixed, or allowed to run as a

function of the kinematics. Here, one particular choice of scale shall be discussed in anticipation of upcoming results that use this same scale. Consider letting μ_R grow proportionally to the sum of the partonic transverse masses, denoted H_T :

$$\mu_R = \frac{H_T}{4} = \frac{1}{4} \left(\sqrt{m_t^2 + p_{T,t}^2} + \sqrt{m_{\bar{t}}^2 + p_{T,\bar{t}}^2} \right), \quad (7.1.27)$$

where p_T denotes the transverse momentum, defined as the momentum in the direction transverse to the incoming beam's axis:

$$p_T = \sqrt{\frac{\hat{s}}{4} - m_t^2} \sin \theta. \quad (7.1.28)$$

To accommodate this choice of dynamical scale, one needs to retain information about the scattering angle θ in the derivation of the partonic cross section. In other words,

$$\frac{d\sigma}{d\sqrt{\hat{s}}} = \frac{2\sqrt{\hat{s}}}{s} \int d\theta \int dY \sum_f f_1(x_1; H_T/4) f_2(x_2; H_T/4) \frac{d\hat{\sigma}}{d\theta}. \quad (7.1.29)$$

In the case of a quark-quark initial state, $d\hat{\sigma}/d\theta$ can be readily read off from equation (7.1.17):

$$\frac{d\hat{\sigma}(q_f + q_{\bar{f}} \rightarrow t\bar{t})}{d\theta} = 2\pi \sin \theta \cdot \frac{2}{9} \frac{g_s^2}{64\pi^2 \hat{s}} \sqrt{1 - \frac{4m_t^2}{\hat{s}}} \left(1 + \frac{4m_t^2}{\hat{s}} + \left(1 - \frac{4m_t^2}{\hat{s}} \right) \cos^2 \theta \right). \quad (7.1.30)$$

As for the gluon-gluon initial state, the differential with respect to \hat{t} in equation (7.1.20) can be converted to a differential in θ by applying the chain rule:

$$\frac{d\hat{\sigma}(gg \rightarrow t\bar{t})}{d\theta} = \frac{d\hat{\sigma}(gg \rightarrow t\bar{t})}{d\hat{t}} \frac{d\hat{t}}{d\theta} = \frac{d\hat{\sigma}(gg \rightarrow t\bar{t})}{d\hat{t}} \sqrt{\hat{s} \left(\frac{\hat{s}}{4} - m_t^2 \right)}. \quad (7.1.31)$$

As a result, equation (7.1.29) together with (7.1.30) and (7.1.31) allow for the implementation of a dynamical renormalization scale.

7.1.4 Conversion to Bins and Conventions

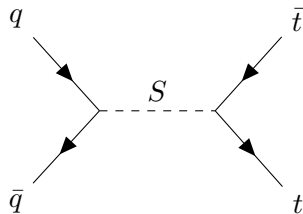
Experimental data of differential cross sections are presented in terms of bins. Consequently, in order to compare to experiment, we need to average the semi-analytical result over the relevant bin. The bins are divided according to

$$\text{bins} [] = [300, 360, 430, 500, 580, 680, 800, 1000, 1200, 1500, 2500] \quad \text{GeV}$$

The conversion within the i^{th} bin is straightforward:

$$\left(\frac{d\sigma}{d\sqrt{\hat{s}}} \right)_i = \frac{1}{\text{bin}[i+1] - \text{bin}[i]} \int_{\text{bin}[i]}^{\text{bin}[i+1]} \frac{d\sigma}{d\sqrt{\hat{s}}} d\sqrt{\hat{s}}. \quad (7.1.32)$$

Throughout this work, the semi-analytical calculations use the following settings. The top quark's mass is always set to 173.3 GeV and the proton-proton center of mass energy is $\sqrt{s} = 13$ TeV. Furthermore, we use the NNPDF31_lo_as_0118 PDF with $\mu_R = \mu_F = H_T/4$.

Figure 7.3: $t\bar{t}$ -production in the heavy scalar boson model from section 6.1.

7.2 Beyond the Standard Model Contribution

In this section, we derive the BSM contribution to $t\bar{t}$ -production as predicted by the two models from sections 6.1 and 6.2, i.e. the heavy scalar and heavy vector model. Let us discuss these in turn, starting with the heavy scalar.

7.2.1 Heavy Scalar

Let us adopt the Lagrangian from equation (6.1.2) as our model and consider top-pair production. The only ingredient that changes compared to the SM calculation done in section 7.1 is the matrix element \mathcal{M} , shown in figure 7.3. Apart from this, the entire derivation is completely analogous. Following the Feynman rules, the squared amplitude for $q\bar{q} \rightarrow S \rightarrow t\bar{t}$ in the BSM is given by

$$\begin{aligned} i\mathcal{M} &= \bar{v}(p_q)c_S u(p_{\bar{q}}) \frac{1}{\hat{s} - m_S^2} \bar{u}(p_t)c_S v(p_{\bar{t}}) \\ &= \frac{c_S^2}{\hat{s} - m_S^2} \bar{v}(p_q)u(p_{\bar{q}})\bar{u}(p_t)v(p_{\bar{t}}). \end{aligned} \quad (7.2.1)$$

Hence, the squared amplitude is given by

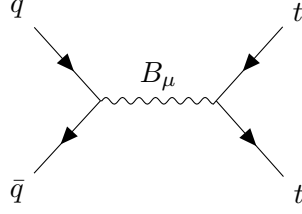
$$|\mathcal{M}|^2 = \left(\frac{c_S^2}{\hat{s} - m_S^2} \right)^2 [\bar{v}(p_q)u(p_{\bar{q}})][\bar{u}(p_t)v(p_{\bar{t}})][\bar{v}(p_{\bar{t}})u(p_t)][\bar{u}(p_{\bar{q}})v(p_q)] \quad (7.2.2)$$

Since the incoming beam of particles is unpolarised we again average over the polarisations, giving two factors of two downstairs. Also, since we don't measure spin in the outgoing beam we sum over it. Using Dirac trace technology we then obtain

$$\begin{aligned} |\bar{\mathcal{M}}|^2 &= \frac{1}{4} \sum_{\text{spins}} |\mathcal{M}|^2 = \frac{1}{4} \left(\frac{c_S^2}{\hat{s} - m_S^2} \right)^2 \text{Tr}[\not{p}_{\bar{q}}\not{p}_q] \text{Tr}[(\not{p}_t + m_t)(\not{p}_{\bar{t}} - m_{\bar{t}})] \\ &= \frac{1}{4} \left(\frac{c_S^2}{\hat{s} - m_S^2} \right)^2 4p_{\bar{q}} \cdot p_q (4p_t \cdot p_{\bar{t}} - 4m_t m_{\bar{t}}), \end{aligned}$$

which after some algebra simplifies to

$$|\bar{\mathcal{M}}|^2 = \left(\frac{c_S^2}{\hat{s} - m_S^2} \right)^2 \hat{s}(\hat{s} - 4m_t^2). \quad (7.2.3)$$

Figure 7.4: $t\bar{t}$ -production in the heavy vector boson model from section 6.2.

Substituting this into equation (7.1.9) for the differential cross section, yields

$$\begin{aligned} d\hat{\sigma}_{BSM}(q_f\bar{q}_f \rightarrow t\bar{t}) &= \frac{1}{2\hat{s}} \left(\frac{c_S^2}{\hat{s} - m_S^2} \right)^2 \hat{s}(\hat{s} - 4m_t^2) \frac{1}{16\pi^2} d\Omega \frac{p_t}{\sqrt{\hat{s}}} \\ &= \frac{1}{4} \left(\frac{c_S^2}{\hat{s} - m_S^2} \right)^2 (\hat{s} - 4m_t^2)^{3/2} \frac{1}{16\pi^2 \sqrt{\hat{s}}} d\Omega, \end{aligned} \quad (7.2.4)$$

which implies that the full partonic cross section is given by

$$\hat{\sigma}_{BSM}(q_f\bar{q}_f \rightarrow t\bar{t}) = \frac{c_S^4}{16\pi\sqrt{\hat{s}}} \frac{(\hat{s} - 4m_t^2)^{3/2}}{(\hat{s} - m_S^2)^2 + \Gamma_{\text{tot}}m_S^2}, \quad (7.2.5)$$

where we have installed the total decay width Γ_{tot} (see appendix C for a derivation):

$$\Gamma_{\text{tot}} = \frac{3c_S^2}{8\pi} m_S \left(1 - \frac{4m_t^2}{m_S^2} \right)^{3/2} + \frac{15c_S^2}{8\pi} m_S. \quad (7.2.6)$$

Finally, plugging this into equation (7.1.25) gives the differential cross section in $\sqrt{\hat{s}}$ at the hadronic level in the BSM:

$$\frac{d\sigma_{BSM}}{d\sqrt{\hat{s}}} = \frac{2\sqrt{\hat{s}}}{s} \frac{c_S^4}{16\pi\sqrt{\hat{s}}} \frac{(\hat{s} - 4m_t^2)^{3/2}}{(\hat{s} - m_S^2)^2 + \Gamma_{\text{tot}}m_S^2} \int_{-\frac{1}{2}\ln\frac{s}{\hat{s}}}^{\frac{1}{2}\ln\frac{s}{\hat{s}}} dY \sum_f f_f \left(\sqrt{\frac{\hat{s}}{s}} e^Y \right) f_{\bar{f}} \left(\sqrt{\frac{\hat{s}}{s}} e^{-Y} \right) \quad (7.2.7)$$

7.2.2 Heavy Vector

We now turn to our second model, i.e. the heavy vector. Adopting the Lagrangian from equation (6.2.1) as our model, the heavy vector boson's contribution to $t\bar{t}$ -production is shown in figure 7.4. Recalling the Feynman rules presented at the end of chapter 6, we find that the associated matrix element \mathcal{M} is given by

$$i\mathcal{M} = [\bar{v}_2 i\gamma^\mu g_B u_1] \frac{i}{\hat{s} - M_B^2} \left(-g_{\mu\nu} + \frac{p_\mu p_\nu}{M_B^2} \right) [\bar{u}_3 i\gamma^\nu g_B v_4]. \quad (7.2.8)$$

Using that in general $\not{p}u = mu$ and $\bar{v}\not{p} = -m\bar{v}$, we conclude that the second term in parenthesis does not contribute:

$$\begin{aligned}
\bar{v}_2\gamma^\mu u_1 p_\mu &= \bar{v}_2\gamma^\mu u_1 p_\mu \\
&= \bar{v}_2\not{p}u_1 \\
&= \bar{v}_2(\not{p}_1 + \not{p}_2)u_1 \\
&= \bar{v}_2(m - m)u_1 = 0.
\end{aligned} \tag{7.2.9}$$

As a result, the total squared amplitude becomes:

$$|\bar{\mathcal{M}}|^2 \equiv \frac{1}{4} \sum_{\text{spin}} |\mathcal{M}|^2 = \frac{g_B^4}{4(\hat{s} - M_B^2)} \sum_{\text{spin}} [\bar{u}_1\gamma_\mu v_2] [\bar{v}_2\gamma_\nu u_1] [\bar{u}_3\gamma^\nu v_4] [\bar{v}_4\gamma^\mu u_3], \tag{7.2.10}$$

which resembles expression (7.1.15). Inspired by this correspondence, we can immediately write down the squared amplitude in the heavy vector model:

$$|\bar{\mathcal{M}}|^2 = \frac{g_B^4}{(\hat{s} - M_B^2)^2} (\hat{s}^2 + 4m_t^2\hat{s} + \cos^2(\theta)(\hat{s}^2 - 4\hat{s}m_t^2)). \tag{7.2.11}$$

Taking the by now usual phase space factors into account, this leads to the following BSM partonic cross section:

$$\hat{\sigma}_{BSM} = \frac{g_B^4}{12\pi} \frac{\sqrt{1 - 4m_t^2/\hat{s}} (1 + 2m_t^2/\hat{s})}{(\hat{s} - M_B^2)^2 + \Gamma_{\text{tot}}M_B^2}, \tag{7.2.12}$$

where Γ_{tot} is the total decay width, given by:

$$\Gamma_{\text{tot}} = \frac{5g_B^2}{12\pi} M_B + \frac{g_B^2}{12\pi} \frac{M_B^2 + 3m_t^2}{M_B} \sqrt{1 - \frac{4m_t^2}{M_B^2}}. \tag{7.2.13}$$

We again refer to appendix C for a derivation of equation (7.2.13).

7.2.3 Interference SM and BSM

One might worry about interference effects between the SM and the BSM in the calculation of $|\bar{\mathcal{M}}|^2$ for $t\bar{t}$ -production. Although this is a legitimate concern, the interference term in fact vanishes due to colour effects, as we show now.

Including the sum over colours, the interference term is proportional to

$$\sum_{\text{colour}} \mathcal{M}_{SM}^\dagger \mathcal{M}_{BSM} \propto \sum_{i,j,k,l} [(t_{ji}^A)(t_A)_{kl}]^* \delta_{ij} \delta_{kl}, \tag{7.2.14}$$

where the delta functions carry indices in colour space resulting from the fact the scalar particle S nor the vector boson B_μ are charged under $SU(3)$. Hence,

$$\sum_{\text{colour}} \mathcal{M}_{SM}^\dagger \mathcal{M}_{BSM} \propto \sum_{i,j,k,l} [(t^A)_{ii}(t_A)_{ll}]^* = 0, \tag{7.2.15}$$

since $\text{Tr}(t^A) = 0$. This shows that the interference term between the SM and BSM vanishes.

$\sqrt{\hat{s}}$ [GeV]	$d\sigma/d\sqrt{\hat{s}}$ [pb GeV ⁻¹]	$\sqrt{\hat{s}}$ [GeV]	$d\sigma/d\sqrt{\hat{s}}$ [pb GeV ⁻¹]
300-360	0.284	680-800	0.327
360-430	2.405	800-1000	0.129
430-500	1.977	1000-1200	$0.437 \cdot 10^{-1}$
500-580	1.230	1200-1500	$0.140 \cdot 10^{-1}$
580-680	0.671	1500-2500	$0.173 \cdot 10^{-2}$

Table 7.1: *FastNLO* results at LO for $t\bar{t}$ -production as differential in the invariant mass of the outgoing top-quark pair at $\sqrt{s} = 13$ TeV. The results were obtained with the following settings. PDF: NNPDF30_nnlo_as_0118, $m_t = 173.3$ GeV, $\mu_R = \mu_F = H_T/4$. The inclusive cross section is 569.130 pb.

7.3 FastNLO and MadGraph

In addition to finding theoretical predictions for $t\bar{t}$ -production along a semi-analytical route as was done in section 7.1 and 7.2, they can also be directly obtained using FastNLO [28] or MadGraph [29].

The FastNLO-framework allows for quick computations of top-quark pair differential distributions using the fastNLO Tables at LO, NLO or NNLO. The corresponding results are shown in Table 7.1 and 7.2 and were obtained with $m_t = 173.3$ GeV, $\mu_R = \mu_F = H_T/4$ and NNPDF30_nnlo_as_0118. From this, the QCD K-values can be read off as the ratio of the NNLO over the LO result, shown in Table 7.3. These are useful for converting LO results to NNLO accuracy.

MadGraph is a Monte-Carlo event generator that allows one to obtain differential distributions for various processes, such as $pp \rightarrow t\bar{t}$. We have generated 100.000 events of $pp \rightarrow t\bar{t}$ at $\sqrt{s} = 13$ TeV (LO), and constructed the resulting differential distribution in the partonic center of mass energy. The results are shown in figure 7.5. Care was taken to let MadGraph run with the same settings as the semi-analytical calculation. That is, with $m_t = 173.3$ GeV, $\mu_R = \mu_F = H_T/4$ and PDF NNPDF31_lo_as_0118. The total inclusive cross section predicted by MadGraph is 568.3 pb. Figure 7.5 also shows the standard model semi-analytical result as computed in section 7.1. This gives an inclusive cross section of 556.47 pb.

Comparing the two, we conclude that the semi-analytical prediction gives an accurate representation of the $pp \rightarrow t\bar{t}$ differential cross section. The difference between MadGraph and the semi-analytical prediction increases towards the tail of the distribution, but this is merely due to the fact that MadGraph has not collected enough statistics there.

$\sqrt{\hat{s}}$ [GeV]	$d\sigma/d\sqrt{\hat{s}}$ [pb GeV ⁻¹]	$\sqrt{\hat{s}}$ [GeV]	$d\sigma/d\sqrt{\hat{s}}$ [pb GeV ⁻¹]
300-360	0.509	680-800	0.477
360-430	3.527	800-1000	0.191
430-500	2.808	1000-1200	$0.652 \cdot 10^{-1}$
500-580	1.754	1200-1500	$0.211 \cdot 10^{-1}$
580-680	0.966	1500-2500	$0.265 \cdot 10^{-2}$

Table 7.2: *FastNLO* results at NNLO for $t\bar{t}$ -production as differential in the invariant mass of the outgoing top-quark pair at $\sqrt{s} = 13$ TeV. The results were obtained with the following settings. PDF: NNPDF30_nnlo_as_0118, $m_t = 173.3$ GeV, $\mu_R = \mu_F = H_T/4$. The inclusive cross section is 828.395 pb.

$\sqrt{\hat{s}}$ [GeV]	K-value	$\sqrt{\hat{s}}$ [GeV]	K-value
300-360	1.792	680-800	1.458
360-430	1.466	800-1000	1.475
430-500	1.420	1000-1200	1.488
500-580	1.427	1200-1500	1.508
580-680	1.440	1500-2500	1.531

Table 7.3: QCD k -values: the ratio of the NNLO result over the LO result. The following settings were used. PDF: NNPDF30_nnlo_as_0118, $m_t = 173.3$ GeV and $\mu_R = \mu_F = H_T/4$.

$\sqrt{\hat{s}}$ [GeV]	$d\sigma/d\sqrt{\hat{s}}$ [pb GeV ⁻¹]	$\sqrt{\hat{s}}$ [GeV]	$d\sigma/d\sqrt{\hat{s}}$ [pb GeV ⁻¹]
300-360	0.215	680-800	0.313
360-430	2.259	800-1000	0.114
430-500	2.051	1000-1200	$0.346 \cdot 10^{-1}$
500-580	1.285	1200-1500	$0.099 \cdot 10^{-1}$
580-680	0.678	1500-2500	$0.103 \cdot 10^{-2}$

Table 7.4: *Binned semi-analytical SM prediction.*

Figure 7.6 shows a comparison between the semi-analytical SM prediction and the FastNLO results, both at LO and NNLO.

7.4 χ^2 Analysis

The measurements of differential cross sections for $t\bar{t}$ -production in proton-proton collisions at 13 TeV are shown in figure 7.7, which are also included in the SMEFiT analysis in [3]. This experiment was conducted by the CMS collaboration [30] and their results are presented at the partonic level, which means that the signal has been unfolded to the the parton level. Here, the top-quarks can effectively be considered as final state particles. The measured inclusive cross section reported in [30] is 240.581 pb. Since only top quarks that decayed into either e/μ or jets have been detected, this result needs to be divided by $2/3$ times the branching ratio $BR(t\bar{t} \rightarrow \text{jets} + \text{leptons})$ in order to arrive at the full inclusive cross section:

$$\sigma_{\text{exp}} = \left[\frac{2}{3} \cdot BR(t\bar{t} \rightarrow \text{jets} + \text{leptons}) \right]^{-1} \cdot 240.581 = 823.908 \text{ pb},$$

where we used that $BR(t\bar{t} \rightarrow \text{jets} + \text{leptons}) = 0.438$ according to [31]. Accounting for this conversion factor, allows us to compare the data for the differential cross section in [30] to our own semi-analytical calculation (at NNLO via QCD K-factors) done in section 7.1. The result is shown in figure 7.8, which also shows the data residuals. We will now start adding the BSM contributions.

7.4.1 Heavy Scalar

Figure 7.9a and 7.9b show the SM and BSM contributions in the heavy scalar model, alongside with the FastNLO and CMS data at $c_S = 0.1$ and $m_S = 1000, 3000$ GeV respectively. The BSM is given in the continuous case as well as binned. One can clearly see that the spike, located at $\sqrt{\hat{s}} = m_S$,

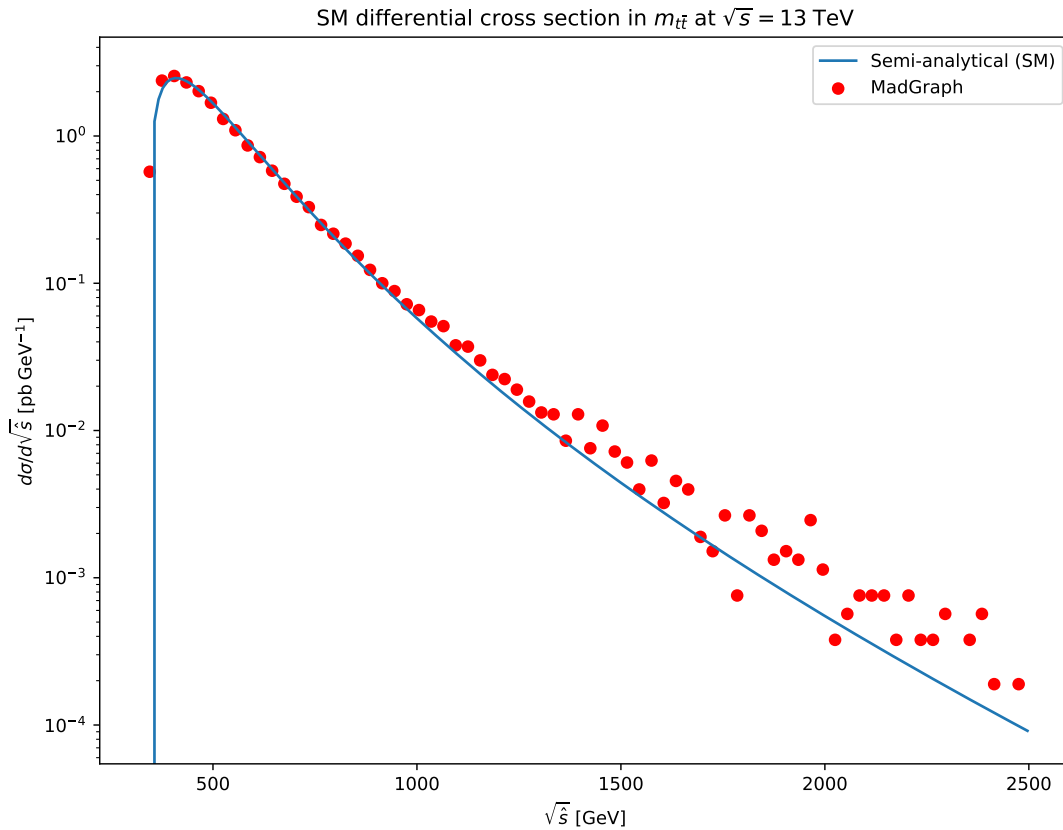
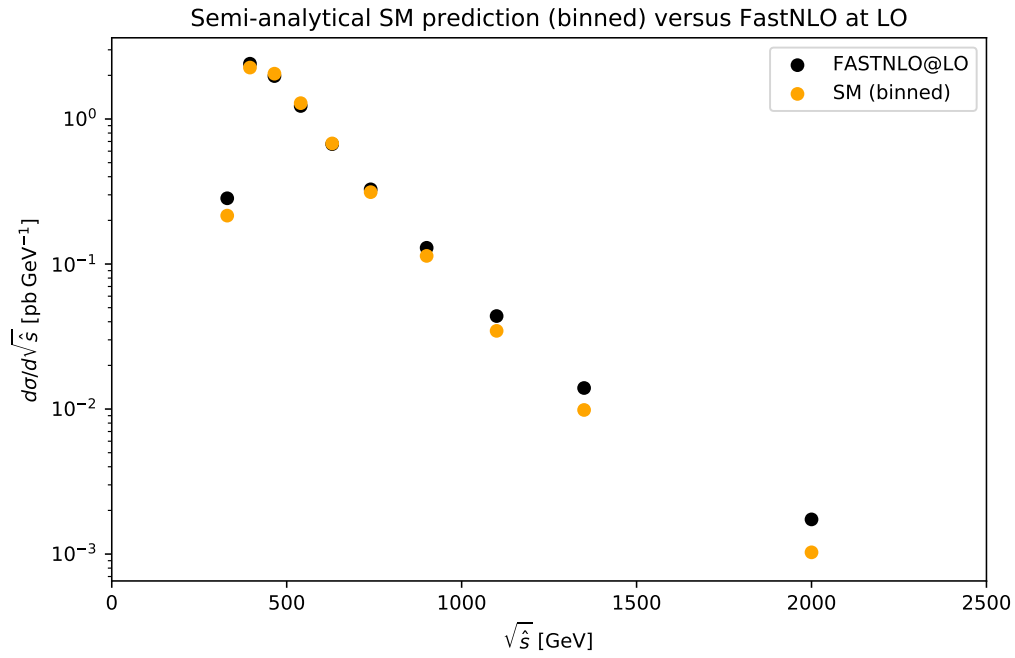
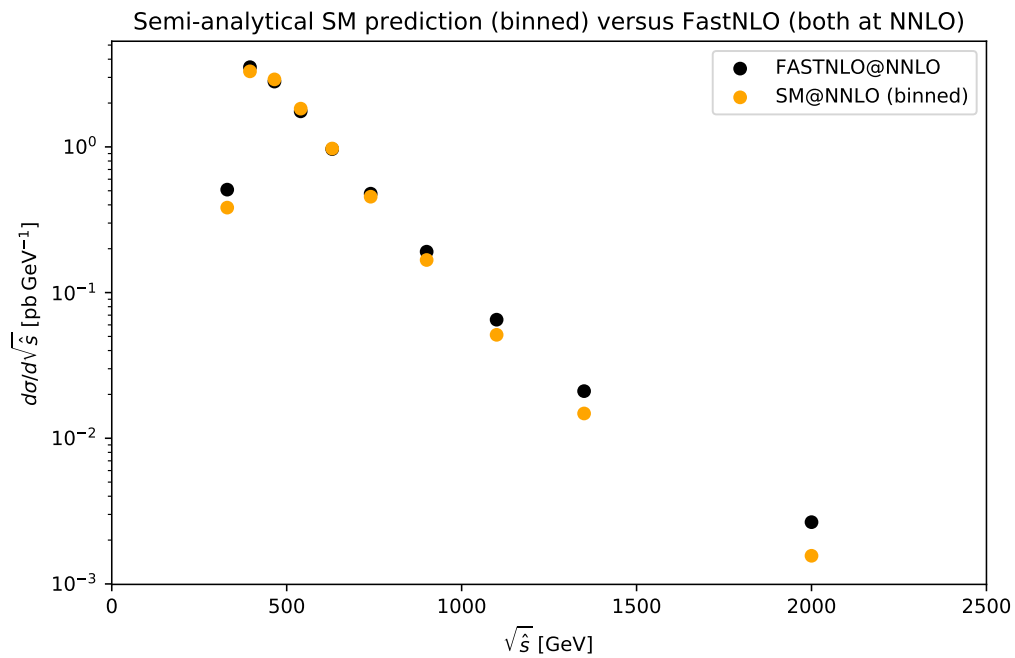


Figure 7.5: Differential cross section in $\sqrt{\hat{s}}$ of $t\bar{t}$ -production in a proton-proton collision at $\sqrt{s} = 13$ TeV, as predicted by the semi-analytical calculation (solid line) and a MadGraph simulation (in dots). Both use $m_t = 173.3$ GeV, $\mu_R = \mu_F = H_T/4$ and PDF NNPDF31_lo_as_0118. The inclusive cross sections are 556.47 pb (semi-analytical) and 568.3 pb (MadGraph).



(a)



(b)

Figure 7.6: *FastNLO* versus binned semi-analytical SM prediction (PDF: NNPFD31_lo_as_0118) at 13 TeV at LO (Fig. (a)) and NNLO (Fig. (b)). At NNLO, the inclusive cross sections are 804.998 pb (SA) and 825.432 pb (*FastNLO*).

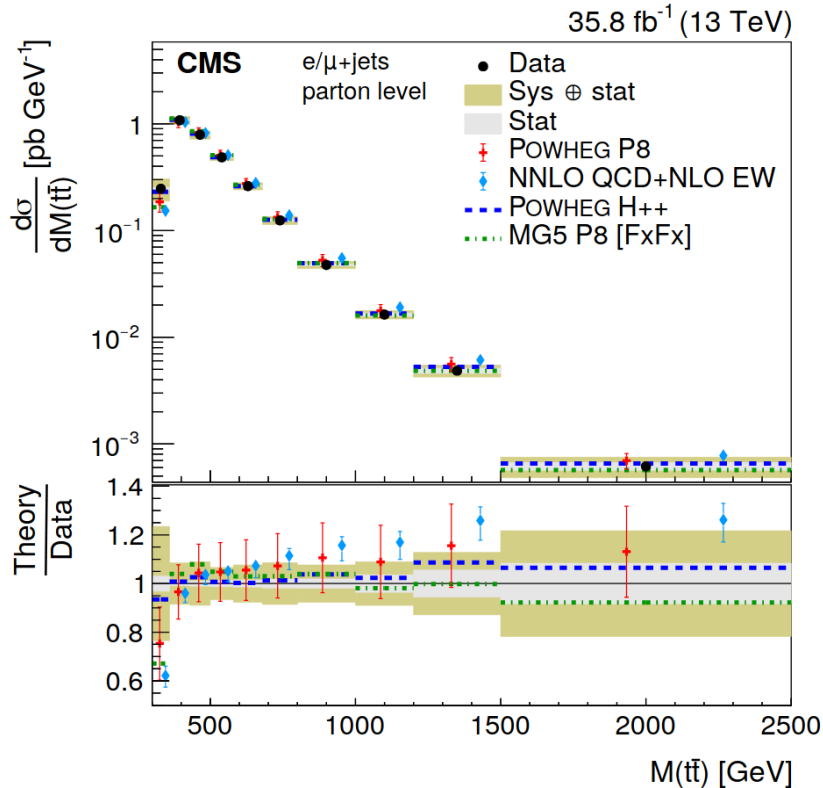


Figure 7.7: *Differential cross section at the parton level as a function of the invariant mass $m_{t\bar{t}}$. Taken from [30].*

makes up the dominant contribution to the BSM prediction. At large values of m_S , the CMS data loses sensitivity, and the SM + BSM prediction essentially reduces to the SM, see figure 7.9b.

Let us now introduce the following figure of merit, a simple χ^2 test, defined by

$$\chi^2(c_S, m_S) = \sum_{\text{bins}} \left(\frac{\sigma_{SM} + \sigma_{BSM}(c_S, m_S) - \sigma_{\text{exp}}}{\delta_{\text{exp}}} \right)^2. \quad (7.4.1)$$

A contour plot of equation (7.4.1) is shown in figure 7.12 at the 95% confidence level (CL) interval. The region in white here represents the pair of points (c_S, m_S) that are excluded at 95% confidence. From the χ^2 -landscape, we can determine bounds on the UV-parameters c_s and m_S . We shall refer to these as bounds from the BSM model. We also include Table 7.6 that gives an overview of the χ^2 in the SM, BSM and FastNLO.

At this stage we can compare the bounds from the BSM model and the bounds from the EFT, which we obtained in section 6.1 of chapter 6 via matching. Let us first recall the best bound that we found there from a four-heavy quark operator (same as equation 6.1.26):

$$\frac{c_S^2}{m_S^2} < 0.0900 \quad \text{TeV}^{-2} \quad (\text{EFT bound from matching}). \quad (7.4.2)$$

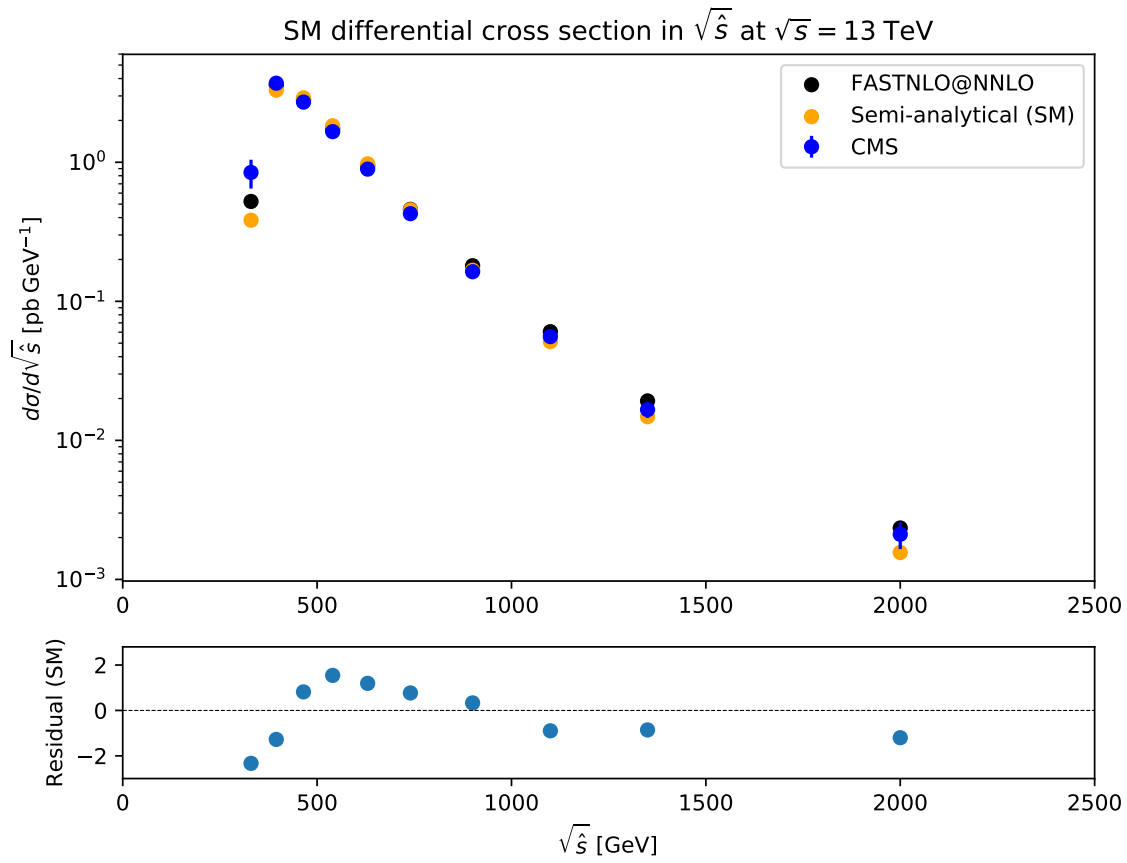


Figure 7.8: *Semi-analytical prediction (at NNLO) versus FastNLO (at NNLO) and experimental data from CMS [30], including the data residuals of the semi-analytical SM prediction.*

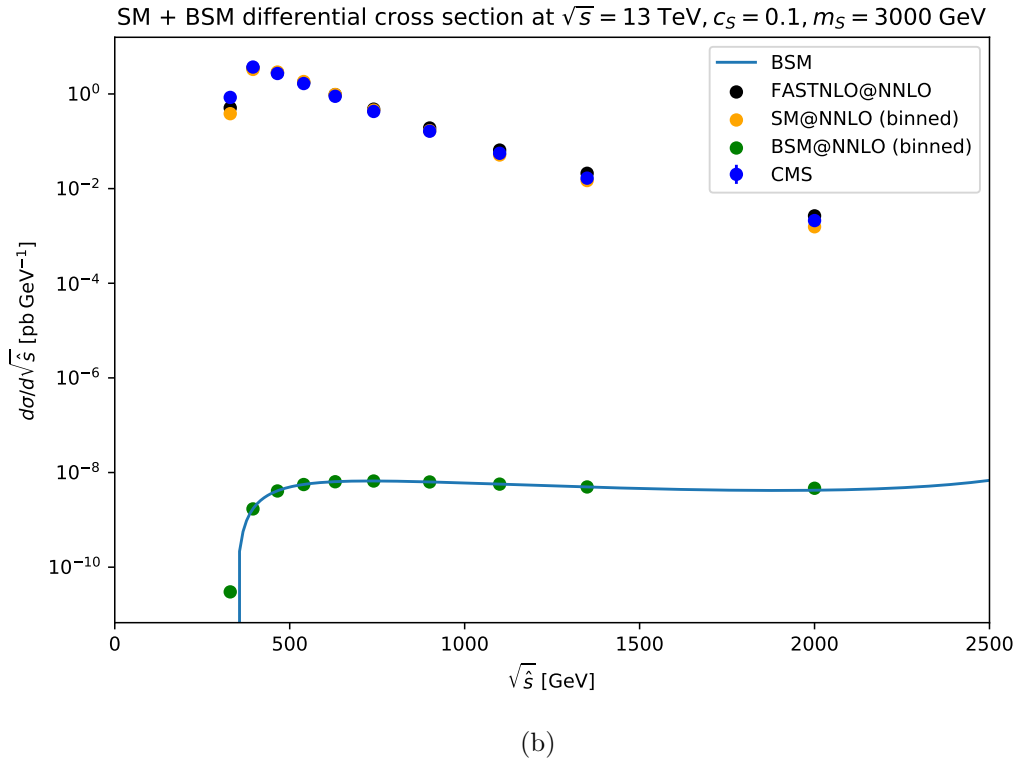
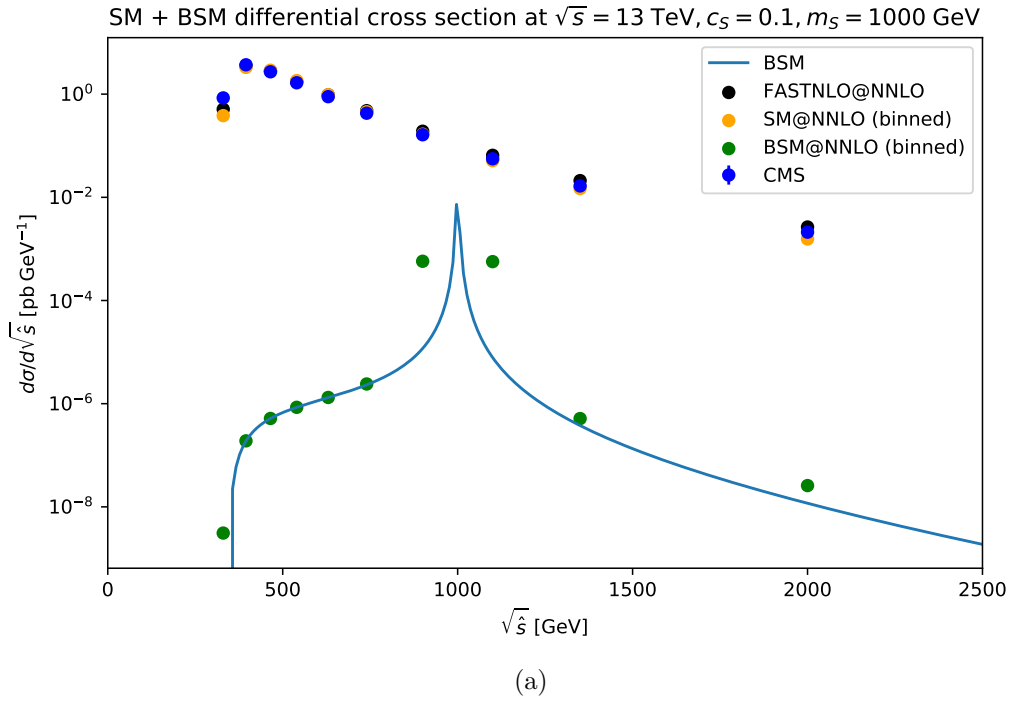


Figure 7.9: *Semi-analytical prediction (SM and BSM) versus FastNLO (at NNLO) and experimental data from CMS [30]. The BSM prediction is given for $c_S = 0.1$ and $m_S = 1000, 3000$ GeV in figure (a) and (b) respectively. Note that the CMS data has no sensitivity around the BSM resonance at $m_S = 3000$ GeV.*

We now consider the following two cases:

- Fixing c_S lets us infer lower bounds on m_S . For example, in a maximally strongly coupled UV-theory, we know that the coupling constant $c_S = 1$, since $c_S > 1$ corresponds to the non-perturbative regime. Therefore, putting $c_S = 1$, we deduce

$$\frac{c_S^2}{m_S^2} = \frac{1}{m_S^2} < 0.0900 \text{ TeV}^{-2} \implies m_S > 3.33 \text{ TeV}.$$

From the χ^2 in figure 7.12 we get a less stringent BSM bound on m_S if $c_S = 1$: $m_S > 2.503$ TeV.

- Next, consider putting $\Lambda = m_S$. This gives an EFT bound on the coupling c_S :

$$\frac{c_S^2}{m_S^2} < 0.0900 \text{ TeV}^{-2} \implies c_S < 0.3m_S \quad \text{with } m_S \text{ its numerical value in TeV}.$$

We can also read off BSM bounds on c_S at the 95% CL from the χ^2 -landscape in figure 7.12. A comparison between these BSM bounds and the EFT bounds is shown in figure 7.10. It shows quite interesting behaviour, for the following reason. Recall that our BSM phenomenology only relied on CMS data from $t\bar{t}$ production. However, the bounds from the EFT were derived from the four-heavy quark operators $QQQQ$, which are only constrained from $t\bar{t}t\bar{t}$ and $t\bar{t}b\bar{b}$ production. So going to the EFT allows us to use experimental data from other production mechanisms than the one we are explicitly considering; the EFT relates different processes. Conversely, this implies that the heavy scalar model also modifies the cross-section for $t\bar{t}t\bar{t}$ and $t\bar{t}b\bar{b}$ production. Indeed, figure 7.11 shows that this is the case. The upshot of this discussion is that an EFT approach proves to be much more versatile than direct BSM searches, since the latter relates different processes and hence maximally exploits the available experimental data to constrain UV physics.

In order to get a quick overview of how the BSM bounds compare to the EFT bounds, we include Table 7.5 that shows a couple of benchmark points at $c_S = 0.25, 0.50, 0.75$ and 1.00.

7.4.2 Heavy Vector

Let us repeat the same analysis also in the case of the heavy vector. Recall equation (6.2.13) from section 6.2 that gave an upper bound on the ratio g_B^2/M_B^2 at order $\mathcal{O}(\Lambda^{-2})$:

$$\frac{g_B^2}{M_B^2} < 0.00633 \text{ TeV}^{-2} \quad (\text{EFT bound from matching}).$$

We now consider the same cases as in section 7.4.1.

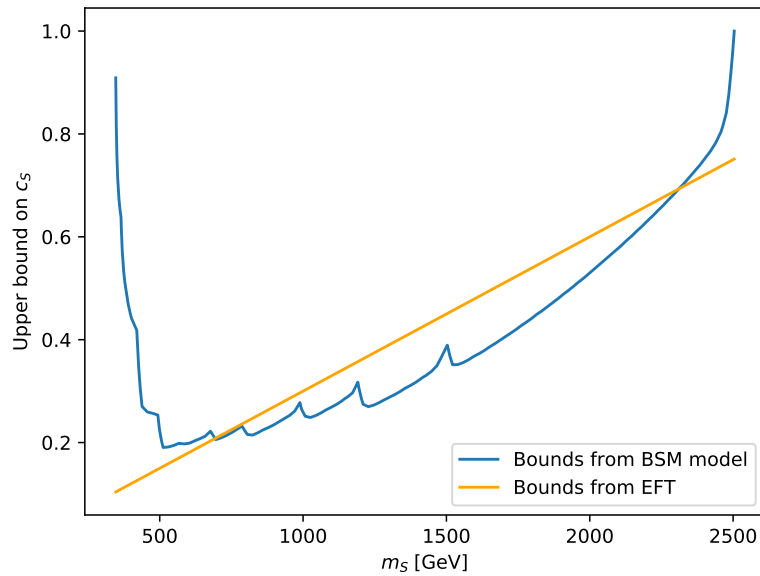


Figure 7.10: A comparison of the upper bounds on the heavy scalar coupling c_s that follow from either a direct χ^2 -analysis on the level of the BSM model or from an EFT analysis. The bounds from the EFT originate from the four-heavy quark operators.

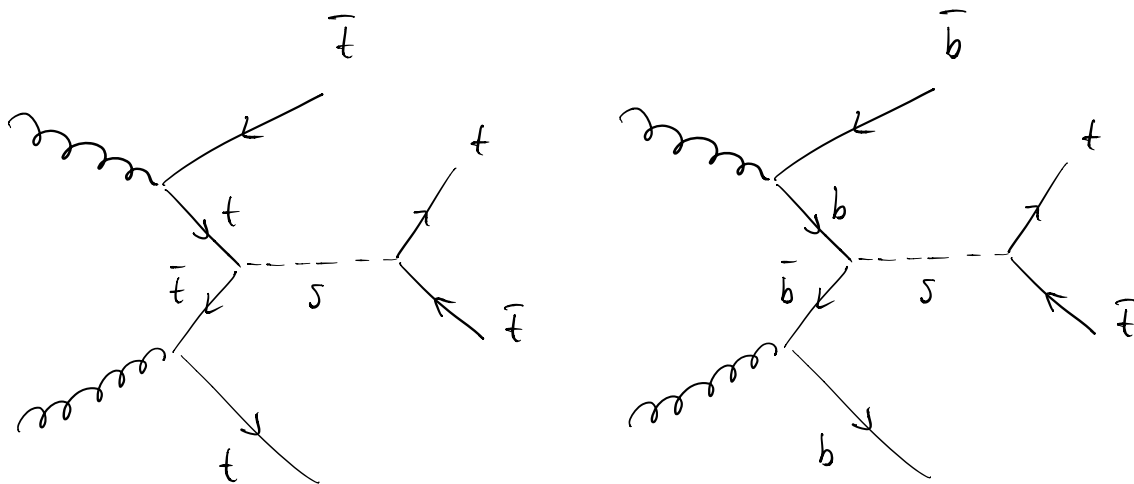


Figure 7.11: The heavy scalar S contributes to $t\bar{t}\bar{t}$ and $t\bar{t}b\bar{b}$ production.

	EFT (TeV)	BSM (TeV)
$c_S = 0.25$	$\Lambda > 0.833$	$m_S > 0.946$
$c_S = 0.50$	$\Lambda > 1.667$	$m_S > 1.934$
$c_S = 0.75$	$\Lambda > 2.500$	$m_S > 2.389$
$c_S = 1.00$	$\Lambda > 3.333$	$m_S > 2.503$

Table 7.5: A comparison between the bounds on Λ in the EFT and M_B in the scalar BSM model for the four benchmark points $c_S = 0.25, 0.50, 0.75$ and 1.00 .

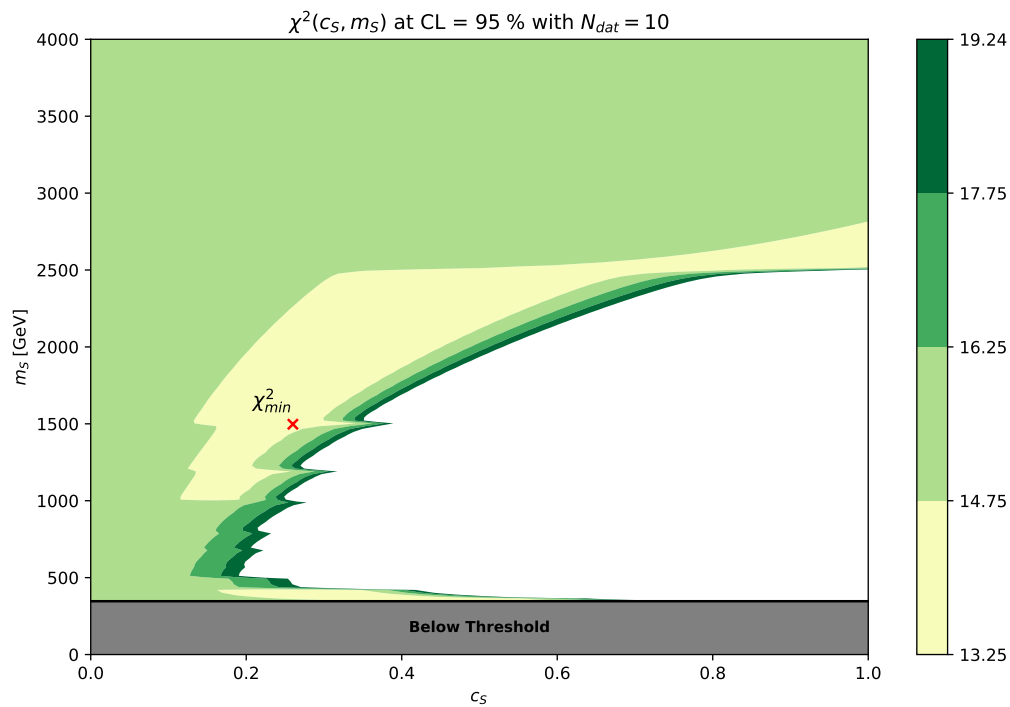


Figure 7.12: χ^2 of the SM + BSM (heavy scalar) prediction at 95% CL as a function of the UV parameters c_S and m_S . The region in white is excluded at 95% CL and the SM is located at the line $c_S = 0$.

Model	χ^2/N
SM	1.521
SM + BSM ($c_S = 0.1, m_S = 3m_t$)	1.541
FastNLO@NNLO (LO PDF)	0.928
FastNLO@NNLO (NNLO PDF)	2.127

Table 7.6: χ^2/N for $N = 10$ data points in the standard model (SM), beyond the standard model (BSM, heavy scalar) and FastNLO (LO PDF)

- In a maximally strongly coupled UV-theory, we again have that the coupling constant $g_B = 1$. Putting $g_B = 1$, we thus get

$$\frac{g_B^2}{M_B^2} = \frac{1}{M_B^2} < 0.00633 \text{ TeV}^{-2} \implies M_B > 12.57 \text{ TeV}.$$

From the χ^2 in figure 7.14 we get a less stringent bound on m_S if $g_B = 1$: $M_B > 2.522 \text{ TeV}$.

- Next, we put $\Lambda = M_B$. This gives a bound on the coupling g_B :

$$\frac{g_B^2}{M_B^2} < 0.00633 \text{ TeV}^{-2} \implies g_B < 0.0796 M_B \quad \text{with } M_B \text{ its numerical value in TeV}.$$

Again, we can also read off the bounds on g_B at the 95% CL from the χ^2 in figure 7.14. A comparison between the χ^2 bound and the one that follows from the SMEFiT analysis is shown in figure 7.13. Note that the BSM-bound blows up at $M_B \approx 2500 \text{ GeV}$, which is a result of the fact that the CMS data has no sensitivity beyond 2500 GeV.

We also present Table 7.7 with benchmark results that show the lower bounds on Λ and M_B for $g_B = 0.25, 0.5, 0.75$ and 1.0 in the EFT and BSM model respectively. It tells us that the EFT gives stronger constraints on Λ than the BSM model, which is simply because the CMS data has no sensitivity beyond 2.5 TeV. In general, this is also what one would expect; an EFT can provide sensitivity for higher values of Λ than direct searches from experiment. This is yet another advantage of an EFT.

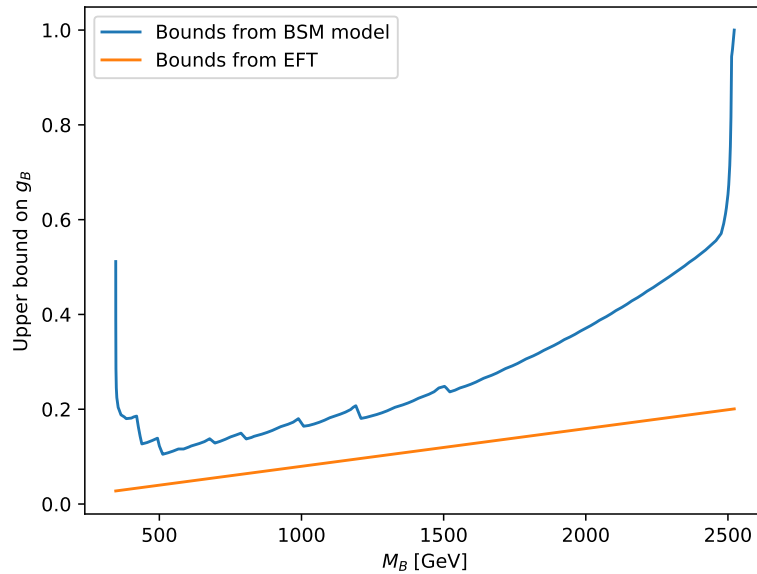


Figure 7.13: A comparison of the upper bound on the heavy vector coupling g_B that follow from either a direct χ^2 -analysis on the level of the BSM model or from an EFT analysis. The bounds from the EFT originate from the two-light-two-heavy operators.

	EFT (TeV)	BSM (TeV)
$g_B = 0.25$	$\Lambda > 3.14$	$M_B > 1.57$
$g_B = 0.50$	$\Lambda > 6.28$	$M_B > 2.35$
$g_B = 0.75$	$\Lambda > 9.43$	$M_B > 2.51$
$g_B = 1.00$	$\Lambda > 12.57$	$M_B > 2.52$

Table 7.7: A comparison between the bounds on Λ in the EFT and M_B in the vector BSM model for the four benchmark points $g_B = 0.25, 0.50, 0.75$ and 1.00 .

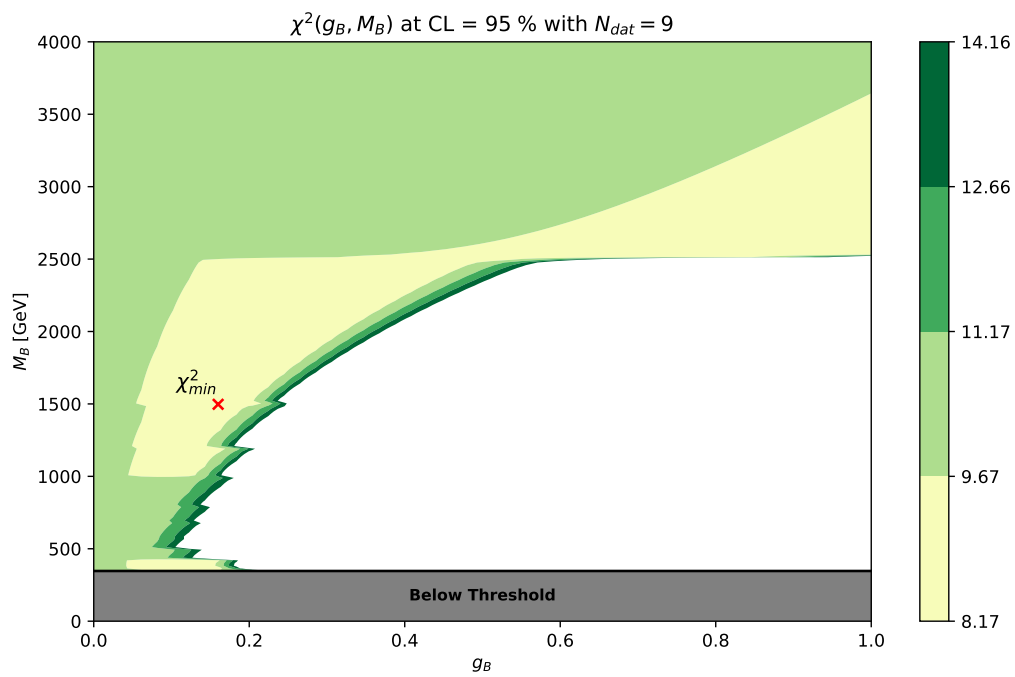


Figure 7.14: χ^2 of the SM + BSM (heavy vector) prediction at 95% CL as a function of the UV parameters g_B and M_B , with nine data points. The SM is located at the line $g_B = 0$.

Chapter 8

Conclusion

In this thesis, we have focused on matching UV-completions of the SM onto the SMEFT. By considering the SM to only be valid up to a finite energy scale Λ , we could extend the SM Lagrangian by higher dimensional (irrelevant) operators. In this framework, the unknown high-energy effects manifested themselves at energy scales below Λ as interactions that were previously not allowed in the SM. Specifically, we showed how high-energy imprints could be captured by including dimension-six operators in the Warsaw basis. In this sense, the SMEFT parameterises high energy effects in a model-independent way; no assumptions about the UV-completions are made. Differential cross sections were also seen to change in the SMEFT, and by comparing these to the high precision data from the LHC we were able to derive bounds on the Wilson coefficients. Specifically, we used Nested Sampling to sample the prior volume in order to locate the region close to maximum likelihood.

Furthermore, we argued in chapter 6 that matching UV-completions onto the SMEFT is another crucial ingredient in our search for new physics. Matching could be carried out alongside the SMEFT bottom-up analysis and restored the model-dependence. We studied two specific UV-completions: the heavy scalar model and the heavy vector model. In both cases, we showed there is no a priori reason the UV completions generate dimension-six operators in the Warsaw basis upon going to the effective regime. However, we were able to express the matching equations in the Warsaw basis nonetheless by making use of the Fierz identities and the relation among the the matrices of the fundamental representation of $SU(3)$. Consequently, we could use the bounds on the four-heavy quark operators to constrain the heavy scalar extension. The heavy vector extension could be constrained by the two-light-two-heavy operators, which led to to tighter constraints than in the heavy scalar model. This was explained by noting that more cross section measurements are sensitive to 2L2H operators than to four-heavy quark operators.

A complementary approach that we studied in chapter 7 in order to find bounds on the UV-parameters involved an explicit BSM phenomenology analysis. Here, we compared the BSM predictions at NNLO with experimental data from CMS for $t\bar{t}$ differentials in the invariant mass of the top-quark pair in pp -collisions at 13 TeV. This direct analysis took only 10 measurements into

account, as opposed to the more than 100 cross section measurements that constrain dimension-six operators in the EFT of the top-quark sector. Using the χ^2 as our figure of merit, we then derived bounds on the UV-parameters.

We ended chapter 7 with comparing the bounds that resulted from the two different methods that we adopted; an explicit BSM phenomenology study and an EFT analysis complemented by the matching equations. The main conclusion is that an EFT analysis provides sensitivity for higher energies than direct searches for new physics. This is one of the big advantages of the EFT-programme. It offers a model-independent, and hence efficient, way of parameterising new physics, while at the same time providing more sensitivity than direct searches. This might come as no surprise, as the EFT programme strives to take into account all available data relevant to specific processes.

As an outlook for possible future research, higher order matching calculations in the heavy scalar model should be considered in order to exploit the relatively stringent bounds on the operator \mathcal{O}_{tG} . It would be interesting to see how NLO results relate to our current LO predictions. Naturally, one could generalise the BSM phenomenology study by allowing also for off-diagonal couplings in generation space; the current matching equations presented in this work already incorporate this. The ultimate goal would be to automate the whole procedure of matching UV-completions onto the SMEFT at tree level by developing a suitable algorithm. This would automate the search for new physics from two complementary sides; an efficient global EFT fit to high precision data and an automatic matching procedure that subsequently translates the resulting bounds to the UV-parameters. This then efficiently scans the whole landscape of BSM theories; a big step towards our dream of finding new physics.

Appendix A

Warsaw Basis

In this first appendix, we provide the complete set of operators that together make up the Warsaw basis that is referred to in chapters 5 and 6 [14]. The four-fermion operators are shown in Table A.1, which are further classified by their chirality (L/R). All other operators, that in addition also include the Higgs-field and/or bosonic fields, can be found in Table A.2. Let us comment on the notation that is used here. The Roman subscripts p, r, s, t represent the generation indices, and the superscripts i, j denote the $SU(2)$ indices (in superscript). Left-handed lepton-doublets are denoted by l_{Lp}^j and the right-handed lepton singlets by e_{Rp} . As for the quarks, left-handed quark-doublets are denoted by $q_{Lp}^{\alpha j}$, where the Greek-index α refers to the colour d.o.f, and right-handed up-type/down-type quark fields are denoted by respectively u_{Rp}^α and d_{Rp}^α . The Higgs field is represented by φ^j . When colour-indices are not explicitly written, a contraction within the same bilinear is assumed.

In Table A.2, X stands for G^A, W^I or B , corresponding to the different gauge field strength tensors. In this thesis, we primarily use the four-fermionic operators from Table A.1.

$(\bar{L}L)(\bar{L}L)$		$(\bar{R}R)(\bar{R}R)$		$(\bar{L}L)(\bar{R}R)$	
Q_{ll}	$(\bar{l}_p \gamma_\mu l_r)(\bar{l}_s \gamma^\mu l_t)$	Q_{ee}	$(\bar{e}_p \gamma_\mu e_r)(\bar{e}_s \gamma^\mu e_t)$	Q_{le}	$(\bar{l}_p \gamma_\mu l_r)(\bar{e}_s \gamma^\mu e_t)$
$Q_{qq}^{(1)}$	$(\bar{q}_p \gamma_\mu q_r)(\bar{q}_s \gamma^\mu q_t)$	Q_{uu}	$(\bar{u}_p \gamma_\mu u_r)(\bar{u}_s \gamma^\mu u_t)$	Q_{lu}	$(\bar{l}_p \gamma_\mu l_r)(\bar{u}_s \gamma^\mu u_t)$
$Q_{qq}^{(3)}$	$(\bar{q}_p \gamma_\mu \tau^I q_r)(\bar{q}_s \gamma^\mu \tau^I q_t)$	Q_{dd}	$(\bar{d}_p \gamma_\mu d_r)(\bar{d}_s \gamma^\mu d_t)$	Q_{ld}	$(\bar{l}_p \gamma_\mu l_r)(\bar{d}_s \gamma^\mu d_t)$
$Q_{lq}^{(1)}$	$(\bar{l}_p \gamma_\mu l_r)(\bar{q}_s \gamma^\mu q_t)$	Q_{eu}	$(\bar{e}_p \gamma_\mu e_r)(\bar{u}_s \gamma^\mu u_t)$	Q_{qe}	$(\bar{q}_p \gamma_\mu q_r)(\bar{e}_s \gamma^\mu e_t)$
$Q_{lq}^{(3)}$	$(\bar{l}_p \gamma_\mu \tau^I l_r)(\bar{q}_s \gamma^\mu \tau^I q_t)$	Q_{ed}	$(\bar{e}_p \gamma_\mu e_r)(\bar{d}_s \gamma^\mu d_t)$	$Q_{qu}^{(1)}$	$(\bar{q}_p \gamma_\mu q_r)(\bar{u}_s \gamma^\mu u_t)$
		$Q_{ud}^{(1)}$	$(\bar{u}_p \gamma_\mu u_r)(\bar{d}_s \gamma^\mu d_t)$	$Q_{qu}^{(8)}$	$(\bar{q}_p \gamma_\mu T^A q_r)(\bar{u}_s \gamma^\mu T^A u_t)$
		$Q_{ud}^{(8)}$	$(\bar{u}_p \gamma_\mu T^A u_r)(\bar{d}_s \gamma^\mu T^A d_t)$	$Q_{qd}^{(1)}$	$(\bar{q}_p \gamma_\mu q_r)(\bar{d}_s \gamma^\mu d_t)$
				$Q_{qd}^{(8)}$	$(\bar{q}_p \gamma_\mu T^A q_r)(\bar{d}_s \gamma^\mu T^A d_t)$
$(\bar{L}R)(\bar{R}L)$ and $(\bar{L}R)(\bar{L}R)$		B -violating			
Q_{ledq}	$(\bar{l}_p^j e_r)(\bar{d}_s q_t^j)$	Q_{duq}	$\varepsilon^{\alpha\beta\gamma} \varepsilon_{jk} [(d_p^\alpha)^T C u_r^\beta] [(q_s^j)^T C l_t^k]$		
$Q_{quqd}^{(1)}$	$(\bar{q}_p^j u_r) \varepsilon_{jk} (\bar{q}_s^k d_t)$	Q_{qqqu}	$\varepsilon^{\alpha\beta\gamma} \varepsilon_{jk} [(q_p^{\alpha j})^T C q_r^{\beta k}] [(u_s^\gamma)^T C e_t]$		
$Q_{quqd}^{(8)}$	$(\bar{q}_p^j T^A u_r) \varepsilon_{jk} (\bar{q}_s^k T^A d_t)$	Q_{qqq}	$\varepsilon^{\alpha\beta\gamma} \varepsilon_{jn} \varepsilon_{km} [(q_p^{\alpha j})^T C q_r^{\beta k}] [(q_s^m)^T C l_t^n]$		
$Q_{lequ}^{(1)}$	$(\bar{l}_p^j e_r) \varepsilon_{jk} (\bar{q}_s^k u_t)$	Q_{duu}	$\varepsilon^{\alpha\beta\gamma} [(d_p^\alpha)^T C u_r^\beta] [(u_s^\gamma)^T C e_t]$		
$Q_{lequ}^{(3)}$	$(\bar{l}_p^j \sigma_{\mu\nu} e_r) \varepsilon_{jk} (\bar{q}_s^k \sigma^{\mu\nu} u_t)$				

Table A.1: Four-fermion operators. Taken from [14].

X^3		φ^6 and $\varphi^4 D^2$		$\psi^2 \varphi^3$	
Q_G	$f^{ABC} G_\mu^{A\nu} G_\nu^{B\rho} G_\rho^{C\mu}$	Q_φ	$(\varphi^\dagger \varphi)^3$	$Q_{e\varphi}$	$(\varphi^\dagger \varphi)(\bar{l}_p e_r \varphi)$
$Q_{\tilde{G}}$	$f^{ABC} \tilde{G}_\mu^{A\nu} G_\nu^{B\rho} G_\rho^{C\mu}$	$Q_{\varphi\Box}$	$(\varphi^\dagger \varphi) \Box (\varphi^\dagger \varphi)$	$Q_{u\varphi}$	$(\varphi^\dagger \varphi)(\bar{q}_p u_r \tilde{\varphi})$
Q_W	$\varepsilon^{IJK} W_\mu^{I\nu} W_\nu^{J\rho} W_\rho^{K\mu}$	$Q_{\varphi D}$	$(\varphi^\dagger D^\mu \varphi)^* (\varphi^\dagger D_\mu \varphi)$	$Q_{d\varphi}$	$(\varphi^\dagger \varphi)(\bar{q}_p d_r \varphi)$
$Q_{\tilde{W}}$	$\varepsilon^{IJK} \tilde{W}_\mu^{I\nu} W_\nu^{J\rho} W_\rho^{K\mu}$				
$X^2 \varphi^2$		$\psi^2 X \varphi$		$\psi^2 \varphi^2 D$	
$Q_{\varphi G}$	$\varphi^\dagger \varphi G_{\mu\nu}^A G^{A\mu\nu}$	Q_{eW}	$(\bar{l}_p \sigma^{\mu\nu} e_r) \tau^I \varphi W_{\mu\nu}^I$	$Q_{\varphi l}^{(1)}$	$(\varphi^\dagger i \overleftrightarrow{D}_\mu \varphi)(\bar{l}_p \gamma^\mu l_r)$
$Q_{\varphi \tilde{G}}$	$\varphi^\dagger \varphi \tilde{G}_{\mu\nu}^A G^{A\mu\nu}$	Q_{eB}	$(\bar{l}_p \sigma^{\mu\nu} e_r) \varphi B_{\mu\nu}$	$Q_{\varphi l}^{(3)}$	$(\varphi^\dagger i \overleftrightarrow{D}_\mu^I \varphi)(\bar{l}_p \tau^I \gamma^\mu l_r)$
$Q_{\varphi W}$	$\varphi^\dagger \varphi W_{\mu\nu}^I W^{I\mu\nu}$	Q_{uG}	$(\bar{q}_p \sigma^{\mu\nu} T^A u_r) \tilde{\varphi} G_{\mu\nu}^A$	$Q_{\varphi e}$	$(\varphi^\dagger i \overleftrightarrow{D}_\mu \varphi)(\bar{e}_p \gamma^\mu e_r)$
$Q_{\varphi \tilde{W}}$	$\varphi^\dagger \varphi \tilde{W}_{\mu\nu}^I W^{I\mu\nu}$	Q_{uW}	$(\bar{q}_p \sigma^{\mu\nu} u_r) \tau^I \tilde{\varphi} W_{\mu\nu}^I$	$Q_{\varphi q}^{(1)}$	$(\varphi^\dagger i \overleftrightarrow{D}_\mu \varphi)(\bar{q}_p \gamma^\mu q_r)$
$Q_{\varphi B}$	$\varphi^\dagger \varphi B_{\mu\nu} B^{\mu\nu}$	Q_{uB}	$(\bar{q}_p \sigma^{\mu\nu} u_r) \tilde{\varphi} B_{\mu\nu}$	$Q_{\varphi q}^{(3)}$	$(\varphi^\dagger i \overleftrightarrow{D}_\mu^I \varphi)(\bar{q}_p \tau^I \gamma^\mu q_r)$
$Q_{\varphi \tilde{B}}$	$\varphi^\dagger \varphi \tilde{B}_{\mu\nu} B^{\mu\nu}$	Q_{dG}	$(\bar{q}_p \sigma^{\mu\nu} T^A d_r) \varphi G_{\mu\nu}^A$	$Q_{\varphi u}$	$(\varphi^\dagger i \overleftrightarrow{D}_\mu \varphi)(\bar{u}_p \gamma^\mu u_r)$
$Q_{\varphi WB}$	$\varphi^\dagger \tau^I \varphi W_{\mu\nu}^I B^{\mu\nu}$	Q_{dW}	$(\bar{q}_p \sigma^{\mu\nu} d_r) \tau^I \varphi W_{\mu\nu}^I$	$Q_{\varphi d}$	$(\varphi^\dagger i \overleftrightarrow{D}_\mu \varphi)(\bar{d}_p \gamma^\mu d_r)$
$Q_{\varphi \tilde{W}B}$	$\varphi^\dagger \tau^I \varphi \tilde{W}_{\mu\nu}^I B^{\mu\nu}$	Q_{dB}	$(\bar{q}_p \sigma^{\mu\nu} d_r) \varphi B_{\mu\nu}$	$Q_{\varphi ud}$	$i(\tilde{\varphi}^\dagger D_\mu \varphi)(\bar{u}_p \gamma^\mu d_r)$

Table A.2: Dimension-six operators other than the four-fermion ones. Taken from [14].

Appendix B

Fierz Identities

Fierz transformations enable one to reorder a product of four Dirac spinors, a trick which we used in chapter 6 to convert dimension-six operators to the Warsaw basis. In this appendix, we provide some background material on this transformation and specifically derive identity 6.1.13 from the main-text:

$$[\bar{\psi}_{L_1} \psi_{R_2}][\bar{\psi}_{R_3} \psi_{L_4}] = \frac{1}{2} [\bar{\psi}_{L_1} \gamma^\mu \psi_{L_4}] [\bar{\psi}_{R_3} \gamma_\mu \psi_{R_2}], \quad (\text{B.0.1})$$

where L, R denote the chirality of the Dirac spinor.

Our starting point is to note that the 4×4 Dirac matrices γ^μ together with appropriate products span the space of all 16×16 dimensional matrices [32]. Taking the following quadrilinears as our basis,

$$\begin{aligned} e_S(1234) &\equiv [\bar{\psi}_1 \psi_2][\bar{\psi}_3 \psi_4] \\ e_V(1234) &\equiv [\bar{\psi}_1 \gamma^\mu \psi_2][\bar{\psi}_3 \gamma_\mu \psi_4] \\ e_T(1234) &\equiv [\bar{\psi}_1 \sigma_{\mu\nu} \psi_2][\bar{\psi}_3 \sigma^{\mu\nu} \psi_4] \\ e_A(1234) &\equiv [\bar{\psi}_1 \gamma^\mu \gamma_5 \psi_2][\bar{\psi}_3 \gamma_\mu \gamma_5 \psi_4] \\ e_P(1234) &\equiv [\bar{\psi}_1 \gamma_5 \psi_2][\bar{\psi}_3 \gamma_5 \psi_4] \end{aligned} \quad (\text{B.0.2})$$

we define \mathbf{F} as a 5×5 matrix that swaps positions 2 and 4 (or equivalently, 1 and 3, as the ordering of the bilinears is irrelevant):

$$\mathbf{e}(1234) = \mathbf{F} \mathbf{e}(1432), \quad (\text{B.0.3})$$

with $\mathbf{e}(1234) = (e_S(1234), e_V(1234), e_T(1234), e_A(1234), e_P(1234))^{\mathbf{T}}$. The exact form of \mathbf{F} is derived in ref. [32] and is copied here for convenience:

$$\mathbf{F} = \frac{1}{4} \begin{pmatrix} 1 & 1 & \frac{1}{2} & -1 & 1 \\ 4 & -2 & 0 & -2 & -4 \\ 12 & 0 & -2 & 0 & 12 \\ -4 & -2 & 0 & -2 & 4 \\ 1 & -1 & \frac{1}{2} & 1 & 1 \end{pmatrix}. \quad (\text{B.0.4})$$

Let us now use equation (B.0.3) to prove (B.0.1). Taking $\bar{\psi}_1 = \bar{\psi}_{L_1}, \psi_2 = \psi_{R_2}, \bar{\psi}_3 = \bar{\psi}_{R_3}$ and $\psi_4 = \psi_{L_4}$ in equation (B.0.2), we find

$$\begin{aligned}
e_S(1234) &= [\bar{\psi}_{L_1} \psi_{R_2}] [\bar{\psi}_{R_3} \psi_{L_4}] \\
&= \frac{1}{4} [e_S(1432) + e_V(1432) + \frac{1}{2} e_T(1432) - e_A(1432) + e_P(1432)] \\
&= \frac{1}{4} [\bar{\psi}_{L_1} \psi_{L_4} \bar{\psi}_{R_3} \psi_{R_2} + \bar{\psi}_{L_1} \gamma^\mu \psi_{L_4} \bar{\psi}_{R_3} \gamma_\mu \psi_{R_2} + \frac{1}{2} \bar{\psi}_{L_1} \sigma_{\mu\nu} \psi_{L_4} \bar{\psi}_{R_3} \sigma^{\mu\nu} \psi_{R_2} \\
&\quad - \bar{\psi}_{L_1} \gamma^\mu \gamma_5 \psi_{L_4} \bar{\psi}_{R_3} \gamma^\mu \gamma_5 \psi_{R_2} + \bar{\psi}_{L_1} \gamma_5 \psi_{L_4} \bar{\psi}_{R_3} \gamma_5 \psi_{R_2}] \\
&= \frac{1}{4} [\bar{\psi}_{L_1} \gamma^\mu \psi_{L_4} \bar{\psi}_{R_3} \gamma_\mu \psi_{R_2} - \bar{\psi}_{L_1} \gamma^\mu \gamma_5 \psi_{L_4} \bar{\psi}_{R_3} \gamma^\mu \gamma_5 \psi_{R_2}], \tag{B.0.5}
\end{aligned}$$

where we have used that $\bar{\psi}_L \psi_L = 0, \bar{\psi}_L \sigma_{\mu\nu} \psi_L = 0$ and $\bar{\psi}_L \gamma_5 \psi_L = 0$. The last term in equation (B.0.5) can be cast in a similar form as the first term, by using that $\bar{\psi}_L \gamma^\mu \gamma_5 \psi_L = -\bar{\psi}_L \gamma^\mu \psi_L$ and $\bar{\psi}_R \gamma^\mu \gamma_5 \psi_R = \bar{\psi}_R \gamma^\mu \psi_R$. With this, we obtain:

$$\begin{aligned}
e_S(1234) &= \frac{1}{4} [\bar{\psi}_{L_1} \gamma^\mu \psi_{L_4} \bar{\psi}_{R_3} \gamma_\mu \psi_{R_2} + \bar{\psi}_{L_1} \gamma^\mu \psi_{L_4} \bar{\psi}_{R_3} \gamma_\mu \psi_{R_2}] \\
&= \frac{1}{2} [\bar{\psi}_{L_1} \gamma^\mu \psi_{L_4}] [\bar{\psi}_{R_3} \gamma_\mu \psi_{R_2}], \tag{B.0.6}
\end{aligned}$$

which proves equation (B.0.1).

Appendix C

Decay Widths

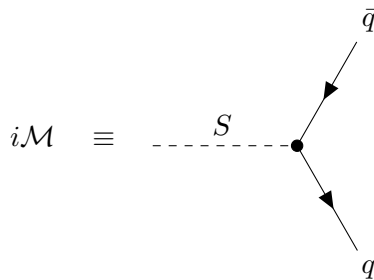
In this last appendix, we consider a particle with mass M that decays into two particles with identical mass m . In that case, the decay width Γ is given by [33]

$$\frac{d\Gamma}{d\Omega} = \frac{|\mathcal{M}|^2}{32\pi^2 s} |p_f| = \frac{|\mathcal{M}|^2}{32\pi^2 s} \frac{1}{2} M \sqrt{1 - \frac{4m^2}{M^2}}, \quad (\text{C.0.1})$$

where $|p_f|$ is the norm of the outgoing particle's momentum. We will now apply (C.0.1) to two special cases that were used in the main-text.

C.1 Heavy Scalar

The heavy scalar particle S , introduced in section 6.1, can decay into two quarks. Here, we derive its corresponding total decay width Γ_{tot} . We define



Since the vertex factor is simply ic_S , we straightforwardly derive

$$\begin{aligned}
|\bar{\mathcal{M}}|^2 &\equiv \sum_{\text{spins}} |\mathcal{M}|^2 \\
&= c_S^2 \sum_{s,s'} [\bar{v}_2^s u_1^{s'}][\bar{u}_1^{s'} v_2^s] \\
&= c_S^2 \text{Tr}[(\not{p}_1 + m_2)(\not{p}_2 - m_2)] \\
&= c_S^2 (4p_1 \cdot p_2 - 4m_q^2) \\
&= c_S^2 (2m_S^2 - 8m_q^2) \\
&= 2c_S^2 m_S^2 \left(1 - \frac{4m_q^2}{m_S^2}\right).
\end{aligned}$$

Including the number of colours, we get:

$$|\bar{\mathcal{M}}|^2 = 6c_S^2 m_S^2 \left(1 - \frac{4m_q^2}{m_S^2}\right). \quad (\text{C.1.1})$$

Substituting this into equation (C.0.1), gives

$$\frac{d\Gamma}{d\Omega} = \frac{|\bar{\mathcal{M}}|^2}{32\pi^2 s} |p_f| = c_S^2 \frac{3m_S}{32\pi^2} \left(1 - \frac{4m_q^2}{m_S^2}\right)^{3/2}. \quad (\text{C.1.2})$$

Performing the integration over the angular variable Ω , gives an extra factor of 4π :

$$\Gamma = \frac{3c_S^2}{8\pi} m_S \left(1 - \frac{4m_q^2}{m_S^2}\right)^{3/2}. \quad (\text{C.1.3})$$

So the total decay width is given by

$$\Gamma_{\text{tot}} = \frac{3c_S^2}{8\pi} m_S \left(1 - \frac{4m_t^2}{m_S^2}\right)^{3/2} + \frac{15c_S^2}{8\pi} m_S. \quad (\text{C.1.4})$$

C.2 Heavy Vector Boson

The heavy vector boson B_μ , as first introduced in section 6.2, can decay into two quarks of the same flavour. Here, we derive the associated matrix element \mathcal{M} . We define

$$i\mathcal{M} \equiv \text{Diagram showing a wavy line labeled } B_\mu \text{ decaying into two quarks } \bar{q} \text{ and } q.$$

The vertex factor is $ig_B\gamma_\mu$, and contracting with the polarization vector, we thus get

$$i\mathcal{M} = \epsilon^\mu(q)\bar{u}_3i\gamma_\mu g_B v_4,$$

which leads to

$$|\mathcal{M}|^2 = g_B^2 [\bar{u}_3\gamma_\mu v_4] [\bar{v}_4\gamma_\nu u_3]\epsilon^\mu(q)\epsilon^\nu(q)^* \quad (\text{C.2.1})$$

Averaging over the incoming polarizations, and summing over the outgoing fermion spins, gives

$$\begin{aligned} |\bar{\mathcal{M}}|^2 &\equiv \frac{1}{3} \sum_{\text{pol}} \sum_{\text{spins}} |\mathcal{M}|^2 \\ &= \frac{g_B^2}{3} \sum_{\text{pol}} \sum_{ss'} [\bar{u}_3^s\gamma_\mu v_4^{s'}] [\bar{v}_4^{s'}\gamma_\nu u_3^s] \epsilon^\mu(q)\epsilon^\nu(q)^* \\ &= \frac{g_B^2}{3} \sum_{\text{pol}} \text{Tr} [(\not{p}_3 + m_q)\gamma_\mu(\not{p}_4 - m_q)\gamma_\nu] \epsilon^\mu(q)\epsilon^\nu(q)^*. \end{aligned} \quad (\text{C.2.2})$$

Using

$$\sum_{\text{pol}} \epsilon_\mu^*(q)\epsilon_\nu(q) = -\left(g_{\mu\nu} - \frac{q_\mu q_\nu}{M_B^2}\right), \quad (\text{C.2.3})$$

we now sum over the three polarizations to get

$$\begin{aligned} |\bar{\mathcal{M}}|^2 &= -\frac{g_B^2}{3} \text{Tr} [(\not{p}_3 + m_q)\gamma_\mu(\not{p}_4 - m_q)\gamma_\nu] \left(g^{\mu\nu} - \frac{q^\mu q^\nu}{M_B^2}\right) \\ &= -\frac{g_B^2}{3} (p_3^\rho p_4^\sigma \text{Tr} [\gamma_\rho\gamma_\mu\gamma_\sigma\gamma_\nu] - m_q^2 \text{Tr} [\gamma_\mu\gamma_\nu]) \left(g^{\mu\nu} - \frac{q^\mu q^\nu}{M_B^2}\right) \\ &= -\frac{g_B^2}{3} (4p_3^\rho p_4^\sigma (g_{\rho\mu}g_{\sigma\nu}) + g_{\rho\nu}g_{\mu\sigma} - g_{\rho\sigma}g_{\mu\nu} - 4m_q^2 g_{\mu\nu})(g^{\mu\nu} - \frac{q^\mu q^\nu}{M_B^2}). \end{aligned} \quad (\text{C.2.4})$$

Contracting the Lorentz-indices then gives

$$\begin{aligned} |\bar{\mathcal{M}}|^2 &= -\frac{4g_B^2}{3} \left(p_{34} + p_{34} - 4p_{34} - 4m_q^2 - 2\frac{(p_3 \cdot q)(p_4 \cdot q)}{M_B^2} + \frac{p_{34}q^2}{M_B^2} \right) \\ &= \frac{4g_B^2}{3} \left(p_{34} + 4m_q^2 + 2\frac{(p_3 \cdot q)(p_4 \cdot q)}{m_B^2} \right). \end{aligned} \quad (\text{C.2.5})$$

Let us now use that in the CM-frame we have $p_3^\mu = (M_B/2, \vec{p}_3)$, $p_4^\mu = (M_B/2, -\vec{p}_3)$ and $q^\mu = (M_B, 0)$.

Then

$$\begin{aligned} |\bar{\mathcal{M}}|^2 &= \frac{4g_B^2}{3} \left(\frac{M_B^2}{2} - m_q^2 + 4m_q^2 + \frac{M_B^2}{2} \right) \\ &= \frac{4g_B^2}{3} (M_B^2 + 3m_q^2). \end{aligned} \quad (\text{C.2.6})$$

Substituting equation (C.2.6) into equation (C.0.1), subsequently gives upon integration

$$\Gamma = \frac{g_B^2}{12\pi} \frac{M_B^2 + 3m_q^2}{M_B} \sqrt{1 - \frac{4m_q^2}{M_B^2}}. \quad (\text{C.2.7})$$

Summing over all quark flavours, and recalling that all quarks are massless except for the top-quark, we finally arrive at

$$\Gamma_{\text{tot}} = \frac{5g_B^2}{12\pi} M_B + \frac{g_B^2}{12\pi} \frac{M_B^2 + 3m_t^2}{M_B} \sqrt{1 - \frac{4m_t^2}{M_B^2}}. \quad (\text{C.2.8})$$

Bibliography

- [1] Georges Aad et al. “Observation of a new particle in the search for the Standard Model Higgs boson with the ATLAS detector at the LHC”. In: *Phys. Lett. B* 716 (2012), pp. 1–29. DOI: 10.1016/j.physletb.2012.08.020. arXiv: 1207.7214 [hep-ex].
- [2] Ilaria Brivio and Michael Trott. “The Standard Model as an Effective Field Theory”. In: *Phys. Rept.* 793 (2019), pp. 1–98. DOI: 10.1016/j.physrep.2018.11.002. arXiv: 1706.08945 [hep-ph].
- [3] Nathan P. Hartland et al. “A Monte Carlo global analysis of the Standard Model Effective Field Theory: the top quark sector”. In: *JHEP* 04 (2019), p. 100. DOI: 10.1007/JHEP04(2019)100. arXiv: 1901.05965 [hep-ph].
- [4] M.D. Schwartz. *Quantum Field Theory and the Standard Model*. Quantum Field Theory and the Standard Model. Cambridge University Press, 2014. ISBN: 9781107034730. URL: <https://books.google.nl/books?id=HbdEAgAAQBAJ>.
- [5] Mark Srednicki. *Quantum Field Theory*. Cambridge University Press, 2007. DOI: 10.1017/CB09780511813917.
- [6] D.J. Scott. “Effective Field Theories for Top Quarks at the LHC and Physics Beyond the Higgs Boson”. PhD thesis. Durham University, 2017. URL: <http://etheses.dur.ac.uk/12439/>.
- [7] Thomas Appelquist and J. Carazzone. “Infrared singularities and massive fields”. In: *Phys. Rev. D* 11 (10 May 1975), pp. 2856–2861. DOI: 10.1103/PhysRevD.11.2856. URL: <https://link.aps.org/doi/10.1103/PhysRevD.11.2856>.
- [8] Enrico Fermi. “Tentativo di una teoria dell’emissione dei raggi beta”. In: *Ric. Sci.* 4 (1933), pp. 491–495.
- [9] Y. Fukuda et al. “Measurement of the flux and zenith angle distribution of upward through going muons by Super-Kamiokande”. In: *Phys. Rev. Lett.* 82 (1999), pp. 2644–2648. DOI: 10.1103/PhysRevLett.82.2644. arXiv: hep-ex/9812014.
- [10] Celine Degrande et al. “Effective Field Theory: A Modern Approach to Anomalous Couplings”. In: *Annals Phys.* 335 (2013), pp. 21–32. DOI: 10.1016/j.aop.2013.04.016. arXiv: 1205.4231 [hep-ph].

- [11] Andrew Kobach. “Baryon Number, Lepton Number, and Operator Dimension in the Standard Model”. In: *Phys. Lett. B* 758 (2016), pp. 455–457. DOI: 10.1016/j.physletb.2016.05.050. arXiv: 1604.05726 [hep-ph].
- [12] Christopher W. Murphy. “Dimension-8 Operators in the Standard Model Effective Field Theory”. In: (Apr. 2020). arXiv: 2005.00059 [hep-ph].
- [13] Cen Zhang and Scott Willenbrock. “Effective-field-theory approach to top-quark production and decay”. In: *Physical Review D* 83.3 (Feb. 2011). ISSN: 1550-2368. DOI: 10.1103/physrevd.83.034006. URL: <http://dx.doi.org/10.1103/PhysRevD.83.034006>.
- [14] B. Grzadkowski et al. “Dimension-six terms in the Standard Model Lagrangian”. In: *Journal of High Energy Physics* 2010.10 (Oct. 2010). ISSN: 1029-8479. DOI: 10.1007/jhep10(2010)085. URL: [http://dx.doi.org/10.1007/JHEP10\(2010\)085](http://dx.doi.org/10.1007/JHEP10(2010)085).
- [15] Vladyslav Shtabovenko, Rolf Mertig, and Frederik Orellana. “FeynCalc 9.3: New features and improvements”. In: (Jan. 2020). arXiv: 2001.04407 [hep-ph].
- [16] Vladyslav Shtabovenko, Rolf Mertig, and Frederik Orellana. “New Developments in FeynCalc 9.0”. In: *Comput. Phys. Commun.* 207 (2016), pp. 432–444. DOI: 10.1016/j.cpc.2016.06.008. arXiv: 1601.01167 [hep-ph].
- [17] R. Mertig, M. Böhm, and A. Denner. “Feyn Calc - Computer-algebraic calculation of Feynman amplitudes”. In: *Computer Physics Communications* 64.3 (1991), pp. 345–359. ISSN: 0010-4655. DOI: [https://doi.org/10.1016/0010-4655\(91\)90130-D](https://doi.org/10.1016/0010-4655(91)90130-D). URL: <http://www.sciencedirect.com/science/article/pii/001046559190130D>.
- [18] W. Buchmüller and D. Wyler. “Effective lagrangian analysis of new interactions and flavour conservation”. In: *Nuclear Physics B* 268.3 (1986), pp. 621–653. ISSN: 0550-3213. DOI: [https://doi.org/10.1016/0550-3213\(86\)90262-2](https://doi.org/10.1016/0550-3213(86)90262-2). URL: <http://www.sciencedirect.com/science/article/pii/0550321386902622>.
- [19] F. Feroz et al. “Importance Nested Sampling and the MultiNest Algorithm”. In: (June 2013). DOI: 10.21105/astro.1306.2144. arXiv: 1306.2144 [astro-ph.IM].
- [20] Bo-Ting Wang et al. “Mapping the sensitivity of hadronic experiments to nucleon structure”. In: *Phys. Rev. D* 98.9 (2018), p. 094030. DOI: 10.1103/PhysRevD.98.094030. arXiv: 1803.02777 [hep-ph].
- [21] Enrico Morgante. “Simplified Dark Matter Models”. In: *Adv. High Energy Phys.* 2018 (2018), p. 5012043. DOI: 10.1155/2018/5012043. arXiv: 1804.01245 [hep-ph].
- [22] Jorge de Blas et al. “Observable Effects of General New Scalar Particles”. In: *JHEP* 04 (2015), p. 078. DOI: 10.1007/JHEP04(2015)078. arXiv: 1412.8480 [hep-ph].

- [23] D. Barducci et al. “Interpreting top-quark LHC measurements in the standard-model effective field theory”. In: (Feb. 2018). Ed. by Juan Antonio Aguilar-Saavedra et al. arXiv: 1802.07237 [hep-ph].
- [24] Christoph Englert, Peter Galler, and Chris D. White. “Effective field theory and scalar extensions of the top quark sector”. In: *Phys. Rev. D* 101.3 (2020), p. 035035. DOI: 10.1103/PhysRevD.101.035035. arXiv: 1908.05588 [hep-ph].
- [25] F. del Aguila, J. de Blas, and M. Perez-Victoria. “Electroweak Limits on General New Vector Bosons”. In: *JHEP* 09 (2010), p. 033. DOI: 10.1007/JHEP09(2010)033. arXiv: 1005.3998 [hep-ph].
- [26] W. Buchmuller and D. Wyler. “Effective Lagrangian Analysis of New Interactions and Flavor Conservation”. In: *Nucl. Phys. B* 268 (1986), pp. 621–653. DOI: 10.1016/0550-3213(86)90262-2.
- [27] Emidio Gabrielli, Antonio Racioppi, and Martti Raidal. “Implications of the effective axial-vector coupling of the gluon on top-quark charge asymmetry at the LHC”. In: *Phys. Rev. D* 85 (7 Apr. 2012), p. 074021. DOI: 10.1103/PhysRevD.85.074021. URL: <https://link.aps.org/doi/10.1103/PhysRevD.85.074021>.
- [28] Michal Czakon, David Heymes, and Alexander Mitov. *fastNLO tables for NNLO top-quark pair differential distributions*. 2017. arXiv: 1704.08551 [hep-ph].
- [29] J. Alwall et al. “The automated computation of tree-level and next-to-leading order differential cross sections, and their matching to parton shower simulations”. In: *JHEP* 07 (2014), p. 079. DOI: 10.1007/JHEP07(2014)079. arXiv: 1405.0301 [hep-ph].
- [30] A. M. Sirunyan et al. “Measurement of differential cross sections for the production of top quark pairs and of additional jets in lepton+jets events from pp collisions at s=13TeV”. In: *Physical Review D* 97.11 (June 2018). ISSN: 2470-0029. DOI: 10.1103/physrevd.97.112003. URL: <http://dx.doi.org/10.1103/PhysRevD.97.112003>.
- [31] M. Tanabashi et al. “Review of Particle Physics”. In: *Phys. Rev. D* 98.3 (2018), p. 030001. DOI: 10.1103/PhysRevD.98.030001.
- [32] Jose F. Nieves and Palash B. Pal. “Generalized Fierz identities”. In: *Am. J. Phys.* 72 (2004), pp. 1100–1108. DOI: 10.1119/1.1757445. arXiv: hep-ph/0306087.
- [33] M. Merk, I. Van Vulpen, and W. Hulsbergen. “Particle Physics 1 Lecture notes for the first year master course on the electroweak part of the Standard Model”. In: (2019). URL: <https://www.nikhef.nl/~wouterh/teaching/PP1/LectureNotes.pdf>.